การคัดแยกอนุภาคในย่านขนาดละเอียดโดยใช้ไฮโดรไซโคลน

นายประธาน วงศ์ศริเวช

สถาบันวิทยบริการ
จุฬาลงกรณ์มหาวิทยาลัย

วิทยานิพนธ์นี้เป็นส่วนหนึ่งของการศึกษาตามหลักสูตรปริญญาวิศวกรรมศาสตรดุษฎีบัณฑิต
สาขาวิศวกรรมเคมี ภาควิชาวิศวกรรมเคมี
คณะวิศวกรรมศาสตร์ จุฬาลงกรณ์มหาวิทยาลัย
ปีการศึกษา 2547
ISBN 974-17-6886-9
ลิขสิทธิ์ของจุฬาลงกรณ์มหาวิทยาลัย

PARTICLE CLASSIFICATION OF FINE SIZE REGION BY USING HYDROCYCLONE

Mr. Pratarn Wongsarivej

สถาบันวิทยบริการ
จุฬาลงกรณ์มหาวิทยาลัย

A Dissertation Submitted in Partial Fulfillment of the Requirements
for the Degree of Doctor of Engineering in Chemical Engineering
Department of Chemical Engineering
Faculty of Engineering
Chulalongkorn University
Academic year 2004

ISBN 974-17-6886-9

Thesis Title	PARTICLE CLASSIFICATION OF FINE SIZE REGION BY USING HYDROCYCLONE
By	Mr. Pratarn Wongsarivej
Filed of study	Chemical Engineering
Thesis Advisor	Professor Wiwut Tanthapanichakoon, Ph.D.
Thesis Co-advisor	Professor Hideto Yoshida, D.Eng.

Accepted by the Faculty of Engineering, Chulalongkorn University in Partial Fulfillment of the Requirements for the Doctor's Degree

…….. Dean of the Faculty of Engineering
(Professor Direk Lavansiri, Ph.D.)

THESIS COMMITTEE

…….. Chairman
(Professor Piyasan Praserthdam, Ph.D.)

……. Thesis Advisor
(Professor Wiwut Tanthapanichakoon, Ph.D.)

…….. Thesis Co-advisor
(Professor Hideto Yoshida, D.Eng.)

…….. Member
(Associate Professor Tawatchai Charinpanitkul, D.Eng.)

…….. Member
(Assistant Professor Muenduen Phisalaphong, Ph.D.)

…….. Member
(Sukasem Kangwantrakool, D.Eng.)

สถาบันวิทยบริการ
จุฬาลงกรณ์มหาวิทยาลัย

ประธาน วงศ์ศริเวช : การคัดแยกอนุภาคในย่านละเอียดโดยใช้ไฮโดรไซโคลน (PARTICLE CLASSIFICATION OF FINE SIZE REGION BY USING HYDROCYCLONE) อ. ที่ปรึกษา : ศ.ดร.วิวัฒน์ ตัณฑะพานิชกุล, อ. ที่ปรึกษาร่วม : ศ. ดร. ฮิเดโตะ โยชิดะ จำนวนหน้า 155 หน้า. ISBN 974-17-6886-9.

ไฮโดรไซโคลนแบบไฟฟ้าไม่เคยมีการวิจัยมาก่อน การลดขนาดของอนุภาคเป็นสิ่งจำเป็นในหลากหลายอุตสาหกรรม งานวิจัยนี้ไฮโดรไซโคลนแบบไฟฟ้าชนิดใหม่ถูกพัฒนาขึ้นและทดสอบโดยใช้สารแขวนลอยของซิลิกาขนาดอนุภาคเฉลี่ย 0.754 ไมครอนและมีความเข้มข้น 0.2% โดยปริมาตร ทดสอบในไฮโดรไซโคลนขนาด 20 มม. อัตราส่วนทดสอบของอันเดอร์โฟล์ต่อทางเข้าคือ 0,0.1, 0.2 และ 0.3 อัตราไหลทดสอบคือ $0.083*10^{-3}$, $0.117*10^{-3}$ และ $0.167*10^{-3}$ ลบม.ต่อวินาที (5, 7 และ 10 ลิตรต่อนาที) pH ของสารแขวนลอยที่ศึกษาคือ 6.0, 8.0, 9.0 และ 10.0 ส่วนกรวยของไฮโดรไซโคลนต่อกับกล่องฝุ่นรูปทรงกระบอกเส้นผ่านศูนย์กลาง 41.8 มม. โดยมีแกนโลหะอยู่ตรงกลางระหว่างผนังโลหะซึ่งสามารถประยุกต์ศักย์ไฟฟ้าขนาด 50 โวลต์ได้ ความยาวของกล่องฝุ่นที่ศึกษาคือ 53 และ 106 มม. เส้นผ่านศูนย์กลางของแกนกลางที่ศึกษามีขนาด 8, 12, 16 และ 20 มม. ทำการศึกษา 3 กรณีแตกต่างกันคือ ก. ไม่มีการประยุกต์ศักย์ไฟฟ้า ข. ขั้วบวกต่อกับแกนกลางและขั้วลบต่อกับด้านผนัง และ ค. ขั้วไฟฟ้าสลับกับกรณี ข.

ทั้งในกรณีที่ไม่มีและมีอันเดอร์โฟล์ไฮโดรไซโคลนที่ต่อกับกล่องฝุ่นแบบยาวจะให้ขนาดอนุภาคที่ 50%, d_{50}เล็กกว่ากรณีที่ต่อกับกล่องฝุ่นแบบสั้น ตามความคาดหมายทั้งกรณีที่ไม่มีและมีอันเดอร์โฟล์จะลดขนาดของ d_{50} เมื่อมีศักย์ไฟฟ้า ยิ่งไปกว่านั้นกรณีที่มีอันเดอร์โฟล์จะให้ d_{50} เล็กกว่ากรณีที่ไม่มีอันเดอร์โฟล์ พบได้ว่ากรณี ค. ศักย์ไฟฟ้าจะแสดงผลต่อ d_{50} มากกว่ากรณี ข. การประยุกต์ศักย์ไฟฟ้าในกรณี ค. สามารถลดขนาดของ d_{50} ได้ 9.6% เทียบกับไม่มีการใช้ศักย์ไฟฟ้า เมื่ออัตราส่วนของอันเดอร์โฟล์ต่อทางเข้ามีค่าสูงขึ้น d_{50} จะมีขนาดเล็กลง ค่าศักย์เซต้าจะเพิ่มขึ้นเมื่อสารแขวนลอยมี pH สูงขึ้น ศักย์ไฟฟ้ามีผลมากขึ้นเมื่อสารแขวนลอยมี pH สูงขึ้น เมื่อ pH สูงขึ้นจะทำให้ d_{50} เล็กลง ผลรวมของศักย์ไฟฟ้าและ pH สามารถลดขนาด d_{50} ได้ 18.8% เทียบกับไม่มีการใช้ศักย์ไฟฟ้า ยิ่งไปกว่านั้นศักย์ไฟฟ้าจะแสดงผลมากยิ่งขึ้นอีกเมื่อเส้นผ่านศูนย์กลางของแกนกลางมีขนาดใหญ่ขึ้น ผลของศักย์ไฟฟ้าร่วมกับแกนกลางขนาดใหญ่สุดและค่า pH สูงสุดสามารถลดขนาด d_{50} ได้ถึง 22.7% เทียบกับไม่มีการใช้ศักย์ไฟฟ้า สภาวะดีที่สุดที่ให้ d_{50} ขนาดเล็กสุดคือการใช้กล่องฝุ่นแบบยาว ระบบทำงานด้วยสารแขวนลอยมี pH สูงสุด แกนกลางมีขนาดใหญ่สุด และต่อขั้วบวกกับด้านผนังโดยใช้กรณีแบบมีอันเดอร์โฟล์ จากผลการทดลองสามารถหาความสัมพันธ์ของ d_{50} ได้

ภาควิชา…….วิศวกรรมเคมี…….ลายมือชื่อนิสิต……..……..

สาขาวิชา……วิศวกรรมเคมี……ลายมือชื่ออาจารย์ที่ปรึกษา……..

ปีการศึกษา…….....2547.....ลายมือชื่ออาจารย์ที่ปรึกษาร่วม……..

4571814821 : MAJOR CHEMICAL ENGINEERING
KEY WORD: PARTICLE / CLASSIFICATION / FINE SIZE / HYDROCYCLONE / ELECTRIC POTENTIAL

PRATARN WONGSARIVEJ : PARTICLE CLASSIFICATION OF FINE SIZE REGION BY USING HYDROCYCLONE. THESIS ADVISOR : PROF. WIWUT TANTHAPANICHAKOON, Ph.D., THESIS CO-ADVISOR : PROF. HIDETO YOSHIDA, D. Eng., 155 pp. ISBN 974-17-6886-9.

The electric hydrocyclone had never been investigated. The reduction of the particle cut size was important in many industrial processes. In this research, a novel electric hydrocyclone was developed and tested. Aqueous suspensions of silica with a median diameter of 0.754 μm and 0.2% volumetric concentration were tested using a 20-mm-diameter hydrocyclone. The ratios of the experimental underflow to the throughput were: 0, 0.1, 0.2 and 0.3. The tested volumetric flow rates were $0.083*10^{-3}$ and $0.117*10^{-3}$ and $0.167*10^{-3}$ m^3/s (5, 7 and 10 L/min). The four investigated pH of the suspension were: 6.0, 8.0, 9.0 and 10.0. The conical part of the electric hydrocyclone was connected to a cylindrical dust box having 41.8 mm diameter. This dust box had a central metal rod cone and a cylindrical metal wall between which the desired 50-volt DC electric potential or no potential was applied. The investigated lengths of the dust box were 53 and 106 mm. The investigated central rod diameters were 8, 12, 16 and 20 mm. The three different cases investigated were: a) no applied electric potential, b) positive potential applied at the central rod side and negative potential at the side wall, and c) the reverse of case b).

In both the presence and absence of the underflow, the hydrocyclone with a long dust box was found to give smaller the 50% particle cut size, d_{50} than that with a short dust box. Both the presence and absence of the underflow expectedly decrease d_{50} when electric potential was applied. Moreover, the presence of the underflow gave smaller d_{50} than the absence of the underflow. It was found that case c) exhibited a stronger effect on the d_{50} than case b). Application of the electric potential in case c) can reduce d_{50} by up to 9.6% compared to the absence of electricity. As expected, the higher the underflow to throughput ratio, the smaller d_{50} becomes. The zeta potential was increased when the suspension had higher pH. The electric potential exhibited a stronger effect when the suspension had higher pH. The higher the pH, the smaller d_{50} becomes. The combined effect of electric potential and pH can reduce d_{50} by up to 18.8% compared to the absence of electricity. Moreover, the electric potential exhibited a stronger effect when the central rod had a larger diameter. The effect of electric potential with the largest central rod diameter and highest pH can reduce d_{50} by up to 22.7% compared to the absence of electricity. The best conditions to obtain the smallest d_{50} were that the long dust box be used, the system was operated with a highest pH suspension, the largest central rod diameter and positive electric potential at the wall be employed in the presence of the underflow. Based on the experimental results, a semi-empirical correlation for d_{50} had been obtained.

Department……Chemical Engineering…Student's signature……

Field of study….Chemical Engineering…Advisor's signature……...

Academic year……2004……...Co-advisor's signature……..…

ACKNOWLEGDEMENTS

The author would like to express my sincere thanks to my advisor, Professor Wiwut Tanthapanichakoon for his greatest advice, deep discussion and constant encouragement throughout this project. The author is very grateful to the late Professor Hideto Yoshida, thesis co-advisor, for his indispensable guidance and supervision, especially, a meaningful contribution to the build-up of strong fruitful cooperation between our two universities. They have given me encouragement to continue during hard times, and lent me strong support when things looked impossible to attain. Through their guidance, I have gained not only valuable knowledge from this work but also widened perspective in its practical applications.

The author received the full-expense scholarship under Royal Golden Jubilee (RGJ) Ph.D. program from Thailand Research Fund (TRF), and earned a Student Exchange Scholarship from Association Education Japan (AIEJ) to do research at Hiroshima University for one year (Oct. 2003-Sept. 2004). This work was also partially supported by Thailand-Japan Technology Transfer Project (TJTTP-JBIC) and TRF-RTA Project of Professor Wiwut Tanthapanichakoon. The excellent facilities support of the Graduate School, Chulalongkorn University and Hiroshima University, are greatly appreciated.

The author respectfully thanks Professor Piyasan Praserthdam, Associate Professor Tawatchai Charinpanitkul, Assistant Professor Muenduen Phisalaphong and Dr. Sukasem Kangwantrakool for their stimulating comments and participation as the thesis committee.

Further, the author is indeed grateful to Assistant Professor Seeroong Prichanont for languages correction, Mr. Kompanart Kaewplang and Mr. Wisarut Jintaworn for their useful suggestions and encouragement. As well, the author thanks the teachers, research assistants, friends, brothers and sisters in Particle Technology and Material Processing Laboratory, Chulalongkorn University. Next, the author appreciates Assist. Prof. Kunihiro Fukui at Hiroshima University for their research collaboration, hospitality, and wonderful experience during the author lived in Japan.

Finally, but far from lease, the love, patience and encouragement of my parents, brothers and wife were indispensable.

CONTENTS

Page

ABSTRACT IN THAI..... iv

ABSTRACT IN ENGLISH..... v

ACKNOWLEDGEMENTS..... vi

CONTENTS..... vii

LIST OF TABLES..... xii

LIST OF FIGURES..... xiii

NOMENCLATURE..... xxi

CHAPTER

I INTRODUCTION

1.1 Introduction..... 1

1.2 Objectives of research work..... 2

1.3 Scopes of research work.....2

1.4 Usefulness of research..... 3

II FUNDAMENTAL KNOWLEDGE

2.1 Basic definition and mass balance equations..... 4

2.1.1 Total efficiency..... 6

2.1.2 Grade efficiency..... 6

2.1.3 The 50% cut size..... 6

2.1.4 The underflow to throughput ratio..... 7

2.1.5 Reduce grade efficiency..... 7

2.1.6 The reduced 50% cut size..... 7

2.2 Liquid flow patterns in hydrocyclone..... 8

2.3 Velocity distributions in hydrocyclone..... 9

2.3.1 Tangential velocity..... 9

2.3.2 Axial velocity.....10

2.3.3 Radial velocity..... 11

2.4 Motion of suspended particles..... 11

2.5 Pressure distribution within the flow and static pressure drop..... 13

2.6 Function, design and merits..... 14

Page

2.6.1 The effect of hydrocyclone proportions…… 15
2.6.2 The effect of operating variables…….. 15
2.6.3 Typical sizes and performance ranges…….. 16
2.6.4 Merits and disadvantages…….. 16
2.6.5 Two basic design types. ……17
2.6.6 Categories of application……...18
2.7 Multiple hydrocyclone in series…….. 19
2.8 Fundamentals of electrostatics…… 21
2.9 Zeta potential…….. 23
III LITERATURE REVIEW
3.1 The equilibrium orbit theory……..... 27
3.2 The residence time theory……..... 29
3.3 The turbulent two phase flow theory……. 31
3.4 Crowding theory…… 34
3.5 The regression models……... 35
3.6 The dimensionless group model…… 39
3.7 Analytical flow model……41
3.8 Numerical simulations of flow…….. 41
3.9 Other researches……43
IV MATERIALS AND METHODS
4.1 Materials and Chemicals…… 47
4.2 Experimental Setup…… 49
4.3 Analytical Instrument……53
4.4 Experimental Procedures…..…….. 55
4.4.1 Presence of the underflow……55
4.4.2 Absence of the underflow……. 56
V RESULTS AND DISCUSSION
5.1 Effect of dust box length on classification efficiency…… 58
in the presence of underflow
5.1.1 Short dust box……58
5.1.1.1 Flow rate $0.0833*10^{-3}$ m^3/s (5 L/min)……58

Page

5.1.1.2 Flow rate 0.1167*10^{-3} m^3/s (7 L/min)……61
5.1.1.3 Flow rate 0.1667*10^{-3} m^3/s (10 L/min)……...62
5.1.2 Long dust box……63
5.1.2.1 Flow rate 0.0833*10^{-3} m^3/s (5 L/min)……63
5.1.2.2 Flow rate 0.1167*10^{-3} m^3/s (7 L/min)…… 65
5.1.2.3 Flow rate 0.1667*10^{-3} m^3/s (10 L/min)…….. 66
5.1.3 Comparison of effect of feed flow rate between short ……. 67
and long dust box in the presence of the underflow
5.1.4 Determination of appropriated feed flow rate for……. 69
subsequent experiments in the presence of the underflow
5.2 Effect of underflow to throughput ratio on classification…….. 70
efficiency in the presence of underflow for the long dust box
5.2.1 Underflow to throughput ratio 0.1……..……..……...70
5.2.2 Underflow to throughput ratio 0.2……..……70
5.2.3 Underflow to throughput ratio 0.3…..……72
5.2.4 Summary of effect of underflow to throughput ratio…… 74
5.3 Effect of dust box length on classification efficiency…… 76
in the absence of the underflow
5.3.1 Short dust box……76
5.3.1.1 Flow rate 0.0833*10^{-3} m^3/s (5 L/min)……76
5.3.1.2 Flow rate 0.1167*10^{-3} m^3/s (7 L/min)……..… 79
5.3.1.3 Flow rate 0.1667*10^{-3} m^3/s (10 L/min)……...80
5.3.2 Long dust box……81
5.3.2.1 Flow rate 0.0833*10^{-3} m^3/s (5 L/min)……81
5.3.2.2 Flow rate 0.1167*10^{-3} m^3/s (7 L/min)……83
5.3.2.3 Flow rate 0.1667*10^{-3} m^3/s (10 L/min)……...84
5.3.3 Comparison of effect of feed flow rate between short…….. 85
and long dust box in the absence of the underflow
5.3.4 Determination of appropriated feed flow rate for……87
subsequent experiments in the absence of the underflow
5.4 Comparison of effect of the underflow…….. 88

Page

5.5 Effect of pH in the absence of the underflow……89
5.5.1 Original pH of suspension 6.0…… 89
5.5.1.1 Flow rate 0.0833*10^{-3} m^3/s (5 L/min)……89
5.5.1.2 Flow rate 0.1167*10^{-3} m^3/s (7 L/min)……89
5.5.2 pH of suspension 8.0……...89
5.5.2.1 Flow rate 0.0833*10^{-3} m^3/s (5 L/min)……89
5.5.2.2 Flow rate 0.1167*10^{-3} m^3/s (7 L/min)……91
5.5.3 pH of suspension 9.0…….....92
5.5.3.1 Flow rate 0.0833*10^{-3} m^3/s (5 L/min)……92
5.5.3.2 Flow rate 0.1167*10^{-3} m^3/s (7 L/min)……94
5.5.4 pH of suspension 10.0……95
5.5.4.1 Flow rate 0.0833*10^{-3} m^3/s (5 L/min)……95
5.5.4.2 Flow rate 0.1167*10^{-3} m^3/s (7 L/min)……97
5.5.5 Summary of effect of pH in the absence of the underflow……98
5.6 Effect of central rod diameter in the absence of the underflow……101
5.6.1 Central rod diameter 8 mm……101
5.6.1.1 pH of suspension 6.0……101
5.6.1.2 pH of suspension 9.0……101
5.6.2 Central rod diameter 12 mm……101
5.6.2.1 pH of suspension 6.0……101
5.6.2.2 pH of suspension 9.0……103
5.6.3 Central rod diameter 16 mm……105
5.6.3.1 pH of suspension 6.0……105
5.6.3.2 pH of suspension 9.0……107
5.6.4 Central rod diameter 20 mm……109
5.6.4.1 pH of suspension 6.0……109
5.6.4.2 pH of suspension 8.0……111
5.6.4.3 pH of suspension 9.0……113
5.6.4.4 pH of suspension 10.0……115
5.6.5 Summary of effect of central rod diameter……117
in the absence of the underflow

Page

5.7 Comparison of effect of pH between central rod diameter……120
8 and 20 mm in the absence of the underflow
5.8 Summary of effects of all parameters on classification…….124
efficiency in the presence of the underflow
5.9 Summary of effects of all parameters on classification…….126
efficiency in the absence of the underflow
5.10 Pressure drop……...128
5.11 Models……131
VI CONCLUSIONS AND FUTURE SUGGESTIONS
6.1 Conclusions……137
6.2 Future Suggestions…….139

REFERENCES…….. 140
APPENDICES…….....146
APPENDIX A Publication of this work……..147
APPENDIX B Current, power, voltage and resistance……..148
APPENDIX C Zeta potential measurement……... 154
VITA……155

สถาบันวิทยบริการ
จุฬาลงกรณ์มหาวิทยาลัย

LIST OF TABLES

Page

Table 4.1 Silica specifications ……..……. 47

Table 4.2 Hydrocyclone proportions…….. 53

Table 5.1 Comparison of 50% particle cut size, % reduction with short……..125
dust box and % reduction with long dust box at feed flow rate
$0.1167*10^{-3}$ m^3/s (7 L/min), pH of suspension 6.0 and central
rod diameter 8 mm in the presence of the underflow

Table 5.2 Comparison of 50% particle cut size, % reduction with short…….....127
dust box and % reduction with long dust box at feed flow rate
$0.1167*10^{-3}$ m^3/s (7 L/min) in the absence of the underflow

สถาบันวิทยบริการ
จุฬาลงกรณ์มหาวิทยาลัย

LIST OF FIGURES

Page

Figure 2.1 Balance of a hydrocyclone……..……..4

Figure 2.2 Schematic diagram of a typical hydrocyclone……... 8

Figure 2.3 Tangential velocity……9

Figure 2.4 Axial velocity……. 10

Figure 2.5 Radial velocity……11

Figure 2.6 The results of the classification process in a hydrocyclone……14

Figure 2.7 The two conventional hydrocyclone designs……. 18

Figure 2.8 Two hydrocyclones in series for clarification…… 19

Figure 2.9 Two hydrocyclones in series for thickening…….. 20

Figure 2.10 Two hydrocyclone in series for clarification and thickening……. 20

Figure 2.11 Electrochemical double layers around particle surface…….. 24
in an applied electric field

Figure 4.1 Frequency size distribution of silica particles used in this work…....48

Figure 4.2 (a) Hydrocyclone and the dust box…..……..……..49

Figure 4.2 (b) Tank, control valve, impeller, flow meter and pressure gauge……..49

Figure 4.3 Schematic diagram of the experimental apparatus……50

Figure 4.4 Schematic diagram of the hydrocyclone…… 52

Figure 4.5 Laser Scattering Particle Size Distribution Analyzer…… 53

Figure 4.6 Zeta potential meter……..……..54

Figure 5.1 Effect of electrical potential on the short dust box of the……..….59
hydrocyclone in the presence of the underflow at underflow
to throughput ratio 0.1, feed flow rate $0.0833*10^{-3}$ m^3/s
(5 L/min), pH of suspension 6.0 and central rod diameter 8 mm.

Figure 5.2 Phenomenon in the presence of the underflow…….. 60

Figure 5.3 Effect of electrical potential on the short dust box of the……. 61
hydrocyclone in the presence of the underflow at underflow
to throughput ratio 0.1, feed flow rate $0.1167*10^{-3}$ m^3/s
(7 L/min), pH of suspension 6.0 and central rod diameter 8 mm.

Page

Figure 5.4 Effect of electrical potential on the short dust box of the……..…….62
hydrocyclone in the presence of the underflow at underflow
to throughput ratio 0.1, feed flow rate 0.1667*10^{-3} m^3/s
(10 L/min), pH of suspension 6.0 and central rod diameter 8 mm.

Figure 5.5 Effect of electrical potential on the long dust box of the……..…..64
hydrocyclone in the presence of the underflow at underflow
to throughput ratio 0.1, feed flow rate 0.0833*10^{-3} m^3/s
(5 L/min), pH of suspension 6.0 and central rod diameter 8 mm.

Figure 5.6 Effect of electrical potential on the long dust box of the……..…..65
hydrocyclone in the presence of the underflow at underflow
to throughput ratio 0.1, feed flow rate 0.1167*10^{-3} m^3/s
(7 L/min), pH of suspension 6.0 and central rod diameter 8 mm.

Figure 5.7 Effect of electrical potential on the long dust box of the……..……..66
hydrocyclone in the presence of the underflow at underflow
to throughput ratio 0.1, feed flow rate 0.1667*10^{-3} m^3/s
(10 L/min), pH of suspension 6.0 and central rod diameter 8 mm.

Figure 5.8 Relationship between 50% particle cut size, d_{50}, and…….68
suspension feed flow rate, Q, when electrical potential was applied
either the short or long dust box (53 or 106 mm) of the
hydrocyclone in the presence of the underflow at underflow to
throughput ratio 0.1, pH of suspension 6.0 and central rod
diameter 8 mm.

Figure 5.9 Effect of electrical potential on the long dust box of the……..……..71
hydrocyclone in the presence of the underflow at underflow
to throughput ratio 0.2, feed flow rate 0.1167*10^{-3} m^3/s
(7 L/min), pH of suspension 6.0 and central rod diameter 8 mm.

Figure 5.10 Effect of electrical potential on the long dust box of the……..……..73
hydrocyclone in the presence of the underflow at underflow
to throughput ratio 0.3, feed flow rate 0.1167*10^{-3} m^3/s
(7 L/min), pH of suspension 6.0 and central rod diameter 8 mm.

Page

Figure 5.11 Relationship between 50% particle cut size, d_{50}, and the…..…… 75
underflow to throughput ratio, R_f, by using the long dust box
(106 mm) of the hydrocyclone at feed flow rate $0.1167*10^{-3}$ m^3/s
(7 L/min), pH of suspension 6.0 and central rod diameter 8 mm
with and without electrical potential.

Figure 5.12 Effect of electrical potential on the short dust box of the……..…….77
hydrocyclone in the absence of the underflow at feed flow rate
$0.0833*10^{-3}$ m^3/s (5 L/min), pH of suspension 6.0 and central
rod diameter 8 mm.

Figure 5.13 Phenomenon in the absence of the underflow…… 78

Figure 5.14 Effect of electrical potential on the short dust box of the……..…….79
hydrocyclone in the presence of the underflow at feed flow rate
$0.1167*10^{-3}$ m^3/s (7 L/min), pH of suspension 6.0 and central
rod diameter 8 mm.

Figure 5.15 Effect of electrical potential on the short dust box of the……..…….80
hydrocyclone in the absence of the underflow at feed flow rate
$0.1667*10^{-3}$ m^3/s (10 L/min), pH of suspension 6.0 and central
rod diameter 8 mm.

Figure 5.16 Effect of electrical potential on the long dust box of the……..……..82
hydrocyclone in the absence of the underflow at feed flow rate
$0.0833*10^{-3}$ m^3/s (5 L/min), pH of suspension 6.0 and central
rod diameter 8 mm.

Figure 5.17 Effect of electrical potential on the long dust box of the……..……..83
hydrocyclone in the absence of the underflow at feed flow rate
$0.1167*10^{-3}$ m^3/s (7 L/min), pH of suspension 6.0 and central
rod diameter 8 mm.

Figure 5.18 Effect of electrical potential on the long dust box of the……..……..84
hydrocyclone in the absence of the underflow at feed flow rate
$0.1667*10^{-3}$ m^3/s (10 L/min), pH of suspension 6.0 and central
rod diameter 8 mm.

Page

Figure 5.19 Relationship between 50% particle cut size, d_{50}, and suspension..... 86
feed flow rate, Q, when electrical potential was applied either the short or long dust box (53 or 106 mm) of the hydrocyclone in the absence of the underflow at pH of suspension 6.0 and central rod diameter 8 mm.

Figure 5.20 Effect of electrical potential on the long dust box of the……..…..90
hydrocyclone in the absence of the underflow at feed flow rate $0.0833*10^{-3}$ m^3/s (5 L/min), pH of suspension 8.0 and central rod diameter 8 mm.

Figure 5.21 Effect of electrical potential on the long dust box of the……..…..91
hydrocyclone in the absence of the underflow at feed flow rate $0.1167*10^{-3}$ m^3/s (7 L/min), pH of suspension 8.0 and central rod diameter 8 mm.

Figure 5.22 Effect of electrical potential on the long dust box of the……..…..93
hydrocyclone in the absence of the underflow at feed flow rate $0.0833*10^{-3}$ m^3/s (5 L/min), pH of suspension 9.0 and central rod diameter 8 mm.

Figure 5.23 Effect of electrical potential on the long dust box of the…..……..94
hydrocyclone in the absence of the underflow at feed flow rate $0.1167*10^{-3}$ m^3/s (7 L/min), pH of suspension 9.0 and central rod diameter 8 mm.

Figure 5.24 Effect of electrical potential on the long dust box of the…..……..96
hydrocyclone in the absence of the underflow at feed flow rate $0.0833*10^{-3}$ m^3/s (5 L/min), pH of suspension 10.0 and central rod diameter 8 mm.

Figure 5.25 Effect of electrical potential on the long dust box of the……..……..97
hydrocyclone in the absence of the underflow at feed flow rate $0.1167*10^{-3}$ m^3/s (7 L/min), pH of suspension 10.0 and central rod diameter 8 mm.

Page

Figure 5.26 Relationship between 50% particle cut size, d_{50}, and pH of…..…… 98
suspension when electrical potential was applied to the long dust box (106 mm) of the hydrocyclone in the absence of the underflow at feed flow rate either $0.0833*10^{-3}$ or $0.1167*10^{-3}$ m^3/s (5 or 7 L/min) and central rod diameter 8 mm.

Figure 5.27 Relationship between weight of silica in the underflow…….. 100
and pH of suspension when electrical potential was applied to the long dust box (106 mm) of the hydrocyclone in the absence of the underflow at feed flow rate either $00833*10^{-3}$ or $0.1167*10^{-3}$ m^3/s (5 or 7 L/min) and central rod diameter 8 mm.

Figure 5.28 Effect of electrical potential on the long dust box of the…….102
hydrocyclone in the absence of the underflow at feed flow rate $0.1167*10^{-3}$ m^3/s (7 L/min), pH of suspension 6.0 and central rod diameter 12 mm.

Figure 5.29 Effect of electrical potential on the long dust box of the…….……104
hydrocyclone in the absence of the underflow at feed flow rate $0.1167*10^{-3}$ m^3/s (7 L/min), pH of suspension 9.0 and central rod diameter 12 mm.

Figure 5.30 Effect of electrical potential on the long dust box of the…….106
hydrocyclone in the absence of the underflow at feed flow rate $0.1167*10^{-3}$ m^3/s (7 L/min), pH of suspension 6.0 and central rod diameter 16 mm.

Figure 5.31 Effect of electrical potential on the long dust box of the……. 108
hydrocyclone in the absence of the underflow at feed flow rate $0.1167*10^{-3}$ m^3/s (7 L/min), pH of suspension 9.0 and central rod diameter 16 mm.

Figure 5.32 Effect of electrical potential on the long dust box of the…….… 110
hydrocyclone in the absence of the underflow at feed flow rate $0.1167*10^{-3}$ m^3/s (7 L/min), pH of suspension 6.0 and central rod diameter 20 mm.

Page

Figure 5.33 Effect of electrical potential on the long dust box of the…..…….. 112
hydrocyclone in the absence of the underflow at feed flow rate $0.1167*10^{-3}$ m^3/s (7 L/min), pH of suspension 8.0 and central rod diameter 20 mm.

Figure 5.34 Effect of electrical potential on the long dust box of the……..…… 114
hydrocyclone in the absence of the underflow at feed flow rate $0.1167*10^{-3}$ m^3/s (7 L/min), pH of suspension 9.0 and central rod diameter 20 mm.

Figure 5.35 Effect of electrical potential on the long dust box of the……..… 116
hydrocyclone in the absence of the underflow at feed flow rate $0.1167*10^{-3}$ m^3/s (7 L/min), pH of suspension 10.0 and central rod diameter 20 mm.

Figure 5.36 Relationship between 50% particle cut size, d_{50}, and central……. 117
rod diameter when electrical potential was applied to the long dust box (106 mm) of the hydrocyclone in the absence of the underflow at feed flow rate $0.1167*10^{-3}$ m^3/s (7 L/min) and either pH of suspension 6.0 or 9.0.

Figure 5.37 Relationship between weight of silica in the underflow and……119
central rod diameter when electrical potential was applied to the long dust box (106 mm) of the hydrocyclone in the absence of the underflow at feed flow rate $0.1167*10^{-3}$ m^3/s (7 L/min) and either pH of suspension 6.0 or 9.0.

Figure 5.38 Comparison of effect of pH between central rod diameter 8…….. 120
and 20 mm when applied positive electrical potential at the side wall and negative electrical potential at the central rod on the long dust box (106 mm) of the hydrocyclone in the absence of the underflow at feed flow rate $0.1167*10^{-3}$ m^3/s (7 L/min) and pH of suspension 6.0, 8.0, 9.0 and 10.0.

Page

Figure 5.39 Relationship between 50% particle cut size, d_{50}, and central…….. 121
rod diameter when electrical potential was applied to the long dust box (106 mm) of the hydrocyclone in the absence of the underflow at feed flow rate $0.1167*10^{-3}$ m^3/s (7 L/min), pH of suspension 6.0, 8.0, 9.0 and 10.0 and either central rod diameter 8 or 20 mm.

Figure 5.40 Relationship between weight of silica in the underflow and…….... 123
pH of suspension when electrical potential was applied to the long dust box (106 mm) of the hydrocyclone in the absence of the underflow at feed flow rate $0.1167*10^{-3}$ m^3/s (7 L/min) and either central rod diameter 8 or 20 mm.

Figure 5.41 Relationship between pressure drop, ΔP, and feed flow rate……..128
Q, when electrical potential was applied to either the short or the long dust box (53 or 106 mm) of the hydrocyclone in the presence and absence of the underflow at pH of suspension 6.0 and central rod diameter 8 mm.

Figure 5.42 Relationship between pressure drop, ΔP, and the underflow…..… 129
to throughput ratio, R_f, when electrical potential was applied to the long dust box (106 mm) of the hydrocyclone in the presence of the underflow at feed flow rate $0.1167*10^{-3}$ m^3/s (7 L/min), pH of suspension 6.0 and central rod diameter 8 mm.

Figure 5.43 Relationship between pressure drop, ΔP, and the central rod……. 130
diameter when electrical potential was applied to the long dust box (106 mm) of the hydrocyclone in the absence of the underflow at feed flow rate $0.1167*10^{-3}$ m^3/s (7 L/min) and pH of suspension 6.0.

Figure 5.44 Correlation results for the d_{50} in the presence of the underflow….. 134
using parameter *K* compared with experimental results

Figure 5.45 Correlation results for the d_{50} in the absence of the underflow……136
using parameter *K* compared with experimental results

Page

Figure B1 Relationship between current and time……..…148
Figure B2 Relationship between power and time……..….149
Figure B3 Relationship between voltage and time……151
Figure B4 Relationship between resistance of suspension and time…….153
Figure C1 Effect of pH on zeta potential…….. 154

สถาบันวิทยบริการ
จุฬาลงกรณ์มหาวิทยาลัย

NOMENCLATURE

C_8-C_{11}	=	Parameters	[-]
C_u	=	Underflow weight concentration	[%]
C_v	=	Feed volumetric concentration	[%]
C_w	=	Feed weight concentration	[%]
Cy_{50}	=	Characteristic cyclone number = 3.5	[-]
d_{50}	=	50% particle cut size	[μm]
d_{50c}	=	Reduced 50% particle cut size	[μm]
D_c	=	Hydrocyclone body diameter	[m]
D_i	=	Inlet diameter	[m]
D_o	=	Overflow diameter	[m]
d_p	=	Particle diameter	[m]
D_u	=	Underflow diameter	[m]
E	=	Electric field strength	[V/m]
F	=	Electrostatic force	[N]
F50	=	Feed size effect	[μm]
G	=	Grade efficiency	[-]
k	=	Hydrodynamic exponent	[-]
K	=	Semi-empirical constant	
k_d	=	Parameter	
L	=	Total length of hydrocyclone	[m]
l	=	Vortex finder length	[m]
L_c	=	Length of the cylindrical section of cyclone	[m]
n	=	Power of r in the equation, $v_t r^n$ = const.	[-]
q	=	Particle charge	[Coulomb]
Q	=	Suspension feed flow rate	[m^3/s]
R_f	=	Underflow to throughput ratio (flow ratio)	[-]
R_i	=	Radius of the inner electrode	[m]
R_o	=	Radius of the outer electrode	[m]
u	=	Particle velocity	[m/s]
V	=	Electric potential	[V]

V	=	Fluid velocity	[m/s]
Ω	=	mobility	[m^2 / V s]
ε	=	Permittivity of water	[F/m]
λ	=	Hindered settling factor, $C_v/(1-C_v)^3$	[-]
μ	=	Viscosity of suspension	[kg/m.s]
θ	=	Full cone angle	[degree]
ρ	=	Density of water	[kg/m^3]
ρ_s	=	Density of silica particle	[kg/m^3]
ζ	=	Zeta potential	[V]

สถาบันวิทยบริการ
จุฬาลงกรณ์มหาวิทยาลัย

CHAPTER I

INTRODUCTION

1.1 Introduction

Cyclones have found wide application in various fields of technology, such as gas cleaning, burning, spraying, atomizing, powder classification etc. They are also used for solid-liquid separation; the cyclones specially designed for liquids are referred to as hydrocyclones, hydraulic cyclones or hydroclones. The basic separation principle employed in hydrocyclones is centrifugal sedimentation, i.e. the suspended particles are subjected to centrifugal acceleration, which makes them separate from the fluid. Unlike centrifuges, hydrocyclones have no moving parts and the necessary vortex motion is performed by the fluid itself.

Hydrocyclone consists of a cylindrical section joined to a conical portion. The suspension of particles in a liquid is injected tangentially through the inlet opening in the upper part of the cylindrical section and, as a result of the tangential entry; a strong swirling motion is developed within the hydrocyclone. A portion of the liquid containing the fine fraction of particles is discharged through a cylindrical tube fixed in the center of the top and projecting some distance into the hydrocyclone, the outlet tube is called the overflow pipe or vortex finder. The remaining liquid and the coarse fraction of the material leave through a circular opening at the apex of the cone, called the underflow orifice.

Recently particle size control is an important problem in many industrial processes, especially production of particles with its size about 1 μm. However, recent separation method in this size region by use of a liquid sedimentation process in most cases requires a large scale and excessively long time for particle separation. Therefore, it is important to study and come up with a reliable hydrocyclone system that can control the cut size of particles about 1 μm.

1.2 Objectives of research work

The main objective of the present work is to carry out a series of experiments on silica fine particles using a novel electric hydrocyclone under various experimental conditions to provide some insight into the particle classification efficiency of hydrocyclone, and the effect of hydrocyclone proportions and operating variables.

The main objective can be broken down into the following.

1. To increase the particle classification efficiency using a novel electric hydrocyclone.
2. To carry out the effect of hydrocyclone proportions, i.e. length of dust box and central rod diameter.
3. To test the effect of operating variables, i.e. feed flow rate, underflow to throughput ratio and finally, the presence and absence of underflow conditions.
4. To investigate the effect of applied electric potential on the hydrocyclone using different conditions.
5. To examine the effect of zeta potential on electric hydrocyclone using various pH of suspension.
6. To determine the best condition in order to obtain the smallest 50% particle cut size.

1.3 Scopes of research work

The scope of the present research encompasses the following tasks.

1. The tested powder in this research is silica with a median diameter of 0.754 μm and density is 2,210 kg/m^3.
2. Deionized water is used in all experiments, which has conductivity 0.7-2.0 $*10^{-4}$ S/m.
3. Suspension of 0.2% solid content by weight is tested in all experiments and constantly controlled at 30 ^oC.
4. The tested hydrocyclone is 20 mm body diameter.

5. The ranges of experimental conditions investigated are following:
   - The ratios of underflow to throughput are 0, 0.1, 0.2 and 0.3.
   - The volumetric flow rates are $0.0833*10^{-3}$, $0.1167*10^{-3}$ and $0.1667*10^{-3}$ m^3/s (5, 7 and 10 L/min).
   - The lengths of the dust box are 53 and 106 mm.
   - The desired 50-volt DC electric potential or no potential is applied.
   - The tested pH of suspension are 6, 8, 9 and 10.
   - The central rod diameters are 8, 12, 16 and 20 mm.
6. The three different conditions investigated are
   - No applied electric potential.
   - Positive potential is applied at the central rod side and negative potential at the side wall.
   - Positive potential is applied at the side wall and negative potential at the central rod side.

1.4 Usefulness of research

A hydrocyclone system which can be used to control the cut size of particles at about 1 μm will be developed and investigated. In addition, an appropriated semi empirical correlation will be used to predict the 50% particle cut size.

สถาบันวิทยบริการ
จุฬาลงกรณ์มหาวิทยาลัย

CHAPTER II

FUNDAMENTAL KNOWLEDGE

It is already understood that the hydrocyclone is a device that causes the centrifugal separation of materials contained in the liquid fed to it. These materials may be particles of solid, bubbles of gas or a second immiscible liquid. In the case of two solids suspended in the feed liquid they may separate because of a difference in size, shape or specific gravity. The terms “hydraulic” or “hydro” have become generally used through the prevalence of applications in which the liquid concerned is water since water is the medium on which by far the largest amount of information is available and on which all of the important research contributions have been based. For a full understanding of the hydrocyclone it is essential that the liquid flow pattern and distribution of velocities within the cyclone body be understood.

2.1 Basic definition and mass balance equations

A single-stage hydrocyclone can be schematically drawn as in **Figure 2.1.**

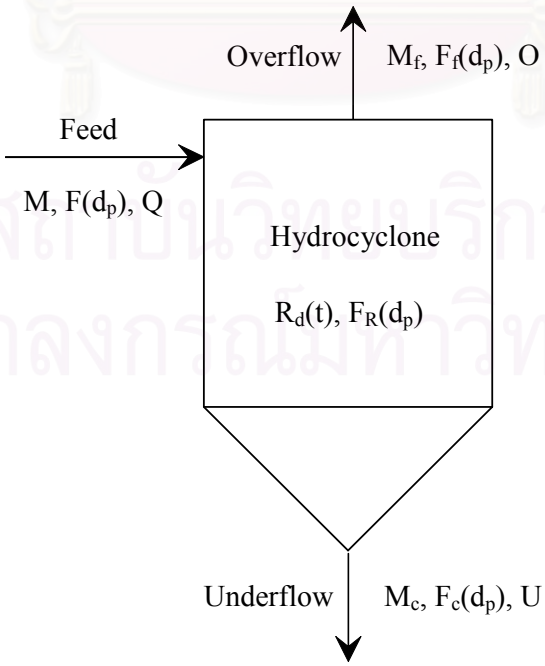

Figure 2.1 Balance of a hydrocyclone

where:

M is the mass flow rate of the feed [kg/s]

M_c is the mass flow rate of the coarse material in the underflow [kg/s]

M_f is the mass flow rate of the fine material in the overflow [kg/s]

$F(d_p)$ is the size distribution frequency of the feed

$F_c(d_p)$ is the size distribution frequency of the coarse material

$F_f(d_p)$ is the size distribution frequency of the fine material

d_p is the particle size

Q is the volumetric flow rate of the feed suspension [m^3/s]

O is the volumetric flow rate of the overflow suspension [m^3/s]

U is the volumetric flow rate of the underflow suspension [m^3/s]

The total mass of the feed must be equal to the sum of the total masses of the products if there is accumulation of material in the equipment, $R_d(t)$:

$$M = M_c + M_f + R_d(t) \tag{2.1}$$

Mass balance must also apply to any size fractions present in the feed if there is no change in particle size of the solids inside the hydrocyclone (no agglomeration or comminution). Hence for each particle size d_p present in the feed:

$$(M)_{d_p} = (M_c)_{d_p} + (M_f)_{d_p} + (R_d(t))_{d_p} \tag{2.2}$$

By definition, the particle size distribution frequency gives the fraction of particles of size d_p in the sample. The total mass of particles of size d_p in the feed is the total mass of the feed M multiplied by the appropriate fraction $F(d_p)$ so that equation 2.2 becomes:

$$MF(d_p) = M_c F_c(d_p) + M_f F_f(d_p) + R_d(t) F_R(d_p) \tag{2.3}$$

2.1.1 Total efficiency

The total efficiency, E_T is defined as the ratio of the mass flow rate of the coarse solid material in the underflow, M_c to the solid mass flow rate of the feed, M.

$$E_T = \frac{M_c + R_d(t)}{M} \tag{2.4}$$

2.1.2 Grade efficiency

For any separator with a size dependent performance, such as a hydrocyclone, the grade efficiency varies with particle size, and a graphical representation of this is called the grade efficiency curve. As the value of the grade efficiency has the character of probability, it is sometimes referred to as the partition probability; the curve then becomes the partition probability curve of Tromp curve. In practice, the grade efficiency curve is a continuous function of particle size d_p. The grade efficiency, $G(d_p)$ can be determined from the particle size distribution data of the feed and underflow streams:

$$G(d_p) = \frac{M_c F_c(d_p) + R_d(t) F_R(d_p)}{M F(d_p)} = \frac{M_c F_c(d_p) + R_d(t) F_R(d_p)}{M_c F_c(d_p) + M_f F_f(d_p) + R_d(t) F_R(d_p)} \tag{2.5}$$

where $F(d_p)$, $F_c(d_p)$ and $F_f(d_p)$ are size distribution frequency corresponding to any size d_p in the feed, coarse and fine streams. $G(d_p)$ is plotted as a function of d_p.

2.1.3 The 50% cut size

The cut size, d_{50} is defined as the particle size corresponding to 50% on the grade efficiency curve.

2.1.4 The underflow to throughput ratio

The underflow to throughput ratio is defined as the fraction of the volumetric feed rate which turns up in the underflow, i.e. the underflow rate divided by the feed rate.

$$R_f = \frac{U}{Q} \tag{2.6}$$

2.1.5 Reduce grade efficiency

The effect of flow splitting (or dead flux) in applications with appreciable and dilute underflow, as is common with hydrocyclones, is to modify the shape of the grade efficiency curve making it appear as if the performance of the hydrocyclone are better than it actually is. The typical grade efficiency curve does not start from the origin but has an intercept, the value of which is usually equal to the underflow to throughput ration, R_f. This is because the very fine particles simply follow the flow and are split between the underflow and the overflow in the same ratio as the fluid. In order to remove the effect of flow splitting from the efficiency definition so that it describes only the true "centrifugal efficiency", the reduced grade efficiency is the following equation:

$$G'(d_p) = \frac{G(d_p) - R_f}{1 - R_f} \tag{2.7}$$

2.1.6 The reduced 50% cut size

The reduced 50% cut size is defined as the size corresponding to 50% on the reduced grade efficiency curve $G'(d_p)$.

2.2 Liquid flow patterns in hydrocyclone

The flow pattern in the hydrocyclone is a spiral within a spiral. Fluid on entry commences downward flow in the outer regions of the cyclone body. This combined with the rotational motion to which it is constrained creates the outer spiral. The existence of a top central outlet and inability under normal feed pressure and flow rate conditions for all of the fluid to leave at the cone apex outlet assists the inward migration of some of the fluid from the external downward moving mass. The amount of inward migration increases as the apex cone is neared and the fluid which flows in this migration stream ultimately reverses its vertical velocity direction and flows upwards to the cyclone overflow outlet via the vortex finder. Since once again it is at the same time rotating the result is an inner spiral.

Mention of the reversal of flow and the existence of an inner and outer spiral can lead to misunderstanding and the mistaken belief that the spirals rotate in opposite directions. This obviously cannot be true. The reversal applies only to the vertical component of velocity and the spirals rotate in the same circular direction. **Figure 2.2** shows a cross-section of a hydrocyclone of conventional design (Svarovsky, 1990).

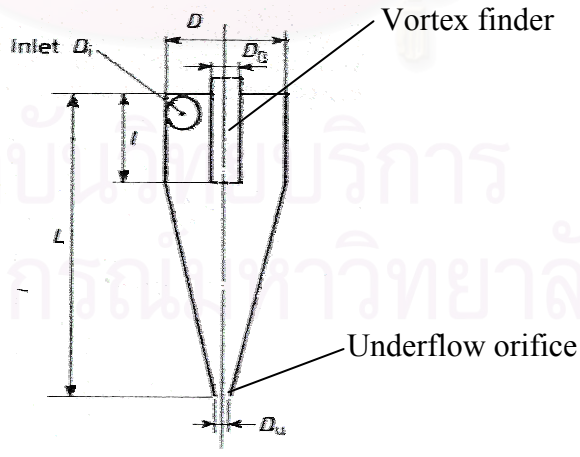

Figure 2.2 Schematic diagram of a typical hydrocyclone

2.3 Velocity distributions in hydrocyclone

The velocity of flow at any point within the hydrocyclone can be resolved into the following three components (Kelsall, 1952).

2.3.1 Tangential velocity

At levels below the rim of the vortex finder, the tangential velocity v_t increases considerably as the radial distance decreases. The radial position of maximum tangential velocity is smaller than the exit radius of the vortex finder (see **Figure 2.3**). The tangential velocity profile can be described by the relationship

$$v_t r^n = \text{const.} \qquad (\text{where } n \text{ is normally } 0.6 \leq n \leq 0.9) \qquad (2.8)$$

As the radius is further increased, the tangential velocity decreases and is proportional to r, this relationship holds until the cylindrical air column (which normally forms in a hydrocyclone discharging at atmospheric pressure) is reached. At levels above the rim of the vortex finder, the break in the rise of v_t occurs at a larger radius. Apart from this phenomenon and the wall effects, v_t is independent of the vertical position so that envelopes of constant tangential velocity are cylinders coaxial with the cyclone (Svarovsky, 1990).

สถาบันวิทยบริการ
จุฬาลงกรณ์มหาวิทยาลัย

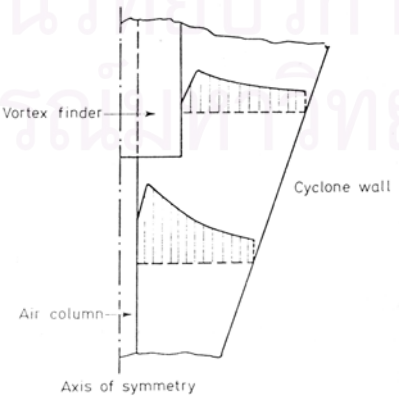

Figure 2.3 Tangential velocity

2.3.2 Axial velocity

As can be seen from **Figure 2.4**, there is a strong downward flow along the outer walls of both the cylindrical and conical portions. This flow is essential for cyclone operation since it moves the particles that have been separated into the underflow orifice. It is not essential to build cyclones with the apex pointing downwards and the cyclone efficiency is only very little influenced by its position relative to the gravity field. The downward current is partially counterbalanced by an upward flow in the core region, depending on the underflow to throughput ratio. There is a well defined locus of zero vertical velocities (LZVV) which follows the profile of the cyclone. Above the rim of the vortex finder, the largest downward velocities again occur near the cyclone wall. At radii between the cyclone wall and the vortex finder, the axial velocity becomes upward. Around the vortex finder strong downward flow may be observed. This is due to wall induced flow which runs inward along the top of the cyclone (Svarovsky, 1990).

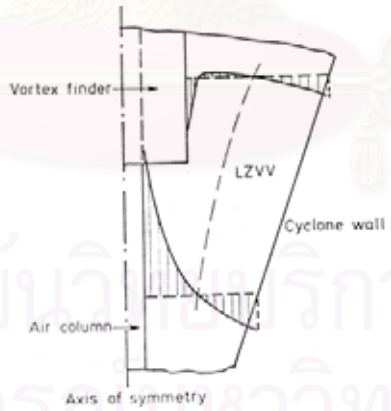

Figure 2.4 Axial velocity

สถาบันวิทยบริการ
จุฬาลงกรณ์มหาวิทยาลัย

2.3.3 Radial velocity

The radial velocity component is normally much smaller than the other two components and they are difficult to measure accurately. As can be seen from **Figure 2.5**, the radial velocity is inward and its magnitude decreases as the radial distance decreases. At levels above the rim of vortex finder, there may be outward recirculatory flows, and near the flat top of the cyclone there are strong inward radial velocities directed towards the root of the vortex finder, thus causing the above mentioned short circuit flow down the outside wall of the vortex finder (Svarovsky, 1990).

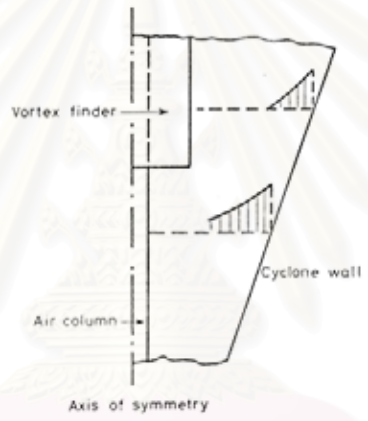

Figure 2.5 Radial velocity

2.4 Motion of suspended particles

When the solid particles enter near the cylindrical wall they can be dispersed radially inwards because of the intensive turbulent mixing in the feed sections. The cylindrical section of the hydrocyclone is usually treated as a preliminary separating zone and the precise separations are thought to be performed in the conical section. As was suggested by Kelsall (1952), any particles present in the downward flows near the conical wall (see **Figure 2.4**) can move radially inwards only if the liquid moves inwards. It is obvious that if a fraction R_f of the feed liquid goes into the underflow, then the same fraction R_f of all particles, independent of their settling rate, must also go with the liquid, together with the particles separated from the remaining fraction of

the liquid 1-R_f leaving in the overflow. This is an important phenomenon peculiar to hydrocyclones and consequently a correction has to be made in evaluation of the true grade efficiency curve.

A particle at any point within the flow in a hydrocyclone is basically subjected to the two kinds of force: one from both the external and internal fields of acceleration (gravity and centrifugal forces) and the other from the drag exerted on the particle by the flow. The gravity effect is normally neglected in hydrocyclones so that only centrifugal and drag forces are taken into account. The movement of a particle in both the tangential and vertical directions is unopposed by any forces so that its velocity components in those directions can be taken to be equal to the corresponding flow velocity components v_t and v_a. Since the centrifugal force acts in the radial direction, it prevents the particle following the inward radial flow (see **Figure 2.5**) and the particle is subjected to "centrifugal elutriation". If the centrifugal force acting on a particle exceeds the drag, the particle moves radially outwards and if the drag is greater, the particle is carried inwards. Since the drag force and the centrifugal force are determined by the values of v_r and v_t respectively, the relative values of v_r and v_t at all positions within the separation zone are decisive for the overall performance of the hydrocyclone.

The problem is that a hydrocyclone may be presented with a whole range of feed slurries: from nearly clean liquids to concentrations of solids of up to 30 or 40% by volume, and from very coarse, fast settling slurries to colloidal, slow settling ones. Let us consider the following two extreme cases:

1. If the feed is very coarse, the particles will settle readily on entry into a ribbon of solids on the wall, swirling into the underflow and the main bulk of the flow inside will be essentially clean liquid.

2. If the feed is very fine, say sub-micron in size, the centrifugal field inside will be insufficient to cause any separation and the concentration anywhere in the hydrocyclone will be essentially the same as in the feed.

Clearly, most real cases will be somewhere in between, when the particle concentration varies with position throughout the hydrocyclone body anywhere between that of the clean liquid and the underflow concentration. Accordingly, the suspension density and apparent viscosity will vary, and different feed solids particle size distributions will result in different spatial distributions of these two variables.

2.5 Pressure distribution within the flow and static pressure drop

Due to the vortex flow in the hydrocyclone, the static pressure in the flow increases radially outward. This centrifugal static head is primarily determined by the distribution of both the tangential fluid velocities and the suspension densities within the flow and it constitutes the major contribution to the total pressure loss across an operating hydrocyclone. The tangential velocity distributions at low solids concentrations can be estimated from simple measurements of radial static pressure. This was the idea behind the early studies of tangential velocity distributions in clean liquid flow. Driessen (1948) was the first to derive an expression relating the tangential velocity v_t, to the radial pressure distribution by assuming the radial velocity component negligible in relation to the tangential component, so that

$$v_t^2 / r = dp / (\rho . dr) \tag{2.9}$$

This relationship was then used to calculate the tangential velocities from static pressure measurements in different places within hydrocyclones run with clean liquids. Driessen and many others following him thus deduced the general expression for tangential velocity profiles in the outer vortex given previously in equation 2.1, where n is an empirical exponent, usually from 0.6 to 0.9. Note that for a free vortex in inviscid flow n=1, while in a forced vortex (solid body rotation) n= -1.

2.6 Function, design and merits

The separation efficiency of a hydrocyclone has a character of probability. This is to do with the probability of the position of the different particles in the entrance to the hydrocyclone, their chances of separation into the boundary layer flow and the general probability character of turbulent flow. Coarse particles are always more likely to be separated than fine particles. Effectively, in the hydrocyclone processes the feed solids by an efficiency curve is called “grade efficiency” which is a percentage increasing with particle size. **Figure 2.6** shows the schematic diagrams of the process; the solids in the feed enter the hydrocyclone and are processed by the grade efficiency curve. There are two products of the hydrocyclone separation: the coarse product (i.e. the solids in the underflow) and the fine product (i.e. the solids in the overflow). Every hydrocyclone is therefore primarily a classifier, although we may use it as a separator by setting the cut size as low as possible to recover as much of the solids as possible into the coarse product.

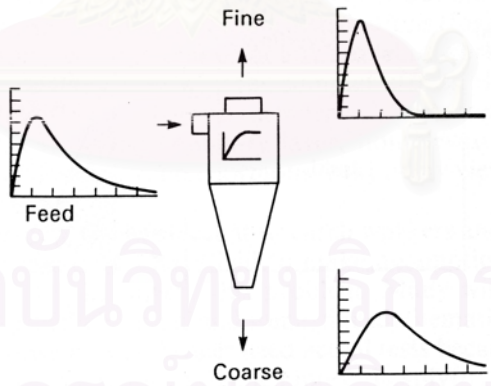

Figure 2.6 The results of the classification process in a hydrocyclone

2.6.1 The effect of hydrocyclone proportions

We need to be concerned with two observations. Firstly, there is a general rule by which every measure which increases resistance to flow improves solids recovery, and vice versa. This applies to all proportions of the hydrocyclone body, within certain reasonable limits, except for the length of the hydrocyclone. A hydrocyclone with relatively small inlet and outlet openings is expected to give higher mass recovery but will offer higher resistance to flow and therefore have lower capacity.

Secondly, one dimension of the hydrocyclone should be made variable or adjustable and that is the underflow orifice diameter. Correct adjustment of this dimension is vital for the best operation of the hydrocyclone because the optimum size of the opening can not be reliably predicted. It is for this reason that the underflow orifice diameter is often regarded as an operating (rather than design) variable. The orifice diameter is best adjusted after start-up of the plant and also during operation whenever some operating conditions change or when the orifice itself gradually wears out.

2.6.2 The effect of operating variables

There is a whole host of operating conditions that affect the performance of hydrocyclones. The most important are the operating pressure drop and the feed concentration. With increasing pressure drop the efficiency of separation increases but the law of diminishing return applies. There is little point in increasing the pressure beyond 5 or 6 bar, the typical operating pressures for larger hydrocyclones is between 1 and 2 bar. With increasing feed concentration the efficiency of separation rapidly falls off and hydrocyclones are therefore operated with dilute feeds whenever high total mass recoveries are sought.

2.6.3 Typical sizes and performance ranges

The diameters of individual hydrocyclones range from 10 mm to 2.5 m, cut sizes for most solids range from 2 to 250 μm, flow rates (capacities) of single units range from 0.1 to 7200 m^3/hr. The operating pressure drops vary from 0.34 to 6 bar, with smaller units usually operated at higher pressures than the large ones. The underflow solids concentrations that can be achieved with hydrocyclones rarely exceed 45 or 50% by volume, depending on the size and design of the unit, operating conditions and the nature of the solids being separated.

In order to make full use of the advantages of the hydrocyclone it is often best to use multiple units, connected either in series or in parallel. In clarification duties for example, the parallel connections allow the more efficient, smaller diameter units to be used to treat high flow rates. On the other hand, the series connections are used to improve overall recoveries in clarification, to produce thicker underflows and clearer overflow simultaneously, to wash solids or to sharpen the classification or sorting.

2.6.4 Merits and disadvantages

The relative merits of hydrocyclones can be summarized as follows:

1. They are extremely versatile in application in that they can be used to clarify liquids, concentrate slurries, classify solids, wash solids, separate two immiscible liquids, degas liquids or sort solids according to density or shape.
2. There are simple, cheap to purchase, install, run and require little in the way of maintenance and support structures.
3. They are small relative to other separators, thus saving space and also giving low residence times, which give them an advantage in terms of the speed of control over the sedimentation classifiers.

4. The existence of high shear forces in the flow is an advantage in classification of solids because it breaks any agglomerates, and also in the treatment of thixotropic and Bingham plastic slurries.

The disadvantages of hydrocyclones may be listed as follows:

1. They are somewhat inflexible once installed and operated, giving low turn down ratios due to the strong dependence of their separation performance on flow rate and feed concentration. They are also inflexible due to their general sensitivity to instabilities in feed flow rate and solids concentration.
2. They are limitations on their separation performance in terms of the sharpness of cut, the range of operating cut size, dewatering performance or the clarification power, some of these characteristics may be improved in multistage arrangements, but at additional costs of power and investment.
3. They are susceptible to abrasion but steps can be taken to reduce abrasive effects.
4. The existence of shear may sometimes turn into a disadvantage because flocculation can not be used to enhance the separation as in the case of gravity thickeners as most flocs do not survive the shear.

2.6.5 Two basic design types

The conventional hydrocyclone is divided to two basic shapes, depending on the inclined angle of the cone (**Figure 2.7**). The narrow-angle design is used more widely than the wide-angle design. The cone angle has a fundamental effect on the existence of circulating flows in the cone, at narrow angles such flows are suppressed and this makes the hydrocyclone efficient for separation of fine particles. At the same time, the wide- angle is used for separation of coarse particles.

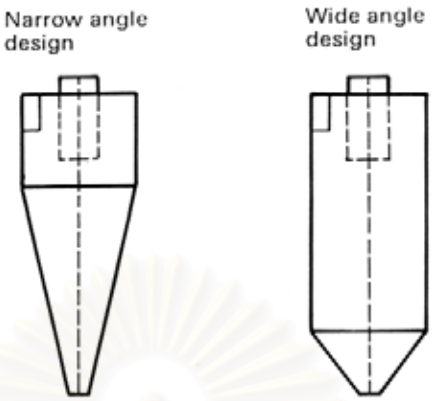

Figure 2.7 The two conventional hydrocyclone designs

2.6.6 Categories of application

Applications of hydrocyclones in industry fall into eight broad categories of two-phase separation with the liquid being the suspending medium:

1. liquid clarification
2. slurry thickening
3. solids washing
4. solids classification by particle size
5. solids sorting according to density or particle shape
6. particle size measurement
7. degassing of liquids
8. separation of two immiscible liquids

Each application listed above has its particular requirements and goals, and it calls for changes in the design and operation of the hydrocyclone to make the hydrocyclone most suitable for each case. In principle, any hydrocyclone separates particles (solids, droplets or gas bubbles) of the dispersed phase from the liquid (continuous phase) on the basis of the density difference between the phases, and the separation depends heavily on particle size or on particle density if the system is not homogeneous.

Particle size which separates at 50% efficiency is referred to as the “cut size” and is commonly used to characterize the performance of a hydrocyclone. This may be understood to be the aperture size of an ideal screen that would give similar recovery as the hydrocyclone: smaller cut size leads to higher recovery. In the first three categories of use listed above, the aim is to set the cut size sufficiently low to obtain high solids recovery. In classification and sorting applications, sharpness of cut is another important factor in assessing the hydrocyclone performance as it controls the amount of misplaced material in the two products.

2.7 Multiple hydrocyclone in series

Serial connections of separators are a common way of improving the performance of single units. In the case of hydrocyclones, due to their low capital and running costs, multiple serial arrangements are quite frequently used. As to which particular layout and arrangement should be used depends on the actual application in question.

If clarification of the liquid is the ultimate purpose and it can not be achieved in a single-pass arrangement, several stages in series in the direction of the overflow may be considered as shown in **Figure 2.8**.

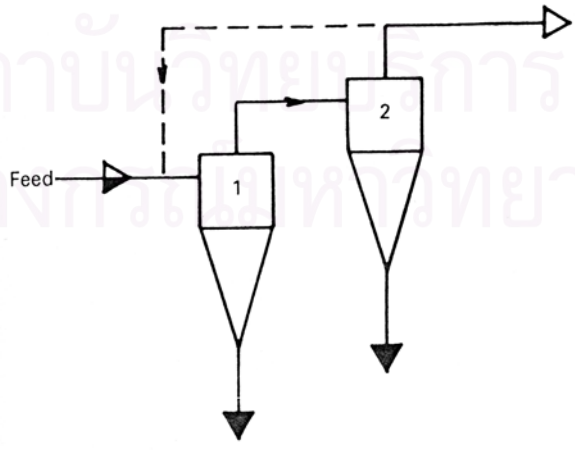

Figure 2.8 Two hydrocyclones in series for clarification

In thickening duties, if the required degree of thickening can not be achieved with one hydrocyclone, two or more in series may be used, this time in the direction of the underflow as shown in **Figure 2.9**.

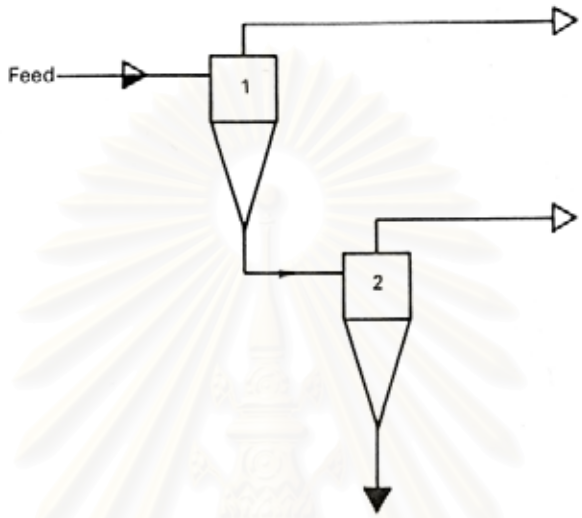

Figure 2.9 Two hydrocyclones in series for thickening

If both clarification and thickening are required simultaneously, a two or three stage arrangement is required where some hydrocyclones are used as clarifiers and others as thickeners as shown in **Figure 2.10**.

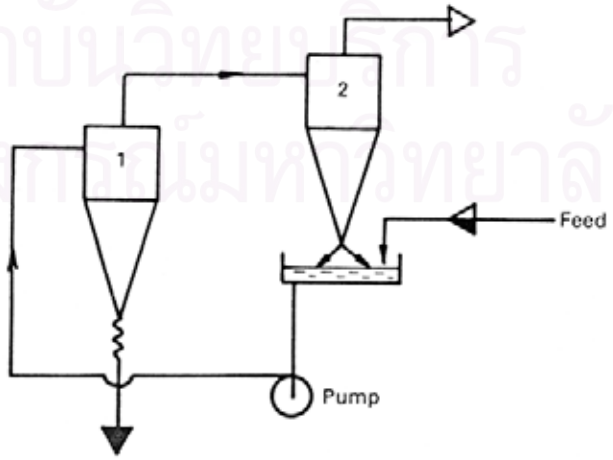

Figure 2.10 Two hydrocyclone in series for clarification and thickening

2.8 Fundamentals of electrostatics

The force reflects the fact that voltage is related to the force applied to a charge and is derived from the electrostatic force law (Coulomb's law):

$$F = qE_r \tag{2.10}$$

where F is force, q is charge on the particle and E is electric field strength.

This force drives the charged particles through the fluid, resulting in an electric current flow. The motion of the charged particles is governed primarily by the combined effects of the electric field as the driving force, with inertia and viscous force as the retarding forces. When the particles attain a constant or terminal velocity, the inertia force is reduced to zero, and the two remaining forces result in an average velocity for the particles which is related to the magnitude of the electric field and the fluid viscosity. The migration velocity attained will be that at which the viscous drag force balances the applied electric force. The constant of proportionally is termed the particle mobility, Ω.

$$u_r = \Omega E_r \tag{2.11}$$

This mobility parameter contains such factors as the charge to cross sectional area ratio of the particle and the viscosity or density of the fluid.

$$\Omega = \frac{q}{3\pi\mu d_p} \tag{2.12}$$

where q is particle charge that can be calculated from

$$q = 2\pi\varepsilon d_p \zeta \tag{2.13}$$

where ε is permittivity of fluid and ζ is the zeta potential of particle.

When the charge on the central rod is relatively low, the ionic space charge density is assumed to be negligible, and Laplace's equation is application. In cylindrical coordinates assuming cylindrical symmetry, with the axis along the axis of the two cylinders, Laplace's equation can be written as (Crowley, 1986):

$$\frac{dE_r}{dr} + \frac{E_r}{r} = 0 \tag{2.14}$$

Integration gives

$$E_r = \left(\frac{1}{r}\right)\frac{V}{\ln(R_o / R_i)} \tag{2.15}$$

where E is the electric field strength, R_i the radius of the inner electrode, R_o the radius of the outer electrode and V the potential across the electrodes.

The migration velocity of the particle obtained as:

$$u_r = \frac{2\varepsilon\zeta}{3\mu}\frac{1}{r}\frac{V}{\ln(R_o / R_i)} \tag{2.16}$$

สถาบันวิทยบริการ
จุฬาลงกรณ์มหาวิทยาลัย

2.9 Zeta potential

Zeta potential is the charge that develops at the interface between a colloidal particle and the liquid medium in which it is suspended may arise by any of several mechanisms. Among these are the dissociation of ionogenic groups in the particle surface and the differential adsorption from solution of ions of different charges into the surface region.

The development of a net charge at the particle surface affects the distribution of ions in the neighboring interfacial region, resulting in an increased concentration of counter ions - ions of charge opposite to that of the particle - close to the surface. The charge on colloidal particles can arise from a number of different mechanisms, including dissociation of acidic or basic groups on the particle surface, or adsorption of a charged species from solution. The particle charge is balanced by an equal and opposite charge carried by ions in the surrounding liquid. These counter ions tend to cluster around the particles in diffuse clouds. This arrangement of particle surface charge surrounded by a diffuse cloud of countercharge is called the electrical double layer that formed in the region of the particle-liquid interface.

.

The double layer may be considered to consist of two parts: an inner region which includes ions bound relatively strongly to the surface (including specifically adsorbed ions) and an outer, or diffuse, region in which the ion distribution is determined by a balance of electrostatic forces and random thermal motion. The potential in this region, therefore, decays as the distance from the surface increases until, at sufficient distance, it reaches the bulk solution value, conventionally taken to be zero. The extent of the diffuse double layer is dependent on the ionic strength of the electrolytes and the valency of each of the ions. Multivalent ions are particularly important. Their effect on the screening of the surface charge is related to the counter-ion valency. The flocculation concentration for divalent counter-ions is on average about 100 times lower than for monovalent ions, and for trivalent ions about 1000 less.

When an external electric field is applied to the suspension, charged particles will migrate toward the electrode of the opposite sign, as illustrated in **Figure 2.11**. This phenomenon is called electrophoresis. Measurements of the electrophoretic velocity of particles give information about their surface potential (Gotoh, 1997).

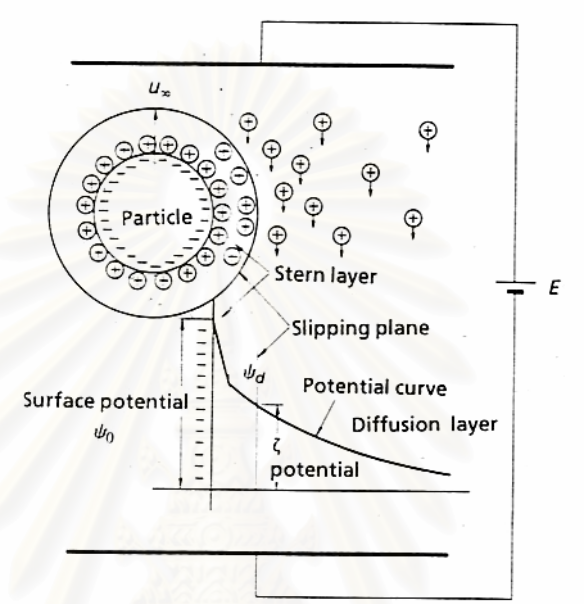

Figure 2.11 Electrochemical double layers around particle surface in an applied electric field

When a particle undergoes electrophoresis, a thin layer of liquid around the Stern layer moves with the particles as if it is fixed on the particle surface. The outer surface of this layer is called the slipping plane, and the potential there is called the zeta potential. Hence, the zeta potential can be correlated with the electrophoretic velocity of particles.

The sign and magnitude of zeta potential, as a function of pH, surfactant, and salt or dispersing agent concentration are indicators of the surface properties of materials. The zeta potential depends on the surface charge density and the double layer thickness. The surface charge density, in turn, depends on the concentration of "potential-determining ions" in the solvent—ions that have a particular affinity for the surface. In many systems, the H^+ ion is potential-determining, and so the zeta

potential depends on pH. The zeta potential is therefore a function of the surface charge of the particle, any adsorbed layer at the interface and the nature and composition of the surrounding medium in which the particle is suspended. It is usually, but not necessarily, of the same sign as the potential actually at the particle surface but, unlike the surface potential, the zeta potential is readily accessible by experiment. Moreover, because it reflects the effective charge on the particles and is therefore related to the electrostatic repulsion between them, zeta potential has proven to be extremely relevant to the practical study and control of colloidal stability and flocculation processes.

Particle size is often considered one of the most important parameters, however, as particle size reduces, the surface area increases significantly in comparison with the volume, so surface properties increasingly determine the dispersions characteristics. The surface charge cannot be measured directly. Instead the charge at a distance from the particle, called the zeta potential is measured. This potential is usually more of interest because particles interact according to the magnitude of this value, rather than the potential at the surface of the particle.

The principal of determining zeta potential by micro electrophoresis is very simple. A controlled electric field is applied via electrodes immersed in the sample suspension and this causes the charged particles to move towards the electrode of opposite polarity. Viscous forces acting upon the moving particle tend to oppose this motion and equilibrium is rapidly established between the effects of the electrostatic attraction and the viscous drag. The particles therefore reach a constant "terminal" velocity.

This velocity is dependent upon the electric field strength or voltage gradient, the dielectric constant and viscosity of the liquid - all of which are known - and the zeta potential. It is usually expressed as the particle mobility which is the velocity under unit field strength. For all practical purposes, the relationship between mobility, Ω, and zeta potential, ζ, is quite simple and, for instance, in water at 25 ^{o} C can be expressed as: $\zeta = 12.85\ \Omega$. In practice, zeta potentials are usually negative, i.e. the

surface is negatively charged, but they can lie anywhere in the range from -100 to +100 mV.

Zeta potential is a measure of the repulsive forces in electrostatically stabilized systems, and, therefore, a measure of relative stability to change. High values - either positive or negative - signify stability; whereas, values approaching zero signify instability. When two particles come so close that their double layers overlap, they repel each other. The strength of this electrostatic force depends on the zeta potential. If the zeta potential is too small (typically less than about 25 mV in magnitude), the repulsive force won't be strong enough to overcome the Van der Waals attraction between the particles, and they will begin to agglomerate. The suspension is said to be unstable when this happens. If the suspension is concentrated and unstable, these agglomerates form networks, and the colloid turns into a paste. A high zeta potential will prevent particle-particle agglomeration and keep the dispersion uniform and free flowing. Therefore, the goal in most formulations is to maximize the zeta potential.

The zeta potential is a consequence of the existence of surface charge, and can give information on electrical interaction forces between the dispersed particles. In many cases, the zeta potential can be used directly as the criterion for assessing product quality. However stability assessment using the zeta potential as the measurable variable may only be useful if the system is sufficiently well understood.

It is worth emphasizing the distinction between surface potential and zeta potential. The zeta potential is the controlling parameter for particle interactions. Modifying the zeta potential requires knowledge of the potential of the surface and its chemistry. Investigation of the interaction of ions with the surface, and their effect on zeta potential is assisted by the determination of zeta potential as a function of a number of parameters. The parameters that it is useful to investigate are pH, conductivity and the concentration of any specifically adsorbed ions or polymers in the system.

CHAPTER III

LITERATURE REVIEW

A vast amount of work had been studied and published concerned with modeling the flow and the separation process in a hydrocyclone. The different approaches to the problem can be shown as follows.

3.1 The equilibrium orbit theory

Criner (1950) and Driessen (1951) originally proposed the equilibrium orbit theory that based on the concept of the equilibrium radius. According to this concept, particles of a given size attain an equilibrium radial orbit position in the cyclone where their terminal settling velocity was equal to the radial velocity of the liquid. Particles were therefore 'elutriated' by the inward radial flow according to the balance of the centrifugal and drag forces, and Stokes' law was usually assumed. The fine particles reached equilibrium on small radii where the flow was moving upwards (and into the overflow), while the coarse particles will stay on large radii, in the downward flow, and finish in the underflow. The dividing line was the locus of zero vertical velocity (LZVV). The particle size, the equilibrium radius of which was coincident with LZVV must then be the cut size d_{50}, which had an equal chance of reporting to either underflow or overflow. Detailed knowledge was required of the inward radial velocities which determine the drag force, as well as of the tangential velocities which cause the centrifugal force. Most authors assumed some simplified shape for LZVV and then work out the average radial velocity through the surface. Most also assumed Stokes' law but some consider a more general relationship for the drag coefficient. Bradley (1965) gave a detailed review of the different approaches and more recently by Svarovsky (1984).

Yoshioka and Hotta (1955) obtained the cut size relationship by assuming that the locus of zero vertical velocity coincided with the surface of an imaginary cone whose apex was at the bottom of the cyclone cone and whose base was at the bottom

of the vortex finder. The flow pattern and velocity data obtained by the authors were used to obtain the following equation:

$$d_{50} = 6.3 * 10^{6}\left(\frac{\mu}{\rho_s - \rho}\right)^{0.5} \frac{D_c^{0.1} D_i^{0.6} D_o^{0.8}}{Q^{0.5}}$$

where the units were D_c, D_i, D_o [m]; Q [L/sec]; μ [kg/ m.s] and ρ_s, ρ [kg/m^3]

Haas (1957) developed equation for use with specified designs of small diameter cyclones and was a development of the Yoshioka and Hotta (1955) equation. It was as follows:

$$d_{50} = 1.07 * 10^{3}\left(\frac{D_c^{3.05}\mu}{Q^{1.14}(\rho_s - \rho)}\right)^{0.5}$$

where the units were D_c [inch]; Q [U.S. gal/min]; μ [lb/ft.s] and ρ_s, ρ [lb/ft^3]

Bradley (1958) obtained an expression for d_{50} using the equilibrium orbit concept. Across surface of zero vertical velocity, the radial velocity component was assumed to be constant and equated to the radial settling velocity of the particle of size d_{50} based on Stokes' Law. Hence an expression for d_{50} was obtained in the form:

$$d_{50} = 2.7\left[\frac{\tan\frac{\theta}{2}\mu(1 - R_f)}{D_c Q(\rho_s - \rho)}\right]^{0.5}\left(\frac{2.3D_o}{D_c}\right)\frac{D_i^2}{\alpha}$$

where the units were D_c, D_i, D_o [inch]; Q [L/min]; μ [cP] and ρ_s, ρ [g/cm^3]. α was inlet velocity loss ration = v_t/v_i.

Bradley and Pulling (1959) were probably the best known and proposed most credible approach to the equilibrium orbit theory. This was based on the discovery of the 'mantle' by the same authors, i.e. an area in the region immediately below the

vortex finder where there was no inward radial velocity. They illustrated known features and added to detailed knowledge of flow patterns by using dye injections into the fluid flowing in hydraulic cyclones. The results were described and the implications on theoretical correlation of efficiency were discussed. Such a correlation can never be precised owing to uncertainties on the path followed by an individual particle. The theoretical approach was given and was shown to provide results which compare favorably with performance data for a particular design of cyclone. The authors modified Bradley's model (1958) as following:

$$d_{50} = 3.2(0.43)^n \frac{D_i^2}{\alpha}\left[\frac{\tan\frac{\theta}{2}\mu(1-R_f)}{D_c Q(\rho_s-\rho)}\right]^{0.5}$$

where the units were D_c, D_i [inch]; Q [L/min]; μ [cP] and ρ_s, ρ [g/cm^3]. α was inlet velocity loss ratio = v_t/v_i.

3.2 The residence time theory

Rietema (1961a) first proposed the residence-time theory and assumed homogeneous distribution of all particles across the inlet. This theory assumed non-equilibrium conditions and considered whether a particle will reach the cyclone wall in the residence time available. The cut size will then be the size of the particle which, if entering precisely in the center of the inlet pipe will just reach the wall in residence time T. In mathematical terms, this mean that the particle radial settling velocity integrated with time should therefore be equal to half the inlet diameter. He proposed a 'characteristic cyclone number' Cy, and suggested that it should be as small as possible considering the variables in it. He proposed the equation as follow:

$$d_{50}^2 \frac{(\rho_s-\rho)L\Delta P}{\mu\rho Q} = Cy_{50} = 3.5$$

where the units were L [mm]; ΔP [atm]; Q [kg/m^3]; μ [cP] and ρ_s, ρ [g/cm^3]

Trawinski (1969) proposed another theoretical approach to cut size prediction that can be classified as another version of the residence-time theory. He used Stokes' law, an effective clarification area an average acceleration in a hydrocyclone to derive an expression for the cut size. He also proposed a rather simplistic correlation for the pressure drop-flow rate relationship.

Kutepov et al. (1977) and Kutepov (1978) developed a Russian theory using residence time theory. This was primarily concerned with overall separation of solids into the overflow and underflow and was based on a stochastic theory of separation processes. Stokes' law was used in describing resistance to particle motion but angular velocity was employed to characterize the spin flow in the hydrocyclone and not the tangential velocity as was more usual. He gave an empirical correlation that expressed as a function of the hydrocyclone design and inlet velocity. As the Russian theory did not use the concept of grade efficiency or cut size, it did not lend itself easily to direct comparison with other theories.

Holland-Batt (1982) proposed a more recent version of the residence-time theory, the so-called 'bulk model'. He simply used the hold-up time of the liquid in the hydrocyclone (flow rate per hydrocyclone volume) as the residence time, average radial fluid velocity (flow rate per wall area of the hydrocyclone) and a general continuity equation for two-dimensional flow to derive an expression for the cut size. He modified his model for the case when non-spherical particles were not characterized by the equivalent Stokes' diameter, and a shape factor must therefore be used. He also considered the case of particle motion outside the Stokes' region.

Medronho (1984) carried out with three sizes of Rietema (1961a)'s optimum design (22, 44 and 88 mm in diameter) at 1% volume feed concentration had reproduced Rietema's results, but only with very dilute underflows: values of Cy about twice as large had been found under more practical operating conditions.

Cilliers and Harrison (1997) illustrated the feasibility of attaining separation of microbial cells from the culture suspension using a 10 mm hydrocyclone. The form of the model equation for recovery had been derived based on the residence time theory. Increasing pressure and temperature exhibited a positive effect on both the recovery and the concentrating effect while increasing in the feed concentration exhibits a negative effect on these. In addition, increasing the vortex diameter resulted in an increasing concentration ratio and a decreasing recovery. Increasing the diameter of the spigot showed the opposing trends.

Dwari, Biswas and Meikap (2004) designed and fabricated a new type of hydrocyclone that can operate in a wide range of variables for sand, sand-ash and sand-FCC systems. A detailed study on performance analysis of hydrocyclone, pressure drop, cut size and particle characterization had been carried out. A mathematical model for predicting particle separation efficiency and cut size had been developed that based on the residence time theory. An experimental finding shows 96% removal efficiency for 175 μm particle with cut size diameter of 75 μm. They modified Rietema (1961) equation as follow:

$$d_{50} = \left[\left(\frac{2Q}{\pi D_c L} - \frac{C_1 v_i R_1}{L} \right) \frac{18 \mu R_1 \rho}{\Delta\rho \Delta P} \right]^{0.5}$$

where C_1 was a constant, R1 was effective distance and Δp was the static pressure drop.

3.3 The turbulent two phase flow theory

Driessen (1948) studied the effect of turbulence on the separation in hydrocyclones. One aspect of interest was how turbulence modifies the tangential velocity profiles, i.e. its effect on the exponent n in the exponential equation for the tangential velocity in his equation. He was the first to derive an expression relating the tangential velocity to the radial pressure distribution by assuming the radial velocity component negligible in relation to the tangential component.

Rietema (1961b) made a detailed investigation into the effect of turbulence on the tangential velocity and estimated the turbulent viscosity with the aid of the tangential velocity profiles measured by Kelsall (1952). This was done using a dimensionless parameter λ.

Bloor and Ingham (1975) published a more rigorous viscous turbulent model of single-phase flow, based on a Prandtl mixing length theory. Although they obtained theoretical velocity profiles, but they used variable radial velocity profiles calculated from a simple mathematical theory. The turbulent viscosity was then related to the rate of strain in the main flow and the distribution of eddy viscosity with radial distance at various levels in the hydrocyclone was derived.

Schubert and Neesse (1980) proposed a separation model based on turbulent two-phase flow. They assumed a homogeneous, stationary turbulence field, with particles moving under Stokes' law and assumed that the particles were smaller than the smallest eddies and that their concentration was 'sufficiently low'. The homogeneous centrifugal force field was one assumption. They derived two general models for turbulent cross-flow classification. These were the suspension partition model and suspension tapping model. The latter model was applied to separation in a hydrocyclone, with the resulting equation for the cut size.

Neesse and Schubert (1984) reported the turbulent two-phase flow model in case of higher solids concentrations where the underflow orifice may restrict the free discharge of the solids. They proposed the existence of a limit in the solids loading and proposed an empirical correlation for the discharge capacity of the underflow orifice.

Schubert, et al. (1986) proposed a set of equations and derived two models for turbulent cross-flow wet classification: the suspension-partition model and the suspension-tapping model. In the former the flow was divided into overflow and underflow without changes in the total cross section, whereas in the latter overflow and underflow were "tapped" from the main flow through small outlet openings.

According to them, the suspension-tapping model was analogously applicable to the separation in hydrocyclones. For performance predictions on the basis of the theory discussed above, the relationship for hydrocyclones was:

$$d_{50} = 0.12\left[\frac{\mu D_c \ln(D_o / D_u)^3}{(\rho_s - \rho)(1 - c_v)^{4.65}(\Delta P / \rho_m)^{0.5}}\right]^{0.5}$$

where ρ_m was suspension density

Duggins and Frith (1987) had challenged the concept of isotropic eddy viscosity and the showed that not only did the eddy viscosity vary with position in the hydrocyclone but its value was different in two mutually perpendicular directions and the ratio of the two values was not constant. They proposed a new method for calculating velocities where the eddy viscosity for the axial and radial momentum equations was calculated from the conventional turbulent model (k-ε model) and the viscosity for the tangential momentum equation from a mixing length expression. This method, therefore, allowed for anisotropy of turbulence in the swirling flow.

Dyakowski and Williams (1993) presented and tested a revised approach to modeling turbulent flow in small diameter (10-44 mm) hydrocyclones. Some of the limitations inherent in the existing approaches, such as the anisotropy of turbulent viscosity and the non-linear interaction between mean vorticity and mean strain rate had been overcome utilizing a k-ε model coupled with equations for calculating normal components of Reynolds stresses. The model predicted correctly the behavior of a conventional water-fed hydrocyclone of various geometries, and had also been used to examine how the flow field can be modified by the insertion of a solid rod in place of the central air core in order to sharpen the classification performance of a hydrocyclone treating particulate suspensions.

Neesse, Dueck and Minkov (2004) concluded that on the basis of the hydrocyclone separation model describing the sedimentation equilibrium of sedimentation flux and turbulent diffusion flux, the separation curve for dilute flow

separation increased monotonically. For dense flow separation, the separation curve shows a non-monotonic course with the typical fish-hook in the fine particle range. The fish-hook reflected the law of disturbed settling in polydisperse dense suspensions. Here, the fine particle entrainment caused by coarse particle settling plays an important part. In accordance with this law, the fine particle settling or the fine particle separation, respectively were not only determined by solid concentration but also by the particle size distribution of the feed.

3.4 Crowding theory

Fahlstrom (1960) was first suggested the crowding theory. He proposed that the cut size was primarily a function of the capacity of the underflow orifice and of the particle size analysis of the feed. He argued that the crowding effect, or hindered discharge through the apex, can swamp the primary interaction to the extent that the cut size can be estimated from the mass recovery to the underflow. He quoted the discharge capacity to be from 1.5 to 3 cm^{-2} h^{-1} in grinding circuits, but this depended on the absolute size of the underflow orifice and it was not realistic for small hydrocyclones. In any case, any crowding effect must surely depend on the physical proximity of the solid particles and this depended on volume rather than mass. He attributed the differences between the analytical cut size and the equiprobable size to the crowding effect. Furthermore, he found the difference to be a function of particle size. This difference was now known to be due to the non-ideal shape of the grade efficiency curve and it existed whether or not underflow crowding takes place.

Bloor and Ingham (1974) modeled the flow in the boundary layer using a correlation for the slurry viscosity as a function of particle concentration and using concentration averaged across the boundary layer.

Bloor, Ingham and Laverack (1980) suggested a scientific proof of the crowning theory from some mathematical modeling. This was a hydrodynamic model of the flow both in the hydrocyclone body and in the boundary layer, but it made no predictions of conditions at underflow because it broke down at the vortex. The model

assumed inviscid flow in the main body and viscous flow in the boundary layer. It allowed plots of particle trajectories, assuming their homogeneous distribution on entry to the hydrocyclone cone.

Laverack (1980) published the flow model in the boundary layer. The model allowed plots to be made of particle concentrations, volume fluxes and layer thickness along the boundary layer. This in turn allowed the effect of increased feed concentration on the conditions in the boundary layer to be studied.

3.5 The regression models

Lynch and Rao (1968) studied the effect of really high feed concentrations on hydrocyclone capacity, in concentration of minerals. Hundreds of experiments were carried out with various cyclone designs and operating conditions, leading to empirical models suitable for mathematical modeling of closed circuit mineral grinding circuits or similar applications. They presented the correlation for the pressure drop-flow rate relationship. Hydrocyclone of 500 mm diameter were tested with silica and copper ore at concentrations of 15-65% by weight.

Lynch, Rao and Prisbrey (1974) and Lynch and Rao (1975) furthermore studied the effect of really high feed concentrations on hydrocyclone capacity in series of experiments using hydrocyclone from 100 to 380 mm in diameter. Limestone was the tested material at concentrations of 15-70% by weight. The model was:

$$\log_{10} d_{50c} = 0.0173 \log_{10} C_w - 0.0695 D_u + 0.0130 D_o + 0.0048 Q + k_d$$

where the units were D_u, D_o [cm] and Q [L/min]

Rao, Nageswararao and Lynch (1976) reported the effect of really high feed concentrations on hydrocyclone capacity in series of tests at concentrations of limestone from 40-70% by weight.

Plitt (1976) took the data of Lynch and Rao (1968) and added his own, with smaller hydrocyclones up to 150 mm diameter tested with silica flour and used the data to derive by regression analysis yet another correlation for the pressure drop-flow rate relationship. The equation for d_{50c} was:

$$d_{50c} = \frac{50.5 D_c^{0.46} D_i^{0.6} D_o^{1.21} e^{0.08 C_v / F50^{0.52}}}{D_u^{0.71} l^{0.38} Q^{0.45} (\rho_s - \rho)^{0.5}}$$

where the units were D_c, D_i, D_o, D_u, l[cm]; Q [L/min]; μ [cP] and ρ_s, ρ [g/cm^3]

Gibson (1979) tested 25 and 50 mm diameter of Mozley hydrocyclones with china clay at concentrations up to 35% by weight and found geometric standard deviations from 1.77 to 2.0 depending on the size of the vortex finder. Larger vortex finders yielded lower standard deviations, thus giving sharper classification.

Apling, Montaldo and Young (1980) applied the formulae proposed by Lynch and Rao (1968) and Plitt (1976) using other hydrocyclone sizes and slurries. He found that it was necessary to change the constants to fit the predicted results to the experimental data.

Flintoff, Plitt and Turak (1987) revised the Plitt (1976) model that had no dependence for feed size characteristics as below:

$$d_{50c} = F_1 \frac{39.7 D_c^{0.46} D_i^{0.6} D_o^{1.21} \mu^{0.5} e^{0.063 C_v^P}}{D_u^{0.71} l^{0.38} Q^{0.45} \left(\frac{\rho_s - 1}{1.6} \right)^k}$$

where the units were D_c, D_i, D_o, D_u, l[cm]; Q [L/min]; μ [cP] and ρ_s, ρ [g/cm^3]. F_1 was calibration parameter for Plitt's equation.

Yopps et al. (1987) studied the effect of silica slurry rheology on hydrocyclone performance. The temperature of the slurry was found to have a predominant effect on the fraction of feed water reporting to the underflow and the sharpness of separation. Increasing the slurry viscosity by lowering the slurry temperature caused the fraction of feed water reporting to the underflow to increase and the sharpness of separation to decrease. Decreasing the slurry viscosity by adding a viscosity modifying reagent caused the fraction of fines bypassing to the underflow to increase.

Kawatra, Bakshi and Rusesky (1996a) studied the effect of viscosity on the cut size of hydrocyclone classifiers using on-line measurement of slurry viscosity. They observed that the cut size was proportional to the 0.35^{th} power of the slurry viscosity. They used this relationship to modify Lynch and Rao (1975) model and predicted the cut size precisely when the viscosities of the slurries were altered by factors other than changing percent solids, such as temperature variation. They also determined that increasing slurry viscosity produced an increase in the underflow to throughput ratio due to the increasing of fluid drag. The modified equation after introducing the viscosity term was:

$$\log_{10} d_{50c} = 0.41 \log_{10} C_v - 0.0695 D_u + 0.0130 D_o + 0.0048 Q + 0.35 \log_{10} \mu + k_d$$

where the units were D_u, D_o [cm]; Q [L/min] and μ [cP]

Kawatra, Bakshi and Rusesky (1996b) studied the effect of slurry viscosity on hydrocyclone classification using on-line viscometer set-up on a hydrocyclone. They observed that the cut size was proportional to the 0.35^{th} power of the slurry viscosity. They used this relationship to modify Plitt (1976) model and predicted the cut size precisely when the viscosities of the slurries were altered by means other than changes in the percent solids. The R_f also trended to increase with increasing viscosity, while the reduced efficiency curve was not affected. The modified equation after introducing the viscosity term was:

$$d_{50c} = \frac{kD_c^{0.46} D_i^{0.6} D_o^{1.21} C_v^{0.41} \mu^{0.35}}{D_u^{0.71} l^{0.38} Q^{0.45} (\rho_s - \rho)^{0.5}}$$

where the units were D_c, D_i, D_o, D_u, l [cm]; Q [L/min]; μ [cP] and ρ_s, ρ [g/cm^3]

Asomah and Napier-Munn (1997) reported the influence of angle of inclination from zero to 112^o to the vertical on hydrocyclone performance. Cyclone diameter varied from 102 to 508 mm. The cyclone inclinations greater than 45^o strongly affect the performance of industrial cyclones. A new empirical model had been developed incorporating angle of inclination and including prediction of cut size, sharpness of separation, water recovery and pressure-flow rate relationship.

$$d_{50c} = D_c^{0.229} \left(\frac{P_{40}}{D_o}\right)^{-0.457} \left(\frac{D_o}{D_u}\right)^{0.948} \left(1 - C_v^{(1-A/180)}\right)^{-2.941} \mathrm{Re}^{-0.155}\ \theta^{0.719} e^{-1.392A/180} B_1$$

where P_{40} was size 40% feed material passing [cm], A was cyclone inclination from vertical [degree] and B_1 was a constant. The units were D_c, D_o, D_u [cm].

Tavares et al. (2002) developed a mathematical model accounting for the effects of slurry rheology on classification, covering a wide range of rheological conditions, both Newtonian and non-Newtonian. Semi-empirical models for estimating the hydrocyclone capacity and corrected cut size and an empirical model of water split had been proposed that based on the residence time theory. They found that hydrocyclone capacity and sharpness of separation were not affected by slurry rheology. Moreover, the plastic viscosity was the most significant parameter for modeling the corrected cut size in 50 and 25 mm diameter hydrocyclones. The equation was:

$$d_{50c} = k_d \left[D_c^{4-b} Q^{b-2} \left(\frac{ab}{\rho_s - \rho}\right) \left(\frac{8\mu\lambda}{\pi D_i^2 r_{50}^{n+1}}\right)^{b-1} \right]^{0.5}$$

where a was consistency index of the fluid, b was slurry type flow behavior index, λ was velocity reduction parameter, n was flow pattern constant and r_{50} was dimensionless radial corresponding to the envelope of zero axial velocity. The units were D_c, D_i [m]; Q [m^3/h]; μ [Pa s] and ρ_s, ρ [kg/m^3].

Nageswararoa, Wiseman and Napier-Munn (2004) provided the latest version of the Nageswararoa (1978) model and Plitt (1976) model in a form that can readily be implemented in any suitable programming language, or within a spreadsheet. They discuss the assumptions and approximations used in developing these models. Differences in model structure and the choice of dependent and independent variables were also considered. Redundancies were highlighted and an assessment made of the general applicability of each of the models, their limitations and the sources of error in their model predictions.

$$\frac{d_{50c}}{D_c} = k_d D_c^{-0.65} \left(\frac{D_o}{D_c}\right)^{0.52} \left(\frac{D_u}{D_c}\right)^{-0.50} \left(\frac{D_i}{D_c}\right)^{0.20} \left(\frac{L_c}{D_c}\right)^{0.20} \theta^{0.15} \left(\frac{P}{\rho_s g D_c}\right)^{-0.22} \lambda^{0.93}$$

where the units were D_c, D_i, D_o, D_u, L_c [m]; Q [m^3/h]; μ [cP], P [kpa]; g [m/s^2] and ρ_s [kg/m^3]

3.6 The dimensionless group model

Gerrard and Liddle (1978) proposed a designed procedure for precisely the selection. As to which particular alternative was adopted depends on the pressure drop that was available or suitable. If this was not determined by some other consideration, optimization of the total cost of the system (running costs and capital costs) may lead to the best design.

Medronho and Svarovsky (1984) developed model and tested to design and scale-up of single or multiple hydrocyclone installations. It was based on fundamental theory combined with dimensional analysis to produce the necessary correlation, the required constant were derived from tests rather than from theory.

Svarovsky (1987) developed model and tested was used to optimize the design and performance of single or multiple hydrocyclone installations. He showed how, for constant solid separation or overflow clarity, the operating pressure drop can be traded off against the flow ratio, and the system optimized. He also analyzed the conclusion of Rietema (1961a) with respect to the optimum size of the feed orifice. The scale-up model based on dimensionless groups simplified hydrocyclone design and allowed the designer to select the best compromise between the capacity and underflow concentration of the solids.

Castilho and Medronho (2000) presented a procedure which allowed the design and performance prediction of hydrocyclones that follow Bradley (1965) and Rietema (1961a) recommended geometries. The procedure results revealed that for a given hydrocyclone diameter and at the same operational conditions, Bradley hydrocyclones provided higher efficiencies while Rietema hydrocyclone gave higher capacities.

Coelho and Medronho (2001) developed a model based on dimensionless groups derived from the equilibrium orbit theory and the residence time theory for performance prediction of hydrocyclones by data obtained with seven hydrocyclones. This model was able to reproduce data from the classical works of Rietema (1961a), Bradley and Pulling (1959) and Kelsall (1952). The product between the Stokes number and the Euler number ($Stk_{50}Eu$) should be constant and a function of feed concentration and water flow ration for a family of geometrically similar hydrocyclones. For different families, this product was also a function of the cyclone geometrical proportions. The reduced cut size can be calculated by:

$$d_{50c} = \frac{1.173 D_c^{0.64}}{D_o^{0.475}\left(L-l\right)^{0.665}}\left[\frac{\mu\rho Q}{\left(\rho_s-\rho\right)\Delta P}\right]^{0.5}\left[\ln\left(\frac{1}{R_f}\right)\right]^{0.395} e^{6.0C_v}$$

where the units were d_{50c}, D_c, D_o, L, l [m]; Q [m3/s]; μ [Pa s]; P [Pa] and ρ_s, ρ [kg/m^3]

3.7 Analytical flow model

Bloor and Ingham (1973a) presented a simple mathematical theory to determine the flow in a conical hydrocyclone. By considering the flow in a region where viscosity was unimportant, an analytical solution of equations of motion was obtained in the form of a truncated series. The results were compared with the experimental work of Kelsall (1952) and good agreement was obtained.

Bloor and Ingham (1973b) developed a method to evaluate theoretically the performance of a conical hydrocyclone. Use was made of the authors' previous analytical model for the detailed fluid dynamics of the system. This was an inviscid rotational flow model which gave an approximate solution comparing favorably with experiment. The performance was shown to depend on two parameters (λ, $\alpha^{*}l/a$) and the results were presented graphically.

Bloor (1987) reported that the entering fluid to the hydrocyclone distributed non-uniformly momentum and the secondary motions produced from realistic entry conditions were of sufficient strength to generate the required levels of vorticity in the hydrocyclone.

3.8 Numerical simulations of flow

Boyson, Ayers and Swithenbank (1982) carried out the numerical calculations of the complete flow field using axially symmetric flow models and solving the full viscous equations of motion. These simulations were suitable for assessing parameters in design optimization provided that they were based on realistic boundary conditions and a comprehensive flow model.

Rhodes, Pericleous and Drake (1987) developed a fundamentally based mathematical model for hydrocyclone prediction. Existing computer codes were used to solve the required partial differential equations that govern the flow. The main

activity was the examination and testing of physical hypotheses relating to fluid and solid behavior.

Malcolm (1988) reported the analytical and numerical solutions of similarity form for inviscid flow in the generating plane of and axi-symmetric conical hydrocyclone below the level of the vortex finder. Results were compared with those based on corresponding approximate solutions derived using the methods of Bloor and Ingham (1974), and differences from the original Bloor and Ingham solution were highlighted. Solutions were found which, if realized physically, would lead to greater separation efficiency of particles with density greater than the fluid. Such solutions were characterized by vertical velocity profiles at a given height which were flater, and inward radial velocities which were smaller, in a region away from the cyclone wall and axis of symmetry.

Bloor, Ingham and Ferguson (1989) produced a numerical simulation for viscous flow in a hydrocyclone at unrealistically low Reynolds numbers. They did not ignore the three-dimensional character of the flow around the entry point and used three different models to simulate the entry flow.

Hsieh and Rajamani (1991) developed a mathematical model of the hydrocyclone based on the physics of fluid flow. The governing Navier-Stokes equations had been solved successfully for the hydrocyclone geometry. The key to the success was the appropriate turbulence model and numerical solution scheme. A number of hydrocyclone that run at various operating conditions had confirmed the model predictions.

Narasimba, Sripriya and Banerjee (2005) used models based on Computational Fluid Dynamics (CFD) techniques to simulate fluid flow in hydrocyclones and predicted the separation efficiency of solid particles in the separator for a wide range of operating and design conditions. The studies revealed that with an increase in feed flow rate and decrease in spigot diameter the cyclone sharpness of separation improved.

3.9 Other researches

Kelsall (1953) investigated the effect of several variables on solid elimination efficiency of 3 in. hydrocyclone. He found that a 0.25 in. feed diameter resulted in maximum efficiencies on this cyclone for wide range of conditions. The importance of turbulent mixing in the feed section due to shock effects and of the short circuit flow down the outside wall of the vortex finder had been demonstrated.

Dahlstrom (1954) developed for one type of hydrocyclone, had been widely and usefully applied to many types.

$$d_{50} = \frac{81\left(D_o D_i\right)^{0.68}}{Q^{0.53}}\left(\frac{1.73}{\rho_s - \rho}\right)^{0.5}$$

where the units were D_i, D_o [inch]; Q [U.S. gal/min]; and ρ_s ,ρ [g/cm^3]

De Gelder (1957) expressed the correlation in terms of the largest particle size which was just not caught, d_o. d_o was related to design and operating variables by:

$$d_o = D_o\left[\frac{0.349\ \mathrm{Re}\left(D_c - \xi D_o\right)}{D_i}\left(\frac{\rho_s}{\rho} - 1\right)\right]^{-0.5}$$

where ξ was constant, dependent on cyclone design and related to the inlet, overflow and hydrocyclone body dimensions.

Matschke and Dahlstrom (1959) modified the Dahlstrom (1954) equation as:

$$d_{50} = \frac{87.2\left(D_o D_i\right)^{0.65}}{Q^{0.60}}\left(\frac{1.73}{\rho_s - \rho}\right)^{0.5}$$

where the units were D_i, D_o [inch]; Q [U.S. gal/min]; and ρ_s ,ρ [g/cm^3]

Mitzmager and Mizrahi (1964) developed a graphical correlation for the pressure drop through small hydrocyclones (3-15 cm diameter), as a function of the flow regime and the principal dimensions of the hydrocyclone, when operating with dilute pulps of water. The correlation had practical value in design and clarifies the relative importance of a number of important variables.

Vallebuona, et al. (1995) reported experimental research on small hydrocyclones. The results showed, in some aspects, coherency with what was already known about conventional larger cyclones. In other aspects, the results were in disagreement with previous findings. Remarkable contribution was the finding about the dependence of the water split on the D_o/D_u ratio and of the d_{50} on the D_o/D_u^2 as follow:

$$d_{50} = C_8 \left(\frac{D_o}{D_u^2} \right)^{C_9} e^{C_{10} C_u} Q^{C_{11}}$$

where the units were D_u, D_o [mm] and Q [L/s]

Nageswararoa (1999) carried out a detailed mathematical analysis of Plitt (1976) – Reid function, based on which the observed variability of the sharpness of classification. It was shown that if the geometric mean between the extreme values of the classification index, m, was taken as the constant value for the system, the errors in the predictions were least. Further, it was noted that the variation in the classification index, observed in industrial practice or as estimated from Plitt's equation for normal operation, was not significant enough to affect prediction of the cyclone performance.

Chen, Zydex and Parma (2000) evaluated seven hydrocyclone models. There were the more theoretically oriented models by Bohnet (1969), Braun (1989) and Mueller (1998), semi-empirical models by Neesse and Schubert (1991) and Svarovsky (1994), plus the empirical models by Flintof, Plitt and Turak (1987) and Krebs Engineers. Plant operation data from the Dow Chemical Company were used to

compare with the predictions from these models. They found that most of the models studied work well for certain cases but none of the models can predicted all applications. The best results were obtained by using more than one model for predictions. Some experimental data were very important in choosing the models.

Chine and Concha (2000) determined the tangential and axial velocity fields of the water flow in a hydrocyclone using two beams, 300 mW laser Doppler velocimeter. They found that the inlet pressure affects only the magnitude of the velocities, but did not change the flow pattern. The tangential velocity was similar in both types of hydrocyclones while the axial velocity was different. In both hydrocyclones the axial velocity was a function of the radial position but, while it was a linear function of the vertical coordinate in the cylindrical hydrocyclone.

Chu, Chen and Lee (2000) designed the structure of hydrocyclone with a series of modification and investigated the comprehensive effects of the structural modifications on operation performance indices of hydrocyclones. Based on the conventional hydrocyclone, the structural modifications with central insertions named winged core, solid core and inner diffuser could increase all the reduced separation efficiency, separation sharpness, cut size, capacity and flow split, and decrease the energy loss coefficient.

Nageswararao (2000) showed that the precision of measurement of the actual efficiency had not been taken into consideration in reporting the occurrence of fish hook effect in hydrocyclone classifiers. In addition, its occurrence was sporadic and random under identical conditions.

Souza et al. (2000) investigated the effects provoked by three different filtering media on the performance of the filtering hydrocyclone which consisted of a Bradley's cyclone whose conical section was replaced by a conical filtering wall. These filtering hydrocyclones were compared to the conventional Bradley's hydrocyclone and displayed increased in both feed flow rates and reduced cut sizes. The reduced cut size equation was:

$$\frac{d_{50c}}{D_c} = \left(0.064 \pm 0.004\right)\left[\frac{\mu D_c}{Q\left(\rho_s - \rho\right)}\right]^{0.5}\left(1 - R_f\right)^2$$

where the units were D_c [m]; Q [m^3/s]; μ [kg/ m.s] and ρ_s, ρ [kg/m^3]

Ogawa and Suzuki (2001) presented the theoretical equation of the cut size which included the gravitational and centrifugal forces acting on the suspended solid particles in the axial flow hydrocyclone. The equation was derived based on the mass balance. The characteristics of the predicted cut size were divided into two regions, one of which was dominated by the gravitational force effect while the other was dominated by the centrifugal force effect. Therefore the maximum value of the cut size will be located between these two regions.

สถาบันวิทยบริการ
จุฬาลงกรณ์มหาวิทยาลัย

CHAPTER IV

MATERIALS AND METHODS

4.1 Materials and Chemicals

The silica used as the test powder was as specified in **Table 4.1**.

Table 4.1 Silica specifications

Company	Denki Kagaku Kogyo Kabushiki Kaisha (DENKA)
Powder ID	SFM-30M
Density	2210 kg/m^3
Mean diameter	0.861 μm
Median diameter	0.754 μm
Mode diameter	1.097 μm
Standard deviation	0.488 μm
Particle surface area	99598 cm^2/ml

Figure 4.1 shows the frequency size distribution of silica particles used in this work. Deionized water with conductivity of 0.7-2.0 $*10^{-4}$ s/m was used in all experiments. Suspensions of 0.2 % solid content by weight were applied in all experiments. Sodium hexametaphosphate, $(NaPO_3)_6$ 0.3 g was used as a dispersing agent in Laser Scattering Particle Size Distribution Analyser, HORIBA LA-920. Sodium Hydroxide was used for pH of suspension adjustment.

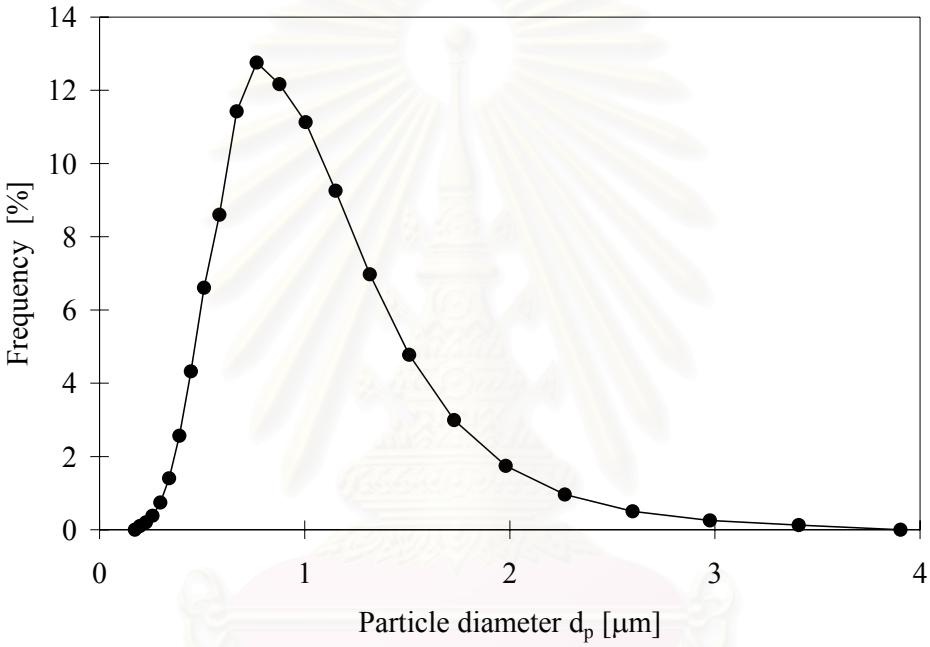

Figure 4.1 Frequency size distribution of silica particles used in this work

สถาบันวิทยบริการ
จุฬาลงกรณ์มหาวิทยาลัย

4.2 Experimental Setup

Figure 4.2 (a) and (b) show the actual arrangement of the experimental apparatus used in the present work and **Figure 4.3** presents its schematic diagram.

Figure 4.2 (a) Hydrocyclone and the dust box

Figure 4.2 (b) Tank, control valve, impeller, flow meter and pressure gauge

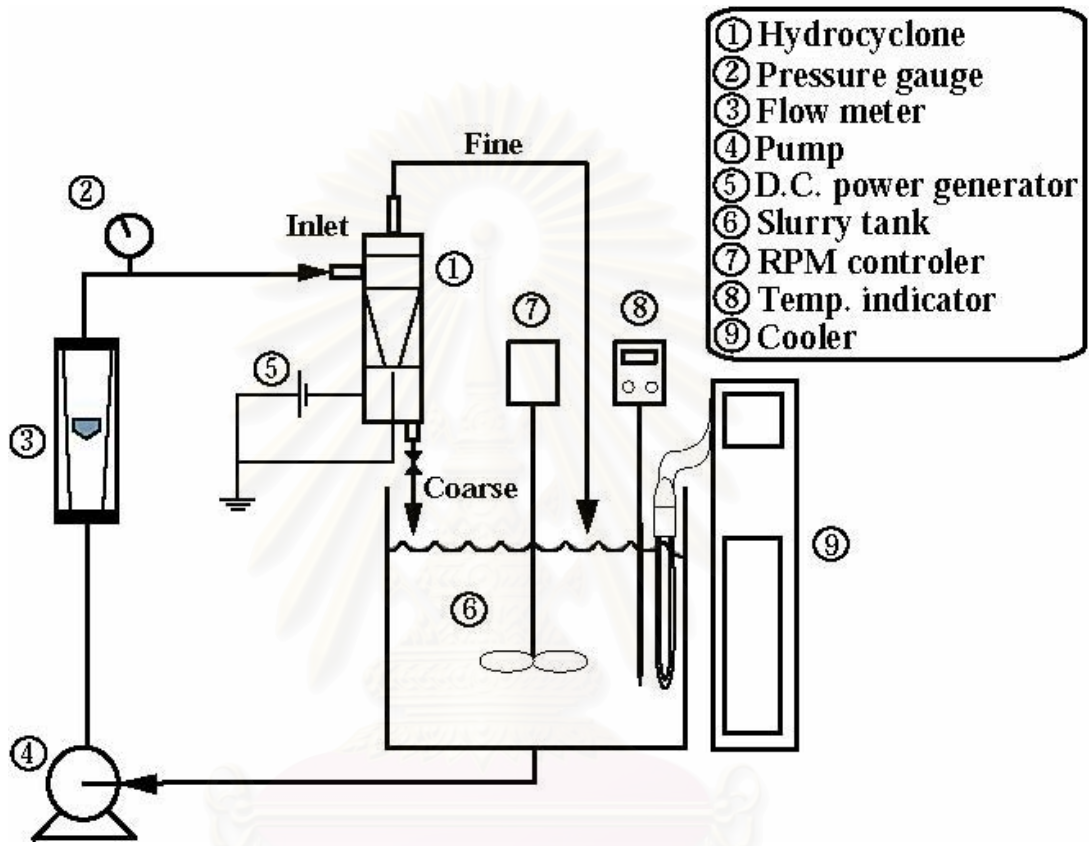

Figure 4.3 Schematic diagram of the experimental apparatus

สถาบันวิทยบริการ
จุฬาลงกรณ์มหาวิทยาลัย

As can be seen in **Figure 4.3**, the experimental apparatus consisted of a tank equipped with impeller (EYELA 120860, MAZELA Z-1210) for mixing at constant agitator speed 250 rpm. The pump was a rubber lined centrifugal pump (NIKUNI Model 20KWD22Z No. 2361D314). The discharged underflow and overflow were returned to the feed tank. The flow meter (SIZ1619, 0-20 L/min) and pressure gauge (MIGISHITA, 0-2.5 Mpa) were installed to measure flow rate and pressure drop. The suspension temperature in the tank was constantly controlled at 30 C^o using a cooler (EYELA CA-1112) and a heater (AWA-1103), and the temperature was observed using temperature indicator (DP-3 AS ONE). pH of the suspension was adjusted by adding a concentrated of NaOH solution. The four investigated pH of suspension were original pH (6.0), 8.0, 9.0 and 10.0. pH of the suspensions were measured by a pH meter (Horiba, pH meter F-22).

Figure 4.4 shows the schematic diagram of the hydrocyclone used in the present work. All design proportions were as shown in **Table 4.2**. The conical part of a modified hydrocyclone was connected to a cylindrical dust box having 41.8 mm diameter. This dust box had a central metal rod cone and a cylindrical metal wall between which the desired 50-volt DC electrical potential or no potential was applied by a DC power generator (BIO RAD POWER PAC3000). The investigated lengths of dust boxes were 53 and 106 mm. The four investigated central rods were 8, 12, 16 and 20 mm diameter. The three different cases investigated were: a) no applied electrical potential, b) positive potential applied at the central rod side and negative potential at the side wall, and c) positive potential applied at the side wall and negative potential at the central rod side.

The ratios of tested underflow rate to throughput were: 0, 0.1, 0.2 and 0.3. The tested volumetric flow rates were $0.0833*10^{-3}$, $0.1167*10^{-3}$ and $0.1667*10^{-3}$ m^3/s (5, 7 and 10 /min). The operating time was 20 minutes to assure that the system was in steady state.

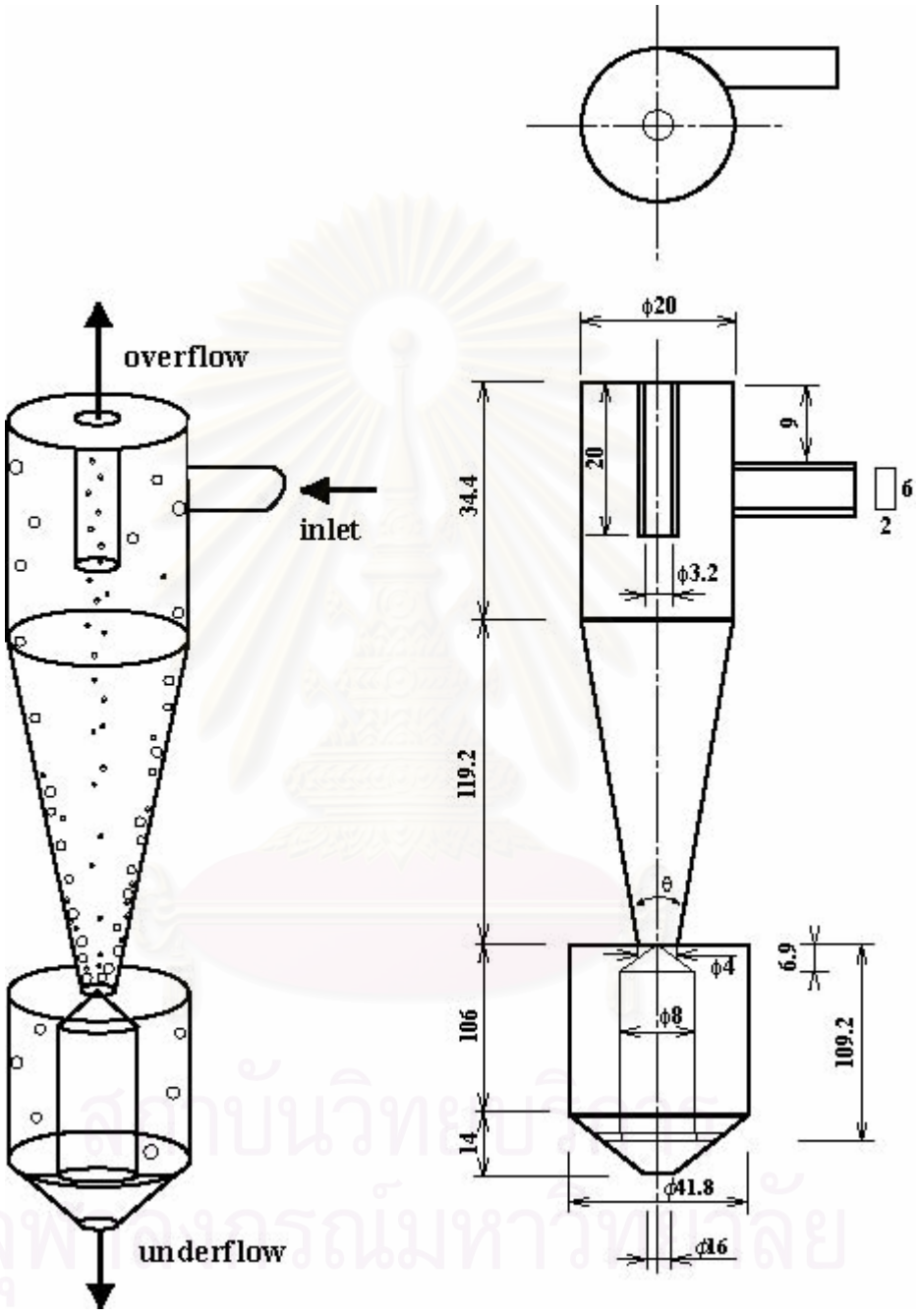

Figure 4.4 Schematic diagram of the hydrocyclone

Table 4.2 Hydrocyclone proportions

D_c [m]	a/D_c	b/D_c	D_o/D_c	D_u/D_c	l/D_c	L/D_c	cone angle (^{o})
0.020	0.10	0.30	0.16	0.20	1.00	7.68	7.68

4.2 Analytical Instrument

The particle size analyses of overflow and underflow were carried out by Laser Scattering Particle Size Distribution Analyzer, HORIBA LA-920 (Japan) as shown in **Figure 4.5** with addition of sodium hexametaphosphate, $(NaPO_3)_6$ 0.3 g as a dispersing agent.

Figure 4.5 Laser Scattering Particle Size Distribution Analyzer

The zeta potentials of suspensions were measured by zeta potential instrument (Zetasizer 2000, MALVERN INSTRUMENTS) as shown in **Figure 4.6**. The effects of pH of suspension on the zeta potential were shown in appendix C. The concentrations of solids in the underflow and overflow samples were carried out by evaporation and weighing. The grade efficiency, G, and the cut size, d_{50}, were evaluated according to the procedure recommended by Svarovsky (1990).

Figure 4.6 Zeta potential meter

4.3 Experimental Procedures

To carry out the classified experiments, the following implementation steps must be carried out carefully to obtain reliable data. Since different procedures were applied in cases of the presence and absence of the underflow, therefore the procedures were separated into two cases.

4.4.1 Presence of the underflow

a. Assemble the inquiring central rod and dust box length to the main body of hydrocyclone.
b. Clean the operating system by circulating water many times until cumulative particles could not be detected in the system.
c. Pour 5 liters deionized water to the feed tank, constantly control water temperature at 30 ^{o}C by using heater and cooler, open the pump and tune the impeller at constant speed of 250 rpm.
d. Weigh of 10 g tested silica and fill to the feed tank.
e. Adjust pH of suspension by adding a concentrated of NaOH solution, inspect the pH value by using a pH meter.
f. Tune the pump speed to obtain the specified feed flow rates.
g. Turn on the control valve under the underflow orifice, measure volume of the underflow against time for calculating underflow to throughput ratio.
h. Check the feed flow rate again. If the desirable feed flow rate was not yet obtained, return to the step f. until the feed flow rate and underflow to throughput ratio were achieved.
i. Select the investigated electrical potential condition then switches either on or off DC power generator at constant 50 volt.
j. Operate the hydrocyclone for 20 minutes (see appendix B) and measure pressure drop.
k. Prepare four 50 cc sample bottles, two bottles for particle size measurement of the overflow and underflow samples (OF1 and UF1), the others were for determining

concentrations of solids in both streams (OF11 and UF11), then weigh the empty bottles.

l. Collect two overflow and two underflow samples, two samples, OF1 and UF1, were for particle size measurement. The others, OF11 and UF11, were placed in the oven at 100 ^{o}C for 12 hours before cooling down and weighing.

m. Calculate the classification efficiency.

n. Turn off the DC power generator, pump, impeller, cooler and heater.

o. Discharge the suspension in the feed tank and clean the system.

4.4.2 Absence of the underflow

a. Assemble the inquiring central rod and dust box length to the main body of hydrocyclone.

b. Clean the operating system by circulating water many times until cumulative particles could not be detected in the system.

c. Pour 5 liters deionized water to the feed tank, constantly control water temperature at 30 ^{o}C by using heater and cooler, open the pump and tune the impeller at constant speed of 250 rpm.

d. Weigh of 10 g tested silica and fill to the feed tank.

e. Adjust pH of suspension by adding a concentrated of NaOH solution, inspect the pH value by using a pH meter.

f. Tune the pump speed to obtain the specified feed flow rates.

g. Shuts off the control valve under the underflow orifice.

h. Check the feed flow rate again. If the desirable feed flow rate was not yet obtained, return to the step f. until the feed flow rate was achieved.

i. Select the investigated electrical potential condition then switches either on or off DC power generator at constant 50 volt.

j. Operate the hydrocyclone for 20 minutes (see appendix B) and measure pressure drop.

k. Prepare two 50 cc sample bottles for particle size measurement of the overflow and underflow samples (OF and UF) and a beaker (BUF), then weighs the empty beaker.

l. Collect the overflow sample, OF and shut off the DC power generator and pump, respectively.
m. Fully open control valve under the underflow orifice then discharge all of the underflow liquid in the dust box to the beaker and measure underflow volume.
n. Divide 50 cc of the underflow liquid to the UF for particle size measurement. The remain underflow liquid in the beaker, BUF was placed in the oven at 100 ^{o}C for 12 hours before cooling down and weighing..
o. Calculate the classification efficiency.
p. Turn off the DC power generator, pump, impeller, cooler and heater.
q. Discharge the suspension in the feed tank and clean the system.

สถาบันวิทยบริการ
จุฬาลงกรณ์มหาวิทยาลัย

CHAPTER V

RESULTS AND DISCUSSION

5.1 Effect of dust box length on the classification efficiency in the presence of the underflow

5.1.1 Short dust box

5.1.1.1 Flow rate $0.0833*10^{-3}$ m^3/s (5 L/min)

The effects of dust box length on the classification efficiency in the presence of the underflow were investigated by using the 0.2% solid content by weight of silica suspension fed into the present hydrocyclone. **Figure 5.1** shows the partial separation efficiency when electrical potential was applied to the short dust box (53 mm) of the hydrocyclone in the presence of the underflow at underflow to throughput ratio 0.1, feed flow rate $0.0833*10^{-3}$ m^3/s (5 L/min), pH of suspension 6.0 and central rod diameter 8 mm. The 50% particle cut sizes, d_{50}, obtained from experiments of applying electrical potential to the hydrocyclone were

a) No potential; 2.350 μm
b) Central side +, wall side -; 2.247 μm
c) Central side -, wall side +; 2.157 μm

It was found that the electrical potential for positive pole at both the central rod and side wall decreased the 50% particle cut size when compared with no application of electrical potential. The effect of the electrical potential when the positive pole was connected to the side wall was stronger than when the positive pole was connected to the central rod.

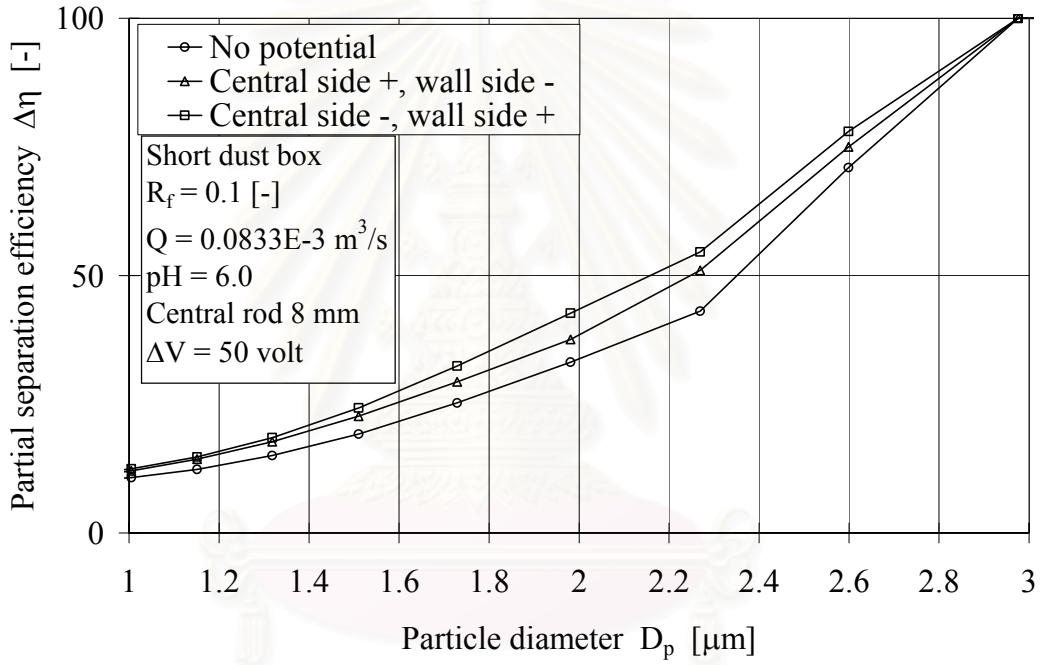

Figure 5.1 Effect of electrical potential on the short dust box of the hydrocyclone in the presence of the underflow at underflow to throughput ratio 0.1, feed flow rate $0.0833*10^{-3}$ m^3/s (5 L/min), pH of suspension 6.0 and central rod diameter 8 mm.

The phenomenon taking place in the hydrocyclone in the presence of the underflow can be described by **Figure 5.2**. At steady state, most of coarse particles, which could be separated by centrifugal force, moved through dust box while only few coarse particles still remained in the dust box. Since silica particles were of negative charge when positive electrical potential was applied to the central rod, a few of silica particles hold on the central rod. Similarly when positive electrical potential was applied to the side wall, some particles hold on the side wall. An amount of accumulative particles, R_d, depended on electrical potential surface area therefore when positive electrical potential was applied at the central rod the amount of attached particles was less than when positive electrical potential was applied at the side wall. The total amount of particles consisted of accumulative particles and the particles removal through the underflow, resulted the total separation efficiency. More amounts of particles expressed the higher separation efficiency. It was meaning that, the classification efficiency in case of positive electrical potential was applied at the central rod and negative electrical potential at the side wall was higher than case of no application of electrical potential but lower than case of positive electrical potential was applied at the side wall and negative electrical potential at the central rod.

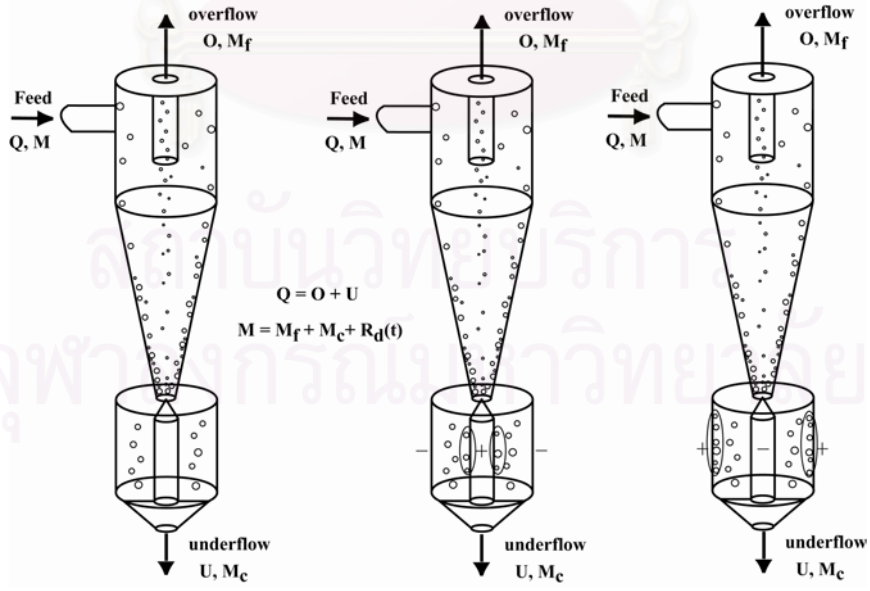

Figure 5.2 Phenomenon in the presence of the underflow

5.1.1.2 Flow rate $0.1167*10^{-3}$ m^3/s (7 L/min)

The effects of dust box length on the classification efficiency in the presence of the underflow were investigated by using the 0.2% solid content by weight of silica suspension fed into the present hydrocyclone. **Figure 5.3** shows the partial separation efficiency when electrical potential was applied to the short dust box (53 mm) of the hydrocyclone in the presence of the underflow at underflow to throughput ratio 0.1, feed flow rate $0.1167*10^{-3}$ m^3/s (7 L/min), pH of suspension 6.0 and central rod diameter 8 mm. The 50% particle cut sizes, d_{50}, obtained from experiments of applying electrical potential to the hydrocyclone were

a) No potential; 2.049 μm
b) Central side +, wall side -; 2.013 μm
c) Central side -, wall side +; 1.972 μm

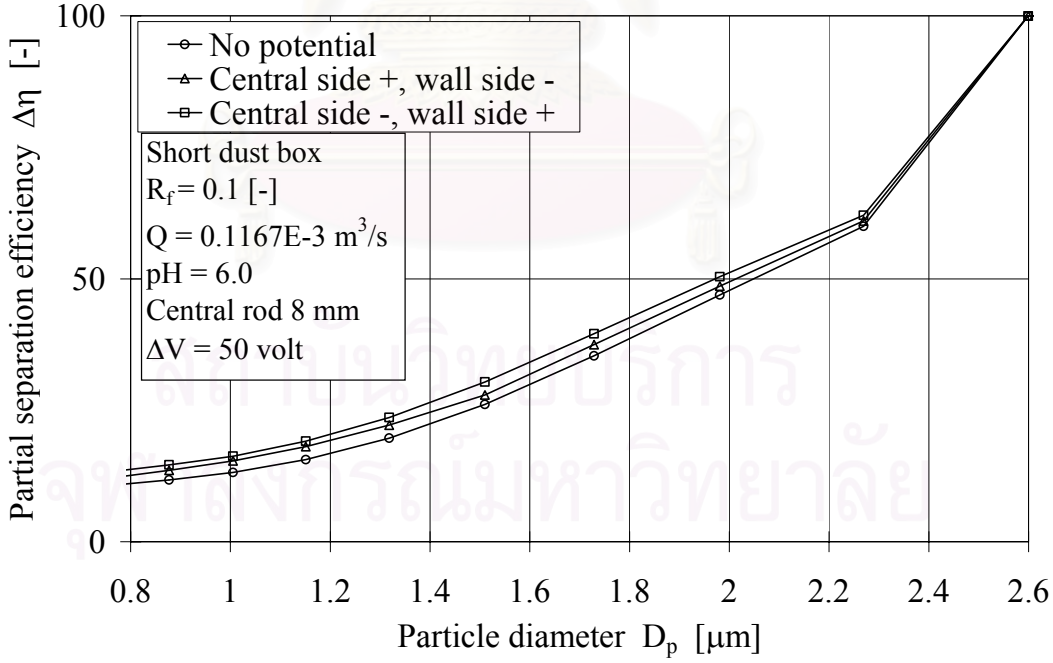

Figure 5.3 Effect of electrical potential on the short dust box of the hydrocyclone in the presence of the underflow at underflow to throughput ratio 0.1, feed flow rate $0.1167*10^{-3}$ m^3/s (7 L/min), pH of suspension 6.0 and central rod diameter 8 mm.

5.1.1.3 Flow rate $0.1667*10^{-3}$ m^3/s (10 L/min)

The effects of dust box length on the classification efficiency in the presence of the underflow were investigated by using the 0.2% solid content by weight of silica suspension fed into the present hydrocyclone. **Figure 5.4** shows the partial separation efficiency when electrical potential was applied to the short dust box (53 mm) of the hydrocyclone in the presence of the underflow at underflow to throughput ratio 0.1, feed flow rate $0.1667*10^{-3}$ m^3/s (10 L/min), pH of suspension 6.0 and central rod diameter 8 mm. The 50% particle cut sizes, d_{50}, obtained from experiments of applying electrical potential to the hydrocyclone were

a) No potential; 1.625 μm
b) Central side +, wall side -; 1.579 μm
c) Central side -, wall side +; 1.558 μm

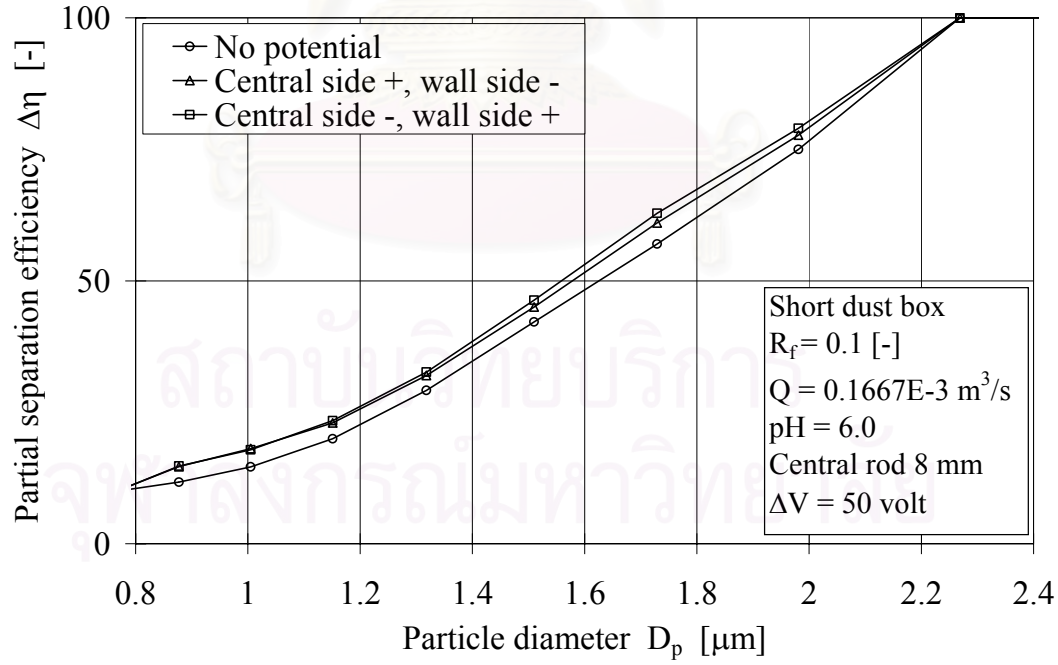

Figure 5.4 Effect of electrical potential on the short dust box of the hydrocyclone in the presence of the underflow at underflow to throughput ratio 0.1, feed flow rate $0.1667*10^{-3}$ m^3/s (10 L/min), pH of suspension 6.0 and central rod diameter 8 mm.

5.1.2 Long dust box

5.1.2.1 Flow rate $0.0833*10^{-3}$ m^3/s (5 L/min)

The effects of dust box length on the classification efficiency in the presence of the underflow were investigated by using the 0.2% solid content by weight of silica suspension fed into the present hydrocyclone. **Figure 5.5** shows the partial separation efficiency when electrical potential was applied to the long dust box (106 mm) of the hydrocyclone in the presence of the underflow at underflow to throughput ratio 0.1, feed flow rate $0.0833*10^{-3}$ m^3/s (5 L/min), pH of suspension 6.0 and central rod diameter 8 mm. The 50% particle cut sizes, d_{50}, obtained from experiments of applying electrical potential to the hydrocyclone were

a) No potential; 2.140 μm
b) Central side +, wall side -; 2.015 μm
c) Central side -, wall side +; 1.932 μm

It was found that the electrical potential for positive pole at both the central rod and side wall decreased the 50% particle cut size when compared with no application of electrical potential. The effect of the electrical potential when the positive pole was connected to the side wall was stronger than when the positive pole was connected to the central rod.

สถาบันวิทยบริการ
จุฬาลงกรณ์มหาวิทยาลัย

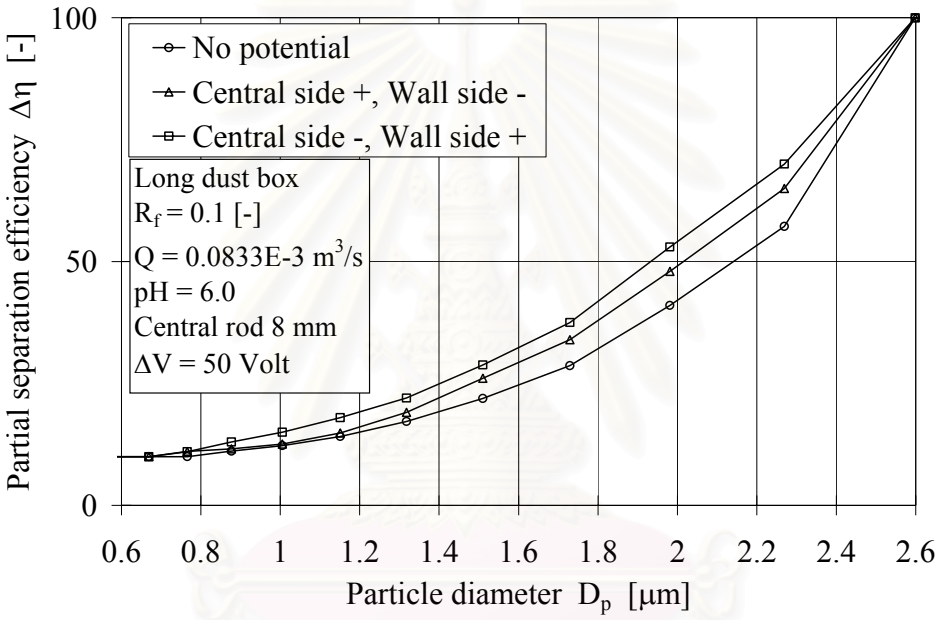

Figure 5.5 Effect of electrical potential on the long dust box of the hydrocyclone in the presence of the underflow at underflow to throughput ratio 0.1, feed flow rate $0.0833*10^{-3}$ m^3/s (5 L/min), pH of suspension 6.0 and central rod diameter 8 mm.

5.1.2.2 Flow rate $0.1167*10^{-3}$ m^3/s (7 L/min)

The effects of dust box length on the classification efficiency in the presence of the underflow were investigated by using the 0.2% solid content by weight of silica suspension fed into the present hydrocyclone. **Figure 5.6** shows the partial separation efficiency when electrical potential was applied to the long dust box (106 mm) of the hydrocyclone in the presence of the underflow at underflow to throughput ratio 0.1, feed flow rate $0.1167*10^{-3}$ m^3/s (7 L/min), pH of suspension 6.0 and central rod diameter 8 mm. The 50% particle cut sizes, d_{50}, obtained from experiments of applying electrical potential to the hydrocyclone were

a) No potential; 1.851 μm
b) Central side +, wall side -; 1.749 μm
c) Central side -, wall side +; 1.696 μm

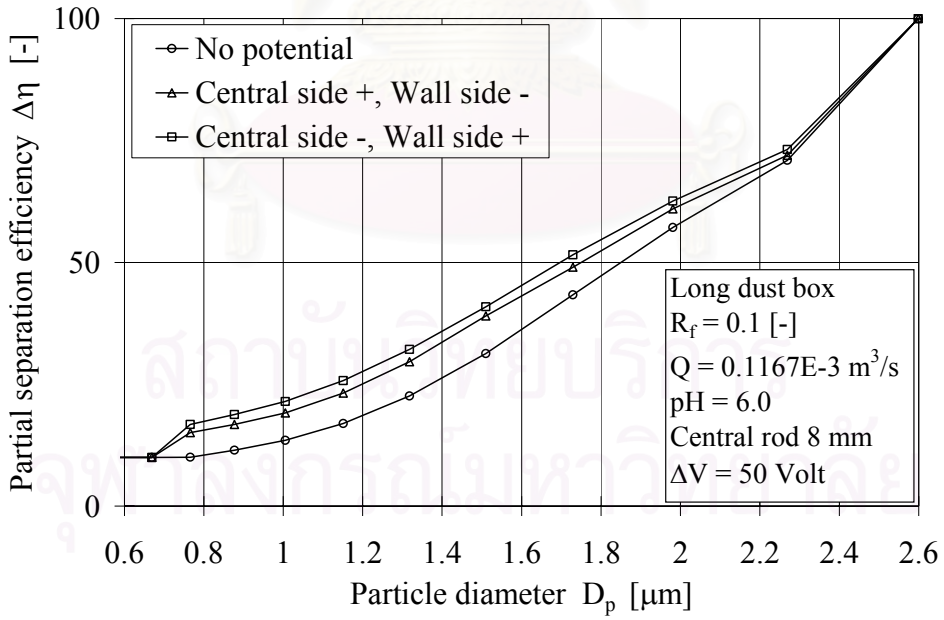

Figure 5.6 Effect of electrical potential on the long dust box of the hydrocyclone in the presence of the underflow at underflow to throughput ratio 0.1, feed flow rate $0.1167*10^{-3}$ m^3/s (7 L/min), pH of suspension 6.0 and central rod diameter 8 mm.

5.1.2.3 Flow rate $0.1667*10^{-3}$ m^3/s (10 L/min)

The effects of dust box length on the classification efficiency in the presence of the underflow were investigated by using the 0.2% solid content by weight of silica suspension fed into the present hydrocyclone. **Figure 5.7** shows the partial separation efficiency when electrical potential was applied to the long dust box (106 mm) of the hydrocyclone in the presence of the underflow at underflow to throughput ratio 0.1, feed flow rate $0.1667*10^{-3}$ m^3/s (10 L/min), pH of suspension 6.0 and central rod diameter 8 mm. The 50% particle cut sizes, d_{50}, obtained from experiments of applying electrical potential to the hydrocyclone were

a) No potential; 1.490 μm
b) Central side +, wall side -; 1.412 μm
c) Central side -, wall side +; 1.368 μm

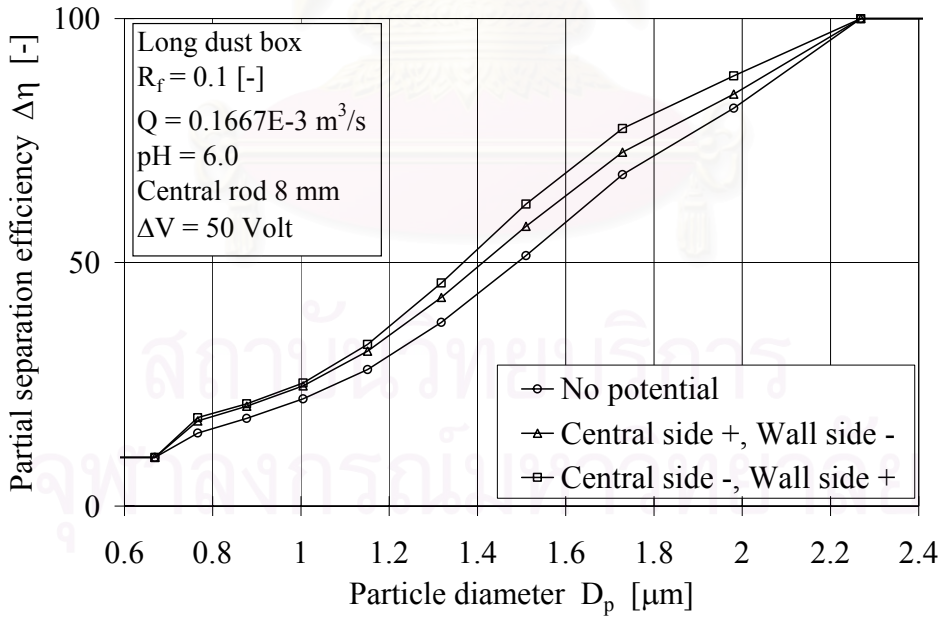

Figure 5.7 Effect of electrical potential on the long dust box of the hydrocyclone in the presence of the underflow at underflow to throughput ratio 0.1, feed flow rate $0.1667*10^{-3}$ m^3/s (10 L/min), pH of suspension 6.0 and central rod diameter 8 mm.

5.1.3 Comparison of effect of feed flow rate between short and long dust box in the presence of the underflow

Figure 5.8 shows the relationship between 50% particle cut size, d_{50}, and suspension feed flow rate, Q, when electrical potential was applied either to the short or the long dust boxes (53 or 106 mm) of the hydrocyclone in the presence of the underflow at underflow to throughput ratio 0.1, pH of suspension 6.0 and central rod diameter 8 mm. The higher the feed flow rate, the smaller the 50% particle cut size. The results confirmed the effect of electrical potential presented in **Figure 5.1** and **Figure 5.3-5.7**.

It was found that the hydrocyclone with a longer dust box exhibited higher classification efficiency because coarse particles had less chance to escape from the vortex finder than that with a short one and the long dust box gave the higher collecting area of the electrodes. The long dust box can reduced the 50% particle cut size by up to 9.66% compared to the short dust box. The lower the feed flow rate, the electrical potential exhibited a stronger effect because the increasing of the retention time to collect the particles of the electrode. The electrical potential decreased the 50% particle cut size by up to 9.72% at the lowest feed flow rate compared to the absence of electricity. In order to obtain the smallest cut size the long dust box should be selected and the system should be operated with positive electrical potential was applied at the side wall and negative electrical potential at the central rod side.

สถาบันวิทยบริการ
จุฬาลงกรณ์มหาวิทยาลัย

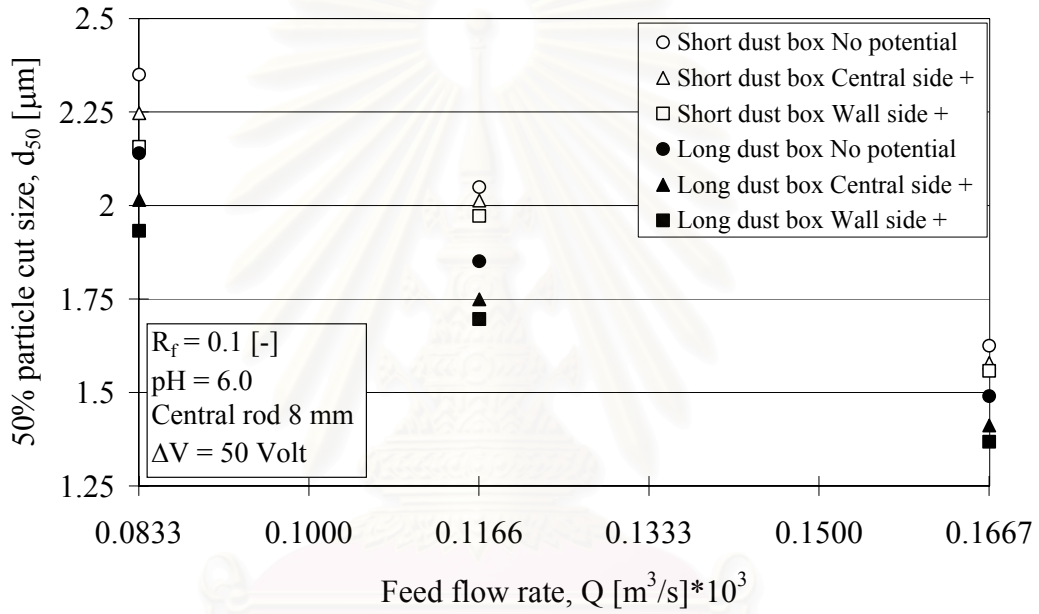

Figure 5.8 Relationship between 50% particle cut size, d_{50}, and suspension feed flow rate, Q, when electrical potential was applied either the short or long dust box (53 or 106 mm) of the hydrocyclone in the presence of the underflow at underflow to throughput ratio 0.1, pH of suspension 6.0 and central rod diameter 8 mm.

5.1.4 Determination of appropriated feed flow rate for subsequent experiments in the presence of the underflow

According to the various feed flow rates in the set of experiments were $0.0833*10^{-3}$, $0.1167*10^{-3}$ and $0.1667*10^{-3}$ m^3/s (5, 7 and 10 L/min), it was found that the suitable feed flow rate for running the experiment in the present hydrocyclone was $0.1167*10^{-3}$ m^3/s. At feed flow rate $0.1167*10^{-3}$ m^3/s, the 50% particle cut sizes were achieved in the range of 1.0-2.0 μm that the major population of particles was in this range as can be seen on the size distribution frequency curve of the feed, **Figure 4.1**.

The experiments using feed flow rate $0.0833*10^{-3}$ m^3/s resulted the 50% particle cut size over 2.0 μm, in this range, the minor population of particles presented therefore the less reliable results were obtained. At the same time, at feed flow rate $0.1667*10^{-3}$ m^3/s, the operated pressure of the system was too high (1.18 Mpa) that the central rod in the dust box could be broken and might resulted in the high risk of physical injury caused by the explosion.

สถาบันวิทยบริการ
จุฬาลงกรณ์มหาวิทยาลัย

5.2 Effect of underflow to throughput ratio on the classification efficiency in the presence of underflow for the long dust box

5.2.1 Underflow to throughput ratio 0.1

See episode 5.1.2.2

5.2.2 Underflow to throughput ratio 0.2

The effects of underflow to throughput ratio on the classification efficiency in the presence of the underflow were investigated by using the 0.2% solid content by weight of silica suspension fed into the present hydrocyclone. **Figure 5.9** shows the partial separation efficiency when electrical potential was applied to the long dust box (106 mm) of the hydrocyclone in the presence of the underflow at underflow to throughput ratio 0.2, feed flow rate $0.1167*10^{-3}$ m^3/s (7 L/min), pH of suspension 6.0 and central rod diameter 8 mm. The 50% particle cut sizes, d_{50}, obtained from experiments of applying electrical potential in the hydrocyclone were

a) No potential; 1.575 μm
b) Central side +, wall side -; 1.497 μm
c) Central side -, wall side +; 1.452 μm

It was found that the electrical potential for positive pole at both the central rod and side wall decreased the 50% particle cut size when compared with no application of electrical potential. The effect of the electrical potential when the positive pole was connected to the side wall was stronger than when the positive pole was connected to the central rod.

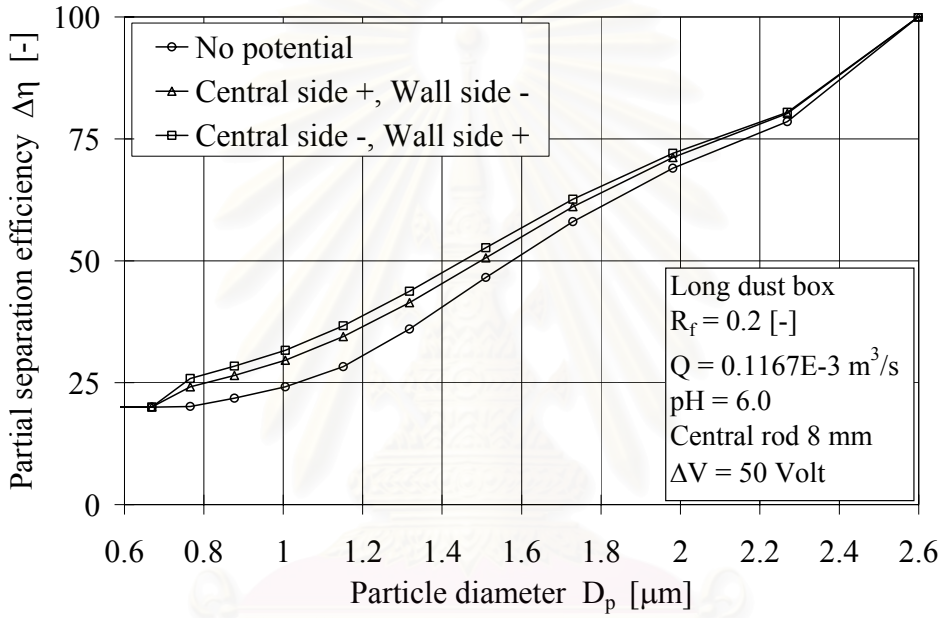

Figure 5.9 Effect of electrical potential on the long dust box of the hydrocyclone in the presence of the underflow at underflow to throughput ratio 0.2, feed flow rate $0.1167*10^{-3}$ m^3/s (7 L/min), pH of suspension 6.0 and central rod diameter 8 mm.

5.2.3 Underflow to throughput ratio 0.3

The effects of underflow to throughput ratio on the classification efficiency in the presence of the underflow were investigated by using the 0.2% solid content by weight of silica suspension fed into the present hydrocyclone. **Figure 5.10** shows the partial separation efficiency when electrical potential was applied to the long dust box (106 mm) of the hydrocyclone in the presence of the underflow at underflow to throughput ratio 0.3, feed flow rate $0.1167*10^{-3}$ m^3/s (7 L/min), pH of suspension 6.0 and central rod diameter 8 mm. The 50% particle cut sizes, d_{50}, obtained from experiments of applying electrical potential in the hydrocyclone were

a) No potential; 1.325 μm
b) Central side +, wall side -; 1.291 μm
c) Central side -, wall side +; 1.255 μm

It was found that the electrical potential for positive pole at both the central rod and side wall decreased the 50% particle cut size when compared with no application of electrical potential. The effect of the electrical potential when the positive pole was connected to the side wall was stronger than when the positive pole was connected to the central rod.

สถาบันวิทยบริการ
จุฬาลงกรณ์มหาวิทยาลัย

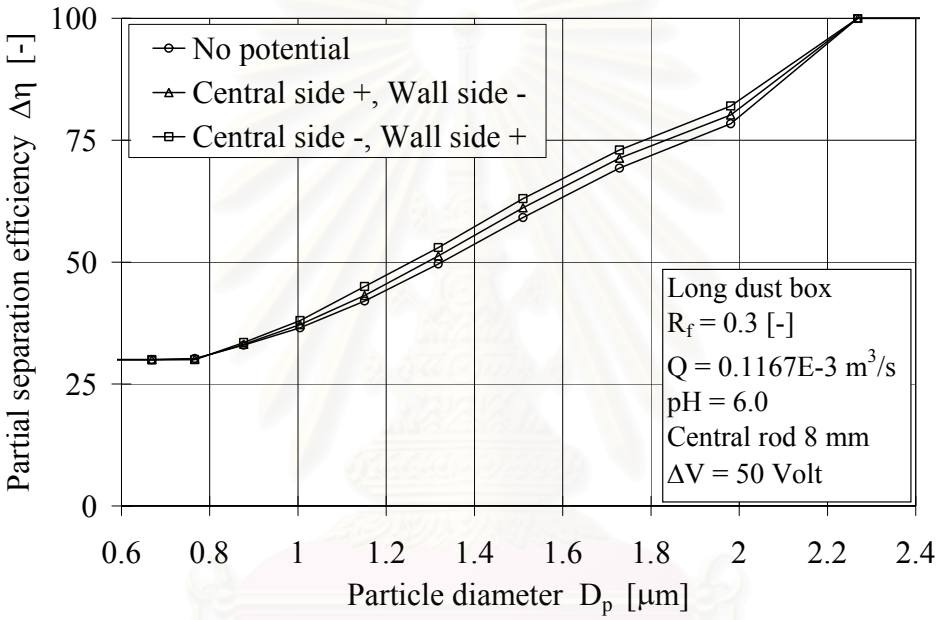

Figure 5.10 Effect of electrical potential on the long dust box of the hydrocyclone in the presence of the underflow at underflow to throughput ratio 0.3, feed flow rate $0.1167*10^{-3}$ m^3/s (7 L/min), pH of suspension 6.0 and central rod diameter 8 mm.

5.2.4 Summary of effect of underflow to throughput ratio

Figure 5.11 shows the relationship between 50% particle cut size, d_{50}, and the underflow to throughput ratio, R_f, by using the long dust box (106 mm) of the hydrocyclone at feed flow rate $0.1167*10^{-3}$ m^3/s (7 L/min), pH of suspension 6.0 and central rod diameter 8 mm with and without electrical potential. As expected, the higher the underflow to throughput ratio, the smaller the particle cut size became. The lower the underflow to throughput ratio, the electrical potential exhibited a stronger effect because the increasing of the retention time to collect the particles of the electrode. The electrical potential decreased the 50% particle cut size by up to 8.37% at the lowest underflow to throughput ratio compared to the absence of electricity. The choice was between high underflow to throughput ratio at low pressure drops and low underflow to throughput ratio at high pressure drops. However, a higher underflow to throughput ratio resulted in a lower solid concentration and vice versa. Depending on the particle size of the feed solids and the cost of further dewatering of the solids in the underflow, the two running costs of dewatering of the solids in the underflow and pressure drop should be weighed against each other and the operating conditions optimized accordingly.

สถาบันวิทยบริการ
จุฬาลงกรณ์มหาวิทยาลัย

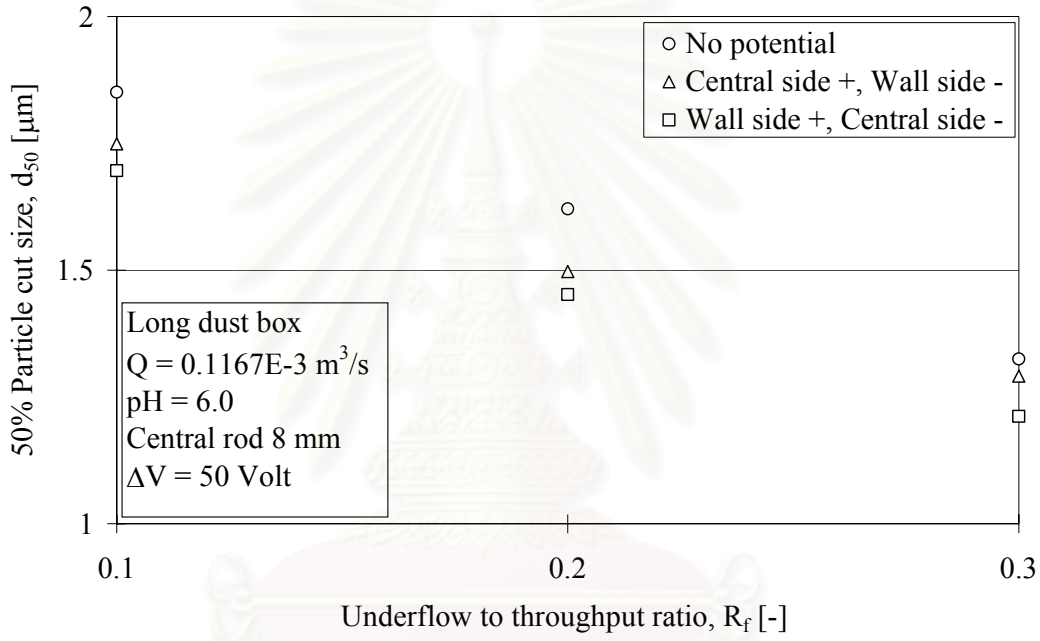

Figure 5.11 Relationship between 50% particle cut size, d_{50}, and the underflow to throughput ratio, R_f, by using the long dust box (106 mm) of the hydrocyclone at feed flow rate $0.1167*10^{-3}$ m^3/s (7 L/min), pH of suspension 6.0 and central rod diameter 8 mm with and without electrical potential.

5.3 Effect of dust box length on the classification efficiency in the absence of the underflow

5.3.1 Short dust box

5.3.1.1 Flow rate $0.0833*10^{-3}$ m^3/s (5 L/min)

The effects of dust box length on the classification efficiency in the absence of the underflow were investigated by using the 0.2% solid content by weight of silica suspension fed into the present hydrocyclone. **Figure 5.12** shows the partial separation efficiency when electrical potential was applied to the short dust box (53 mm) of the hydrocyclone in the absence of the underflow at feed flow rate $0.0833*10^{-3}$ m^3/s (5 L/min), pH of suspension 6.0 and central rod diameter 8 mm. The 50% particle cut sizes, d_{50}, obtained from experiments of applying electrical potential to the hydrocyclone were

a) No potential; 2.540 μm
b) Central side +, wall side -; 2.430 μm
c) Central side -, wall side +; 2.350 μm

It was found that the electrical potential for positive pole at both the central rod and side wall decreased the 50% particle cut size when compared with no application of electrical potential. The effect of the electrical potential when the positive pole was connected to the side wall was stronger than when the positive pole was connected to the central rod.

ศูนย์วิทยทรัพยากร
จุฬาลงกรณ์มหาวิทยาลัย

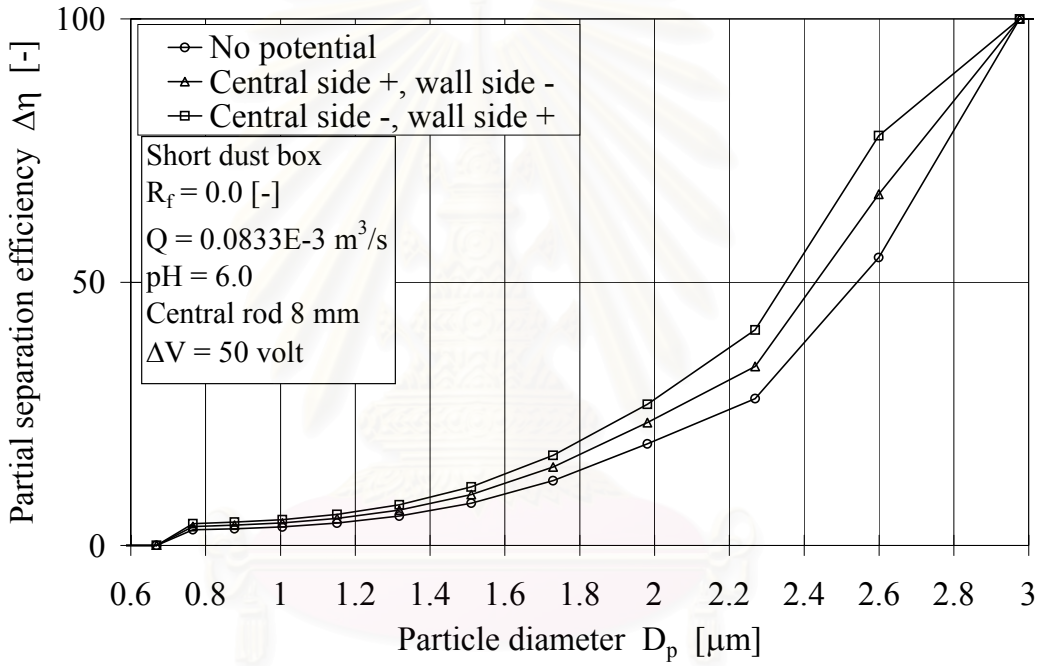

Figure 5.12 Effect of electrical potential on the short dust box of the hydrocyclone in the absence of the underflow at feed flow rate $0.0833*10^{-3}$ m^3/s (5 L/min), pH of suspension 6.0 and central rod diameter 8 mm.

The phenomenon taking place in the hydrocyclone in the absence of the underflow can be described by **Figure 5.13**. In this case, all coarse particles were collected in the dust box. At steady state, amount of particles that suspended in the dust box was constant to maintain force balance in the hydrocyclone. When positive electrical potential was applied to the central rod, a few silica particles hold on the central rod. Similarly, when positive electrical potential was applied to the side wall, some particles hold on the side wall. An amount of accumulative particles, R_d depended on electrical potential surface area; therefore, when positive electrical potential was applied to the central rod, the amount of accumulative particles was less than when positive electrical potential was applied to the side wall. The separation efficiency was proportional to amount of collected particles. It was meaning that, the classification efficiency in case of positive electrical potential was applied at the central rod and negative electrical potential at the side wall was higher than case of no application of electrical potential but lower than case of positive electrical potential was applied at the side wall and negative electrical potential at the central rod.

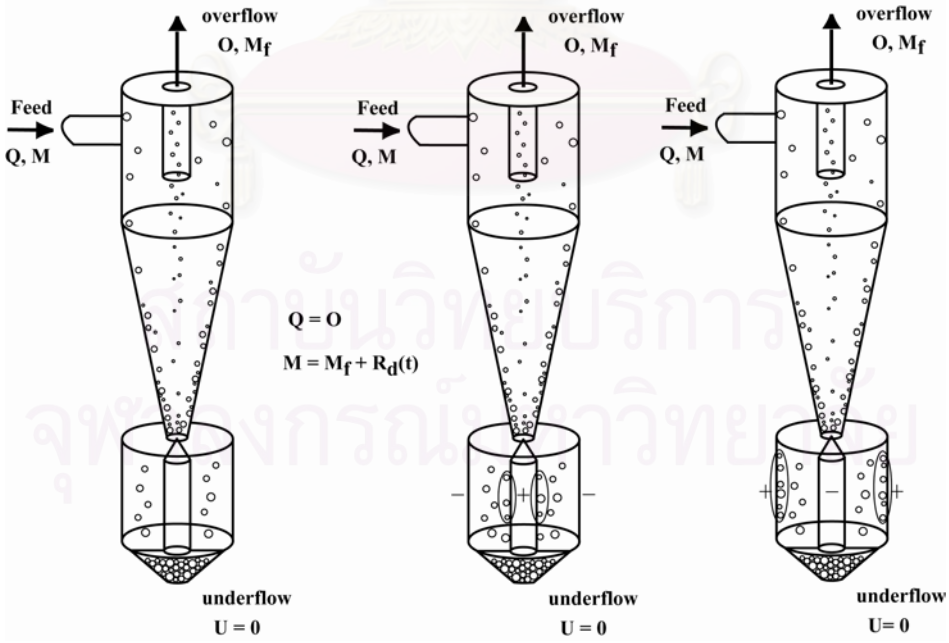

Figure 5.13 Phenomenon in the absence of the underflow

5.3.1.2 Flow rate $0.1167*10^{-3}$ m^3/s (7 L/min)

The effects of dust box length on the classification efficiency in the absence of the underflow were investigated by using the 0.2% solid content by weight of silica suspension fed into the present hydrocyclone. **Figure 5.14** shows the partial separation efficiency when electrical potential was applied to the short dust box (53 mm) of the hydrocyclone in the absence of the underflow at feed flow rate $0.1167*10^{-3}$ m^3/s (7 L/min), pH of suspension 6.0 and central rod diameter 8 mm. The 50% particle cut sizes, d_{50}, obtained from experiments of applying electrical potential to the hydrocyclone were

a) No potential; 2.260 μm
b) Central side +, wall side -; 2.132 μm
c) Central side -, wall side +; 2.107 μm

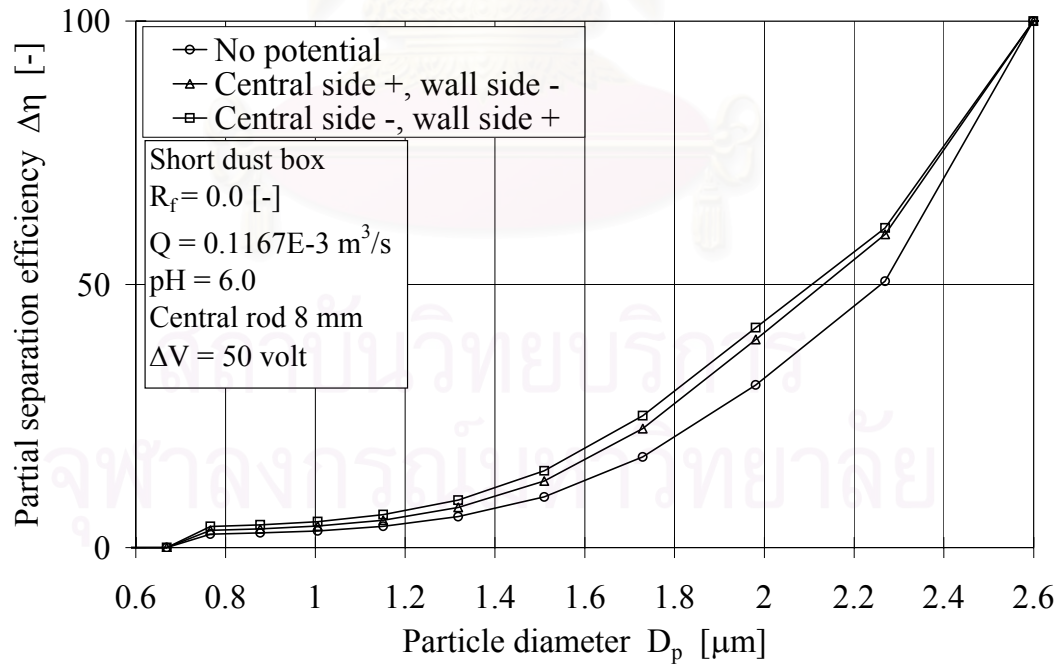

Figure 5.14 Effect of electrical potential on the short dust box of the hydrocyclone in the presence of the underflow at feed flow rate $0.1167*10^{-3}$ m^3/s (7 L/min), pH of suspension 6.0 and central rod diameter 8 mm.

5.3.1.3 Flow rate $0.1667*10^{-3}$ m^3/s (10 L/min)

The effects of dust box length on the classification efficiency in the absence of the underflow were investigated by using the 0.2% solid content by weight of silica suspension fed into the present hydrocyclone. **Figure 5.15** shows the partial separation efficiency when electrical potential was applied to the short dust box (53 mm) of the hydrocyclone in the absence of the underflow at feed flow rate $0.1667*10^{-3}$ m^3/s (10 L/min), pH of suspension 6.0 and central rod diameter 8 mm. The 50% particle cut sizes, d_{50}, obtained from experiments of applying electrical potential to the hydrocyclone were

a) No potential; 1.858 μm
b) Central side +, wall side -; 1.750 μm
c) Central side -, wall side +; 1.691 μm

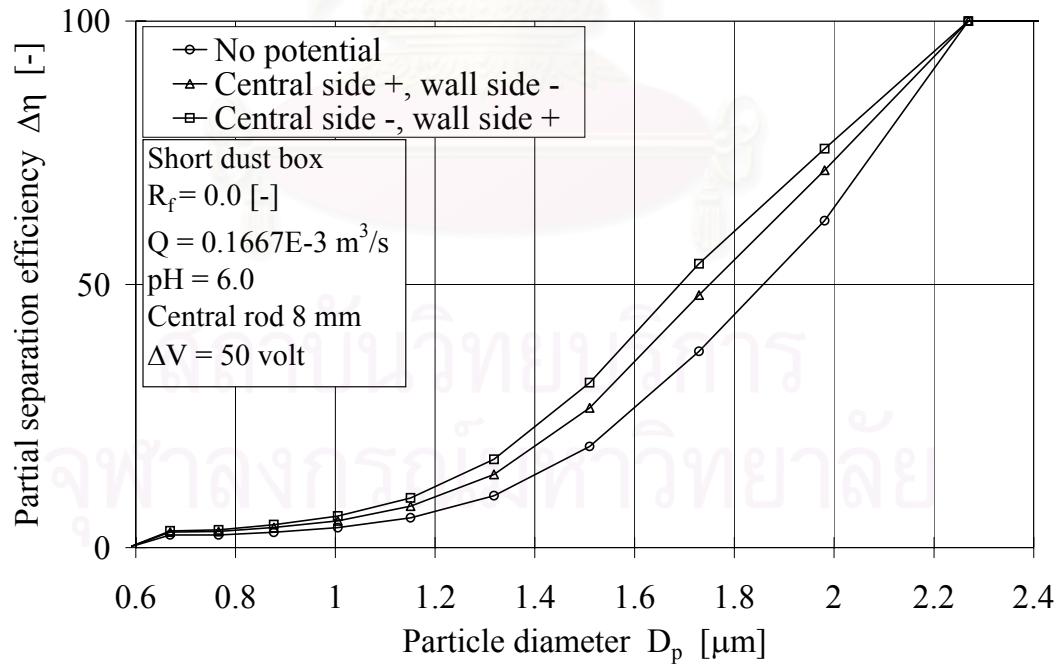

Figure 5.15 Effect of electrical potential on the short dust box of the hydrocyclone in the absence of the underflow at feed flow rate $0.1667*10^{-3}$ m^3/s (10 L/min), pH of suspension 6.0 and central rod diameter 8 mm.

5.3.2 Long dust box

5.3.2.1 Flow rate $0.0833*10^{-3}$ m^3/s (5 L/min)

The effects of dust box length on the classification efficiency in the absence of the underflow were investigated by using the 0.2% solid content by weight of silica suspension fed into the present hydrocyclone. **Figure 5.16** shows the partial separation efficiency when electrical potential was applied to the long dust box (106 mm) of the hydrocyclone in the absence of the underflow at feed flow rate $0.0833*10^{-3}$ m^3/s (5 L/min), pH of suspension 6.0 and central rod diameter 8 mm. The 50% particle cut sizes, d_{50}, obtained from experiments of applying electrical potential to the hydrocyclone were

a) No potential; 2.225 μm
b) Central side +, wall side -; 2.172 μm
c) Central side -, wall side +; 2.022 μm

It was found that the electrical potential for positive pole at both the central rod and side wall decreased the 50% particle cut size when compared with no application of electrical potential. The effect of the electrical potential when the positive pole was connected to the side wall was stronger than when the positive pole was connected to the central rod.

สถาบันวิทยบริการ
จุฬาลงกรณ์มหาวิทยาลัย

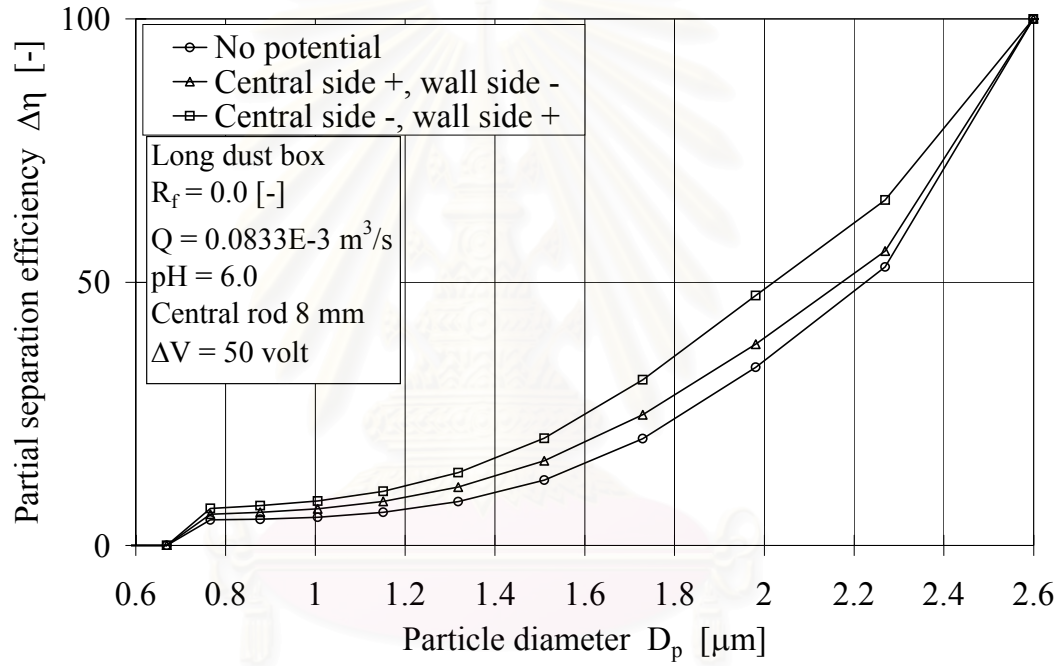

Figure 5.16 Effect of electrical potential on the long dust box of the hydrocyclone in the absence of the underflow at feed flow rate $0.0833*10^{-3}$ m^3/s (5 L/min), pH of suspension 6.0 and central rod diameter 8 mm.

5.3.2.2 Flow rate $0.1167*10^{-3}$ m^3/s (7 L/min)

The effects of dust box length on the classification efficiency in the absence of the underflow were investigated by using the 0.2% solid content by weight of silica suspension fed into the present hydrocyclone. **Figure 5.17** shows the partial separation efficiency when electrical potential was applied to the long dust box (106 mm) of the hydrocyclone in the absence of the underflow at feed flow rate $0.1167*10^{-3}$ m^3/s (7 L/min), pH of suspension 6.0 and central rod diameter 8 mm. The 50% particle cut sizes, d_{50}, obtained from experiments of applying electrical potential to the hydrocyclone were

a) No potential; 2.044 μm
b) Central side +, wall side -; 1.964 μm
c) Central side -, wall side +; 1.856 μm

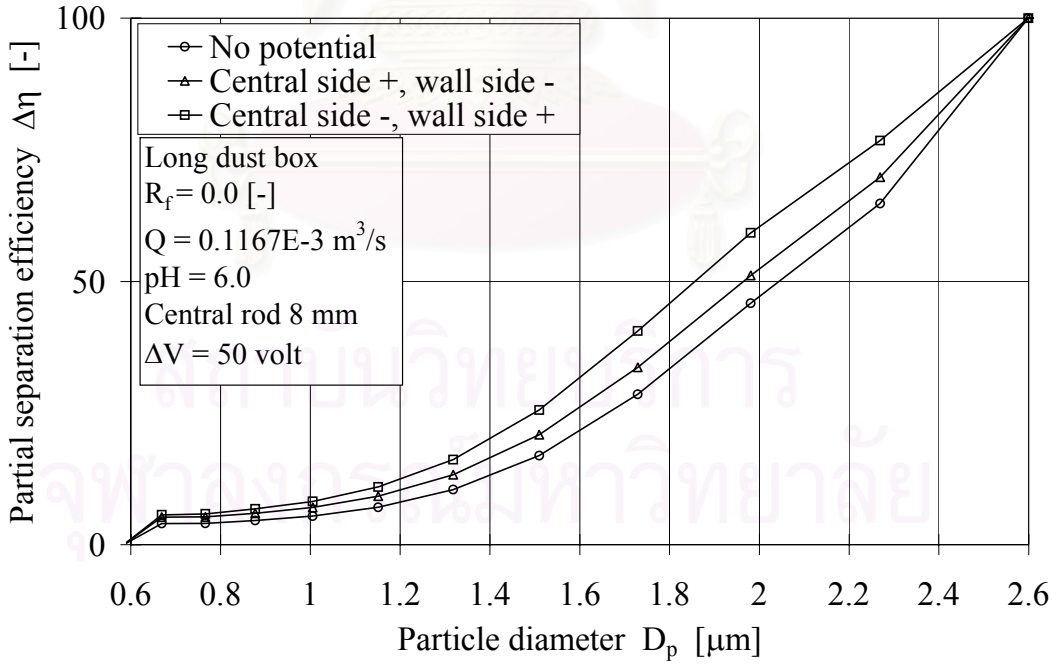

Figure 5.17 Effect of electrical potential on the long dust box of the hydrocyclone in the absence of the underflow at feed flow rate $0.1167*10^{-3}$ m^3/s (7 L/min), pH of suspension 6.0 and central rod diameter 8 mm.

5.3.2.3 Flow rate $0.1667*10^{-3}$ m^3/s (10 L/min)

The effects of dust box length on the classification efficiency in the absence of the underflow were investigated by using the 0.2% solid content by weight of silica suspension fed into the present hydrocyclone. **Figure 5.18** shows the partial separation efficiency when electrical potential was applied to the long dust box (106 mm) of the hydrocyclone in the absence of the underflow at feed flow rate $0.1667*10^{-3}$ m^3/s (10 L/min), pH of suspension 6.0 and central rod diameter 8 mm. The 50% particle cut sizes, d_{50}, obtained from experiments of applying electrical potential to the hydrocyclone were

a) No potential; 1.642 μm
b) Central side +, wall side -; 1.522 μm
c) Central side -, wall side +; 1.484 μm

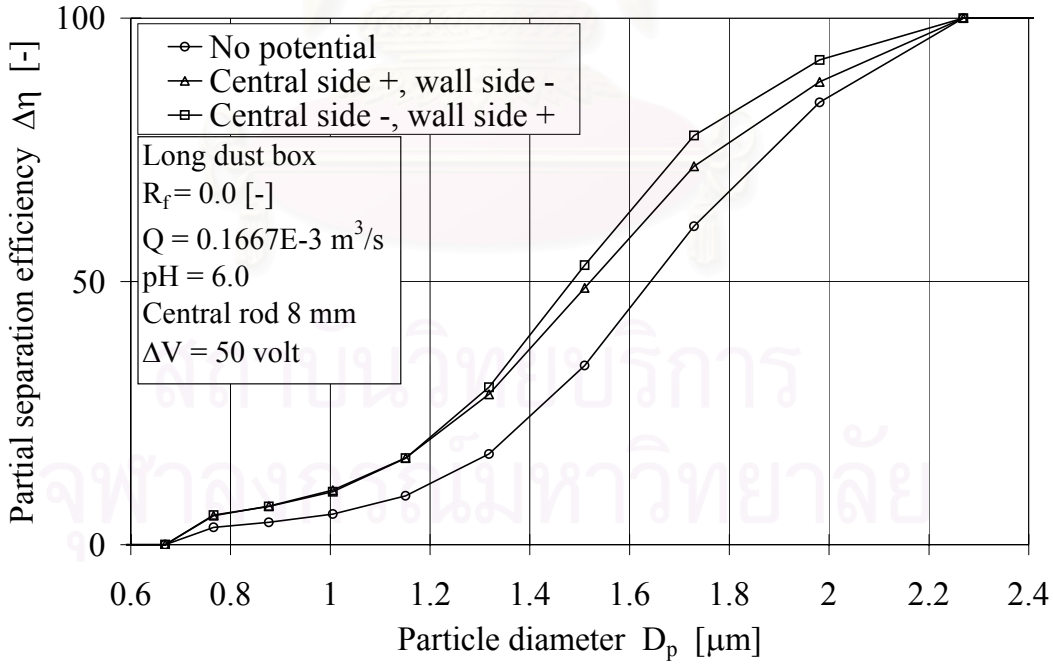

Figure 5.18 Effect of electrical potential on the long dust box of the hydrocyclone in the absence of the underflow at feed flow rate $0.1667*10^{-3}$ m^3/s (10 L/min), pH of suspension 6.0 and central rod diameter 8 mm.

5.3.3 Comparison of effect of feed flow rate between short and long dust box in the absence of the underflow

Figure 5.19 shows the relationship between 50% particle cut size, d_{50} and suspension feed flow rate, Q, when electrical potential was applied either to the short or the long dust boxes (53 or 106 mm) of the hydrocyclone in the absence of the underflow at pH of suspension 6.0 and central rod diameter 8 mm. The higher the feed flow rate, the smaller the 50% particle cut size became. The results confirmed the effect of electrical potential in **Figure 5.12** and **Figure 5.14-5.18**.

It was found that the hydrocyclone with a longer dust box exhibited higher classification efficiency because coarse particles had less chance to escape from the vortex finder than that with a short one. The long dust box can reduced the 50% particle cut size by up to 12.40% compared to the short dust box. The feed flow rates had not significant affected corresponding to the electrical potential because there was no underflow. Therefore the retention time to collect the particles of the electrode was the same at all feed flow rates. The electrical potential decreased the 50% particle cut size by up to 9.62% compared to the absence of electricity. In order to obtain the smallest cut size the long dust box should be selected and the system was operated with positive electrical potential was applied at the side wall and negative electrical potential at the central rod side.

สถาบันวิทยบริการ
จุฬาลงกรณ์มหาวิทยาลัย

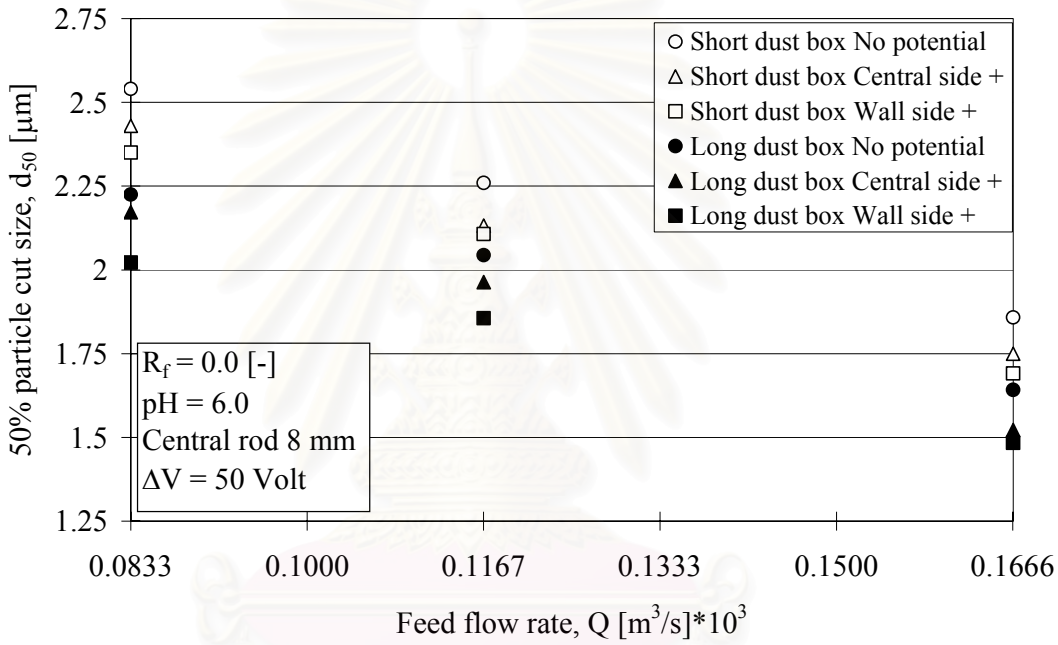

Figure 5.19 Relationship between 50% particle cut size, d_{50}, and suspension feed flow rate, Q, when electrical potential was applied either the short or long dust box (53 or 106 mm) of the hydrocyclone in the absence of the underflow at pH of suspension 6.0 and central rod diameter 8 mm.

5.3.4 Determination of appropriated feed flow rate for subsequent experiments in the absence of the underflow

According to the various feed flow rates in the set of experiments were $0.0833*10^{-3}$, $0.1167*10^{-3}$ and $0.1667*10^{-3}$ m^3/s (5, 7 and 10 L/min). It was found that, the suitable feed flow rate for running the experiment in the present hydrocyclone was $0.1167*10^{-3}$ m^3/s. At feed flow rate $0.1167*10^{-3}$ m^3/s, the 50% particle cut sizes were achieved in the range of 1.0-2.0 μm that the major population of particles was in this range as can be seen on the size distribution frequency curve of the feed, **Figure 4.1**.

The experiments using feed flow rate $0.0833*10^{-3}$ m^3/s resulted the 50% particle cut size over 2.0 μm, in this range, the minor population of particles presented therefore the less reliable results were obtained. At the same time, at feed flow rate $0.1667*10^{-3}$ m^3/s, the operated pressure of the system was too high (1.18 Mpa) that the central rod in the dust box could be broken and might resulted in the high risk of physical injury caused by the explosion.

สถาบันวิทยบริการ
จุฬาลงกรณ์มหาวิทยาลัย

5.4 Comparison of effect of the underflow

According to the previous experimental results (**Figure 5.8 and 5.19**), it was found that in both the presence and absence of the underflow, the hydrocyclone with a long dust box exhibited higher classification efficiency than that with a short dust box. In both the presence and absence of the underflow, the electrical potential for positive pole at both the central rod and side wall decreased the 50% particle cut size when compared with no application of electrical potential. The presence of the underflow gave better classification efficiency than the absence of the underflow. In both the presence and absence of the underflow, effect of electrical potential when the positive pole was connected to the side wall was stronger than when the positive pole was connected to the central rod. The best conditions of the presence and absence of the underflow to obtain the smallest cut size were that the long dust box be used, the system was operated with positive electrical potential was applied at the side wall and negative electrical potential was applied at the central rod side. When compared the smallest 50% particle cut size that obtained between the presence and absence of the underflow, it was found that, the presence of the underflow in corporate with electrical potential resulted the 50% particle cut size smaller than that the absence of the underflow at the same conditions. Therefore, the conditions that had potentially to study and develop in order to accomplish the smallest 50% particle cut size were the presence of the underflow incorporated with electrical potential and absolutely with the long dust box. Unfortunately, the miss analyzed of the experimental results in the presence of the underflow caused to give the reverse conclusions. The further experiments were only concentrated in the absence of the underflow.

สถาบันวิทยบริการ
จุฬาลงกรณ์มหาวิทยาลัย

5.5 Effect of pH in the absence of the underflow

5.5.1 Original pH of suspension 6.0

5.5.1.1 Flow rate $0.0833*10^{-3}$ m^3/s (5 L/min)

See episode 5.3.2.1

5.5.1.2 Flow rate $0.1167*10^{-3}$ m^3/s (7 L/min)

See episode 5.3.2.2

5.5.2 pH of suspension 8.0

5.5.2.1 Flow rate $0.0833*10^{-3}$ m^3/s (5 L/min)

The effects of pH of suspension on the classification efficiency in the absence of the underflow were investigated by using the 0.2% solid content by weight of silica suspension fed into the present hydrocyclone. We adjusted the pH of suspension by adding concentrated of NaOH solution to the silica suspension. **Figure 5.20** shows the partial separation efficiency when electrical potential was applied to the long dust box (106 mm) of the hydrocyclone in the absence of the underflow at feed flow rate $0.0833*10^{-3}$ m^3/s (5 L/min), pH of suspension 8.0 and central rod diameter 8 mm. The 50% particle cut sizes, d_{50}, obtained from experiments of applying electrical potential to the hydrocyclone were

a) No potential; 2.201 μm
b) Central side +, wall side -; 2.161 μm
c) Central side -, wall side +; 2.005 μm

It was found that the electrical potential for positive pole at both the central rod and side wall decreased the 50% particle cut size when compared with no application of electrical potential. The effect of the electrical potential when the positive pole was connected to the side wall was stronger than when the positive pole was connected to the central rod.

According to the measurement of zeta potential of silica particle at various pH of suspension (see Appendix B), it was found that pH affect on the value of zeta potential. The zeta potential proportionally increased in the negative value with the pH of suspension. The higher the zeta potential resulted the stronger the effect of electrical potential on the silica particles. The phenomenon taking place in the hydrocyclone at the higher pH of suspension condition was the same as **Figure 5.13** merely the electric force was greater than that the lower pH of suspension condition.

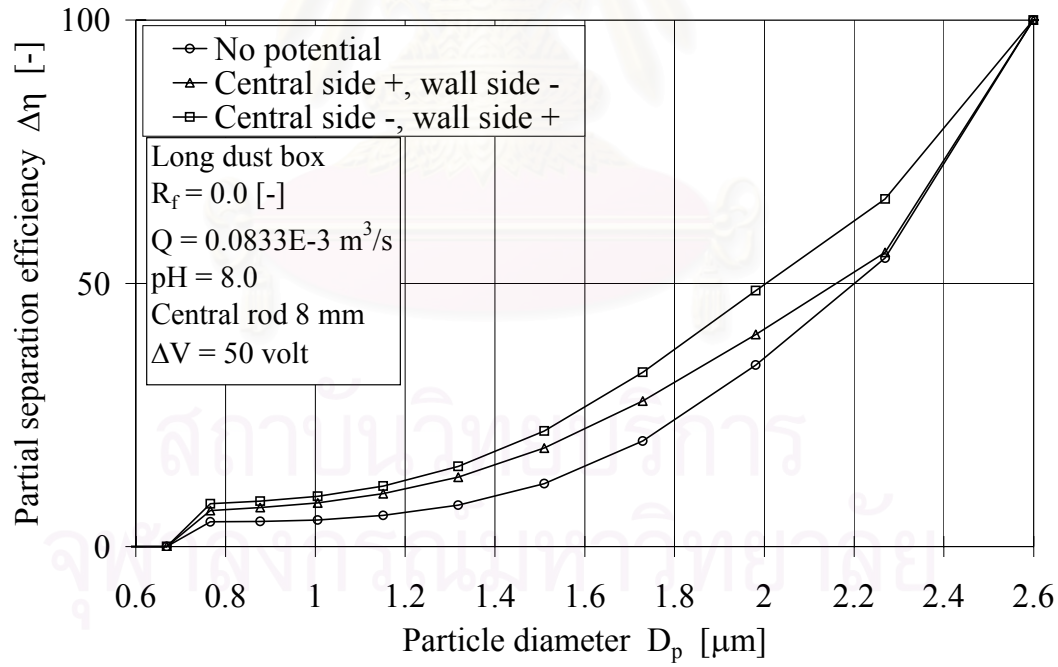

Figure 5.20 Effect of electrical potential on the long dust box of the hydrocyclone in the absence of the underflow at feed flow rate $0.0833*10^{-3}$ m^3/s (5 L/min), pH of suspension 8.0 and central rod diameter 8 mm.

5.5.2.2 Flow rate $0.1167*10^{-3}$ m^3/s (7 L/min)

The effects of pH of suspension on the classification efficiency in the absence of the underflow were investigated by using the 0.2% solid content by weight of silica suspension fed into the present hydrocyclone. We adjusted the pH of suspension by adding concentrated of NaOH solution to the silica suspension. **Figure 5.21** shows the partial separation efficiency when electrical potential was applied to the long dust box (106 mm) of the hydrocyclone in the absence of the underflow at feed flow rate $0.1167*10^{-3}$ m^3/s (7 L/min), pH of suspension 8.0 and central rod diameter 8 mm. The 50% particle cut sizes, d_{50}, obtained from experiments of applying electrical potential to the hydrocyclone were

a) No potential; 1.961 μm
b) Central side +, wall side -; 1.875 μm
c) Central side -, wall side +; 1.785 μm

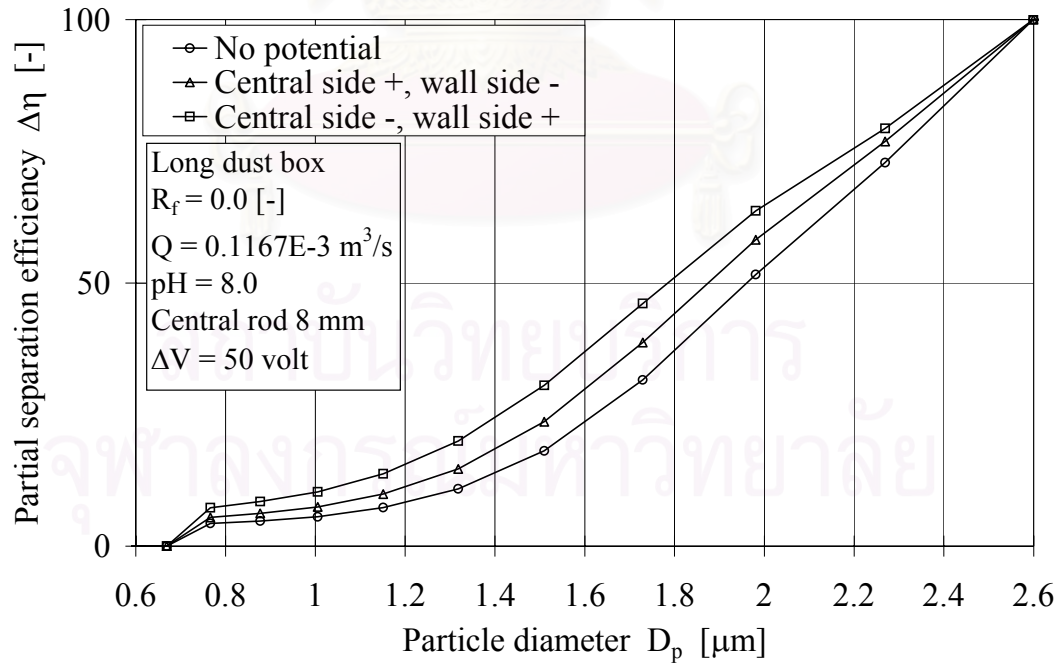

Figure 5.21 Effect of electrical potential on the long dust box of the hydrocyclone in the absence of the underflow at feed flow rate $0.1167*10^{-3}$ m^3/s (7 L/min), pH of suspension 8.0 and central rod diameter 8 mm.

5.5.3 pH of suspension 9.0

5.5.3.1 Flow rate $0.0833*10^{-3}$ m^3/s (5 L/min)

The effects of pH of suspension on the classification efficiency in the absence of the underflow were investigated by using the 0.2% solid content by weight of silica suspension fed into the present hydrocyclone. We adjusted the pH of suspension by adding concentrated of NaOH solution to the silica suspension. **Figure 5.22** shows the partial separation efficiency when electrical potential was applied to the long dust box (106 mm) of the hydrocyclone in the absence of the underflow at feed flow rate $0.0833*10^{-3}$ m^3/s (5 L/min), pH of suspension 9.0 and central rod diameter 8 mm. The 50% particle cut sizes, d_{50}, obtained from experiments of applying electrical potential to the hydrocyclone were

a) No potential; 2.193 μm
b) Central side +, wall side -; 2.149 μm
c) Central side -, wall side +; 1.995 μm

It was found that the electrical potential for positive pole at both the central rod and side wall decreased the 50% particle cut size when compared with no application of electrical potential. The effect of the electrical potential when the positive pole was connected to the side wall was stronger than when the positive pole was connected to the central rod.

จุฬาลงกรณ์มหาวิทยาลัย

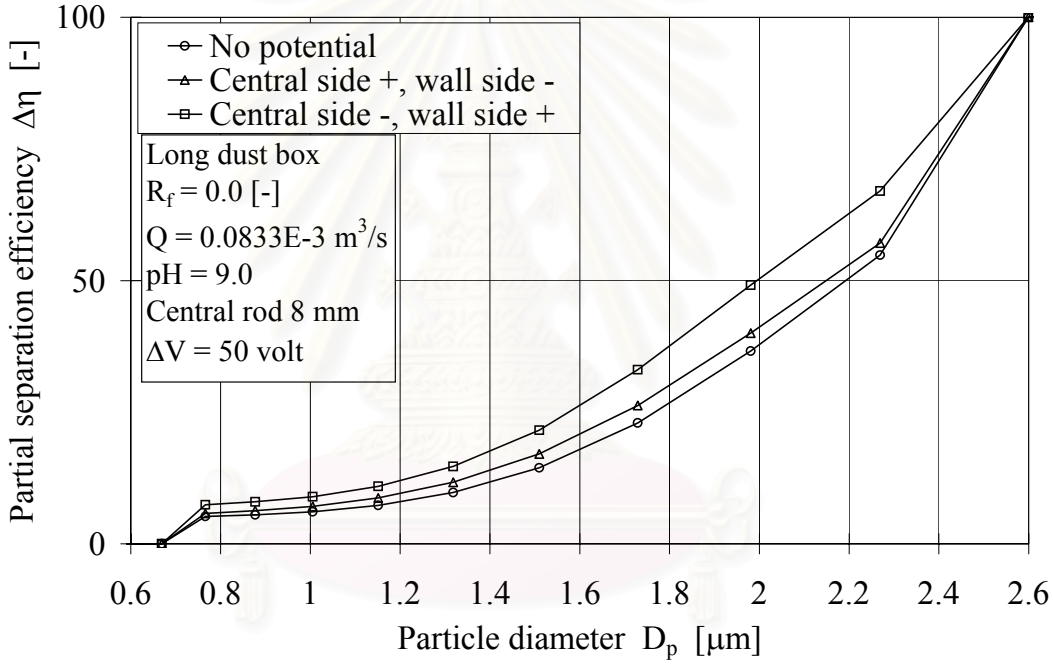

Figure 5.22 Effect of electrical potential on the long dust box of the hydrocyclone in the absence of the underflow at feed flow rate $0.0833*10^{-3}$ m^3/s (5 L/min), pH of suspension 9.0 and central rod diameter 8 mm.

5.5.3.2 Flow rate $0.1167*10^{-3}$ m^3/s (7 L/min)

The effects of pH of suspension on the classification efficiency in the absence of the underflow were investigated by using the 0.2% solid content by weight of silica suspension fed into the present hydrocyclone. We adjusted the pH of suspension by adding concentrated of NaOH solution to the silica suspension. **Figure 5.23** shows the partial separation efficiency when electrical potential was applied to the long dust box (106 mm) of the hydrocyclone in the absence of the underflow at feed flow rate $0.1167*10^{-3}$ m^3/s (7 L/min), pH of suspension 9.0 and central rod diameter 8 mm. The 50% particle cut sizes, d_{50}, obtained from experiments of applying electrical potential to the hydrocyclone were

a) No potential; 2.033 μm
b) Central side +, wall side -; 1.859 μm
c) Central side -, wall side +; 1.757 μm

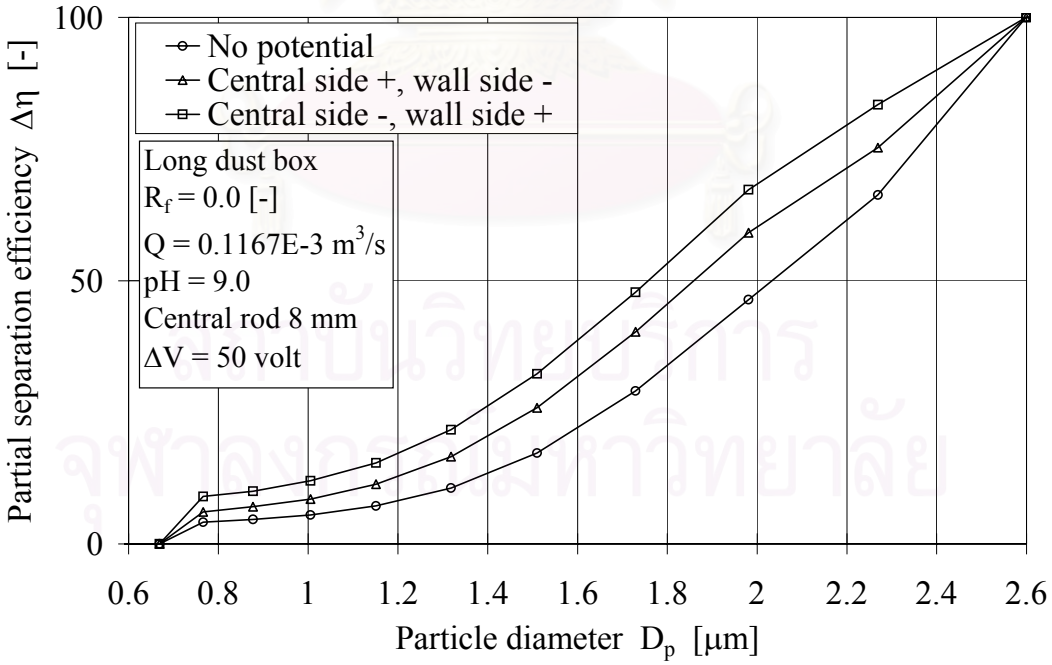

Figure 5.23 Effect of electrical potential on the long dust box of the hydrocyclone in the absence of the underflow at feed flow rate $0.1167*10^{-3}$ m^3/s (7 L/min), pH of suspension 9.0 and central rod diameter 8 mm.

5.5.4 pH of suspension 10.0

5.5.4.1 Flow rate $0.0833*10^{-3}$ m^3/s (5 L/min)

The effects of pH of suspension on the classification efficiency in the absence of the underflow were investigated by using the 0.2% solid content by weight of silica suspension fed into the present hydrocyclone. We adjusted the pH of suspension by adding concentrated of NaOH solution to the silica suspension. **Figure 5.24** shows the partial separation efficiency when electrical potential was applied to the long dust box (106 mm) of the hydrocyclone in the absence of the underflow at feed flow rate $0.0833*10^{-3}$ m^3/s (5 L/min), pH of suspension 10.0 and central rod diameter 8 mm. The 50% particle cut sizes, d_{50}, obtained from experiments of applying electrical potential to the hydrocyclone were

a) No potential; 2.226 μm
b) Central side +, wall side -; 2.123 μm
c) Central side -, wall side +; 1.991 μm

It was found that the electrical potential for positive pole at both the central rod and side wall decreased the 50% particle cut size when compared with no application of electrical potential. The effect of the electrical potential when the positive pole was connected to the side wall was stronger than when the positive pole was connected to the central rod because the side wall has more surface area than the central rod.

จุฬาลงกรณ์มหาวิทยาลัย

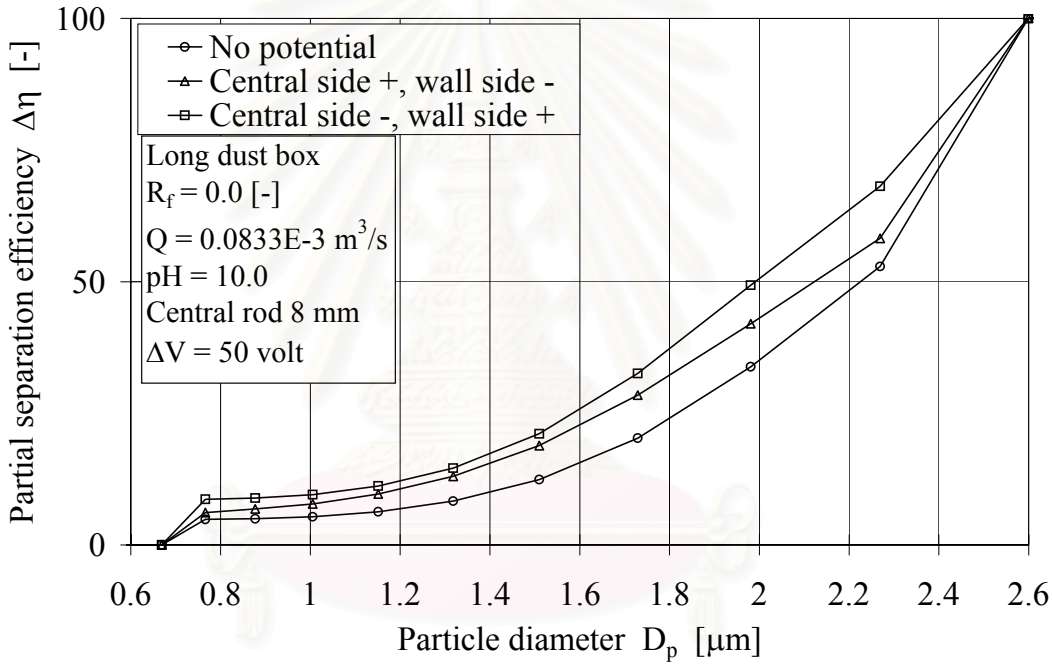

Figure 5.24 Effect of electrical potential on the long dust box of the hydrocyclone in the absence of the underflow at feed flow rate $0.0833*10^{-3}$ m^3/s (5 L/min), pH of suspension 10.0 and central rod diameter 8 mm.

5.5.4.2 Flow rate $0.1167*10^{-3}$ m^3/s (7 L/min)

The effects of pH of suspension on the classification efficiency in the absence of the underflow were investigated by using the 0.2% solid content by weight of silica suspension fed into the present hydrocyclone. We adjusted the pH of suspension by adding concentrated of NaOH solution to the silica suspension. **Figure 5.25** shows the partial separation efficiency when electrical potential was applied to the long dust box (106 mm) of the hydrocyclone in the absence of the underflow at feed flow rate $0.1167*10^{-3}$ m^3/s (7 L/min), pH of suspension 10.0 and central rod diameter 8 mm. The 50% particle cut sizes, d_{50}, obtained from experiments of applying electrical potential to the hydrocyclone were

a) No potential; 2.029 μm
b) Central side +, wall side -; 1.842 μm
c) Central side -, wall side +; 1.648 μm

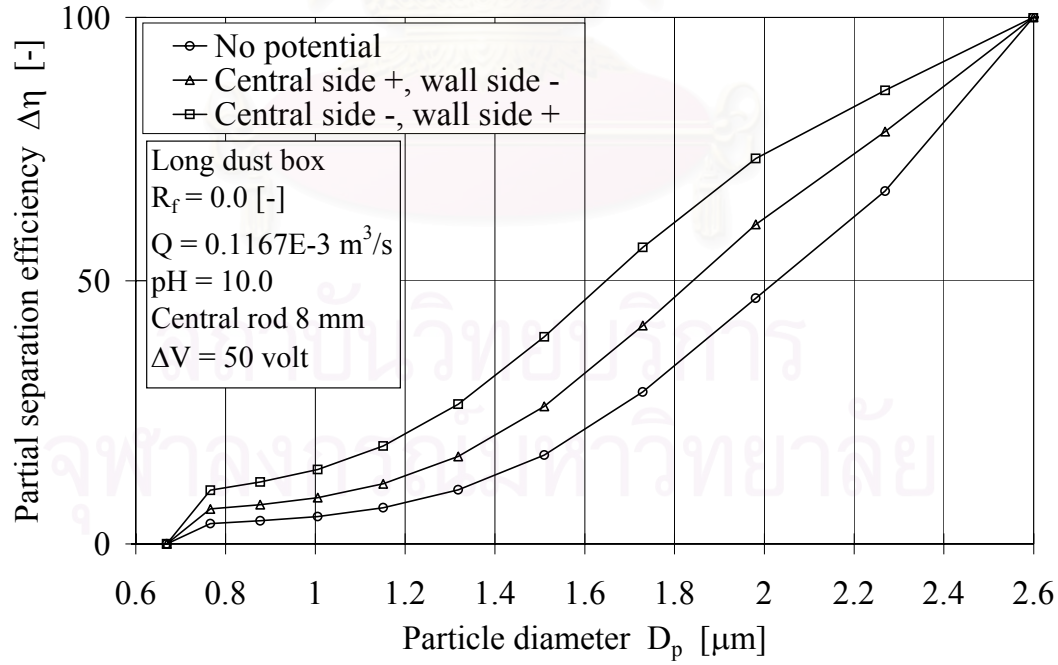

Figure 5.25 Effect of electrical potential on the long dust box of the hydrocyclone in the absence of the underflow at feed flow rate $0.1167*10^{-3}$ m^3/s (7 L/min), pH of suspension 10.0 and central rod diameter 8 mm.

5.5.5 Summary of effect of pH in the absence of the underflow

Figure 5.26 shows the relationship between 50% particle cut size d_{50} and pH of suspension when electrical potential was applied to the long dust box (106 mm) of the hydrocyclone in the absence of the underflow at feed flow rate either $0.0833*10^{-3}$ or $0.1167*10^{-3}$ m^3/s (5 or 7 L/min) and central rod diameter 8 mm. The higher the pH of suspension, the smaller the 50% particle cut size becomes. The results summarized the effect of electrical potential in **Figure 5.16-5.17** and **Figure 5.20-5.25**. Subsequently, the higher the feed flow rate, the smaller the 50% particle cut size.

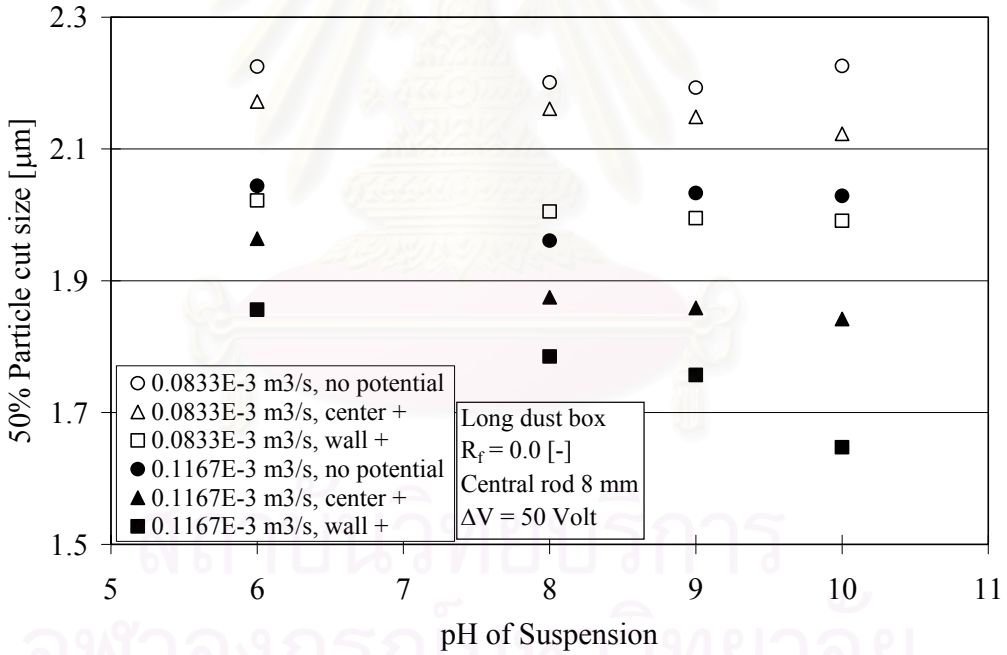

Figure 5.26 Relationship between 50% particle cut size, d_{50}, and pH of suspension when electrical potential was applied to the long dust box (106 mm) of the hydrocyclone in the absence of the underflow at feed flow rate either $0.0833*10^{-3}$ or $0.1167*10^{-3}$ m^3/s (5 or 7 L/min) and central rod diameter 8 mm.

It was found that the electrical potential exhibited a stronger effect when the suspension had higher pH because particles had higher zeta potential. The effect of pH of suspension at 10.0 with electrical potential can reduced the 50% particle cut size by up to 11.21% compared to the pH of suspension at 6.0 with electrical potential. Moreover, the electrical potential with reinforcement of pH can reduced the 50% particle cut size by up to 18.78% compared to the absence of electricity. At the high pH of suspension condition, particles had high zeta potential caused to the high electrostatic force that mean not only the silica particles in the dust box easily hold on the positive electrode but also amount of attached particles was increased. Amount of attached particles depended on the magnitude of electrostatic force and surface area of electrode. Therefore, amount of attached particles when suspension has higher pH was more than that amount of attached particles when suspension has lower pH. Subsequently, amount of attached particles when positive electrical potential was applied to the side wall was more than that amount of attached particles when positive electrical potential was applied to the central rod because the side wall had more surface area than the central rod as shown in **Figure 5.27**. The separation efficiency was proportional to amount of collected particles. It was meaning that, the classification efficiency in case of positive electrical potential was applied at the central rod and negative electrical potential at the side wall was higher than case of no application of electrical potential but lower than case of positive electrical potential was applied at the side wall and negative electrical potential at the central rod. However, the pH of suspension was no effect when the system was operated with no application of electrical potential.

In order to obtain the smallest cut size the long dust box should be selected and the system was operated with positive electrical potential applied at the side wall and negative electrical potential at the central rod side with the reinforcement of the high pH of suspension.

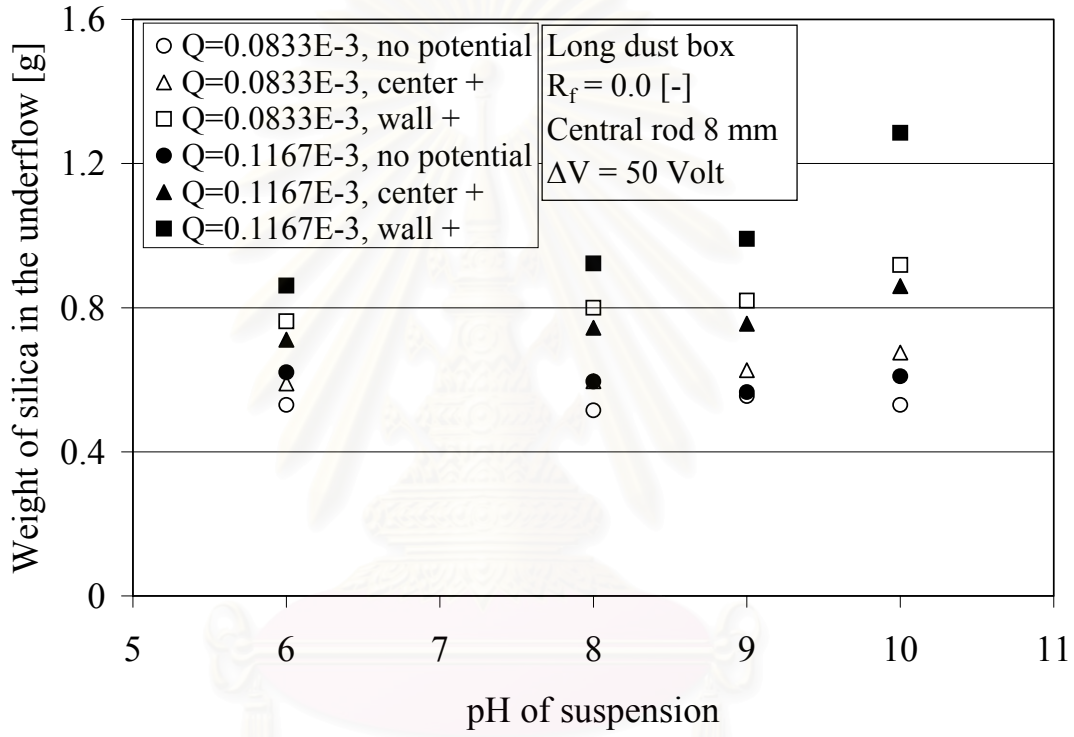

Figure 5.27 Relationship between weight of silica in the underflow and pH of suspension when electrical potential was applied to the long dust box (106 mm) of the hydrocyclone in the absence of the underflow at feed flow rate either $00833*10^{-3}$ or $0.1167*10^{-3}$ m^3/s (5 or 7 L/min) and central rod diameter 8 mm.

5.6 Effect of central rod diameter in the absence of the underflow

5.6.1 Central rod diameter 8 mm

5.6.1.1 pH of suspension 6.0

See episode 5.5.1.2

5.6.1.2 pH of suspension 9.0

See episode 5.5.3.2

5.6.2 Central rod diameter 12 mm

5.6.2.1 pH of suspension 6.0

The effects of central rod diameter on the classification efficiency in the absence of the underflow were investigated by using the 0.2% solid content by weight of silica suspension fed into the present hydrocyclone. **Figure 5.28** shows the partial separation efficiency when electrical potential was applied to the long dust box (106 mm) of the hydrocyclone in the absence of the underflow at feed flow rate $0.1167*10^{-3}$ m^3/s (7 L/min), pH of suspension 6.0 and central rod diameter 12 mm. The 50% particle cut sizes, d_{50}, obtained from experiments of applying electrical potential to the hydrocyclone were

a) No potential; 1.985 μm
c) Central side -, wall side +; 1.830 μm

It was found that the electrical potential for positive pole at the side wall decreased the 50% particle cut size when compared with no application of electrical potential.

The series of experiments for study effects of central rod diameter consisted only of two different conditions were: a) no application of electrical potential and c) positive electrical potential was applied at the side wall and negative electrical potential at the central rod. Since not only all of the previous experiments showed that case c) with positive electrical potential was applied at the side wall and negative electrical potential at the central rod exhibited a stronger effect than case b) with positive electrical potential was applied at the central rod and negative electrical potential at the side wall but also the limitation of the study time. Therefore, case b) was ignored in this study.

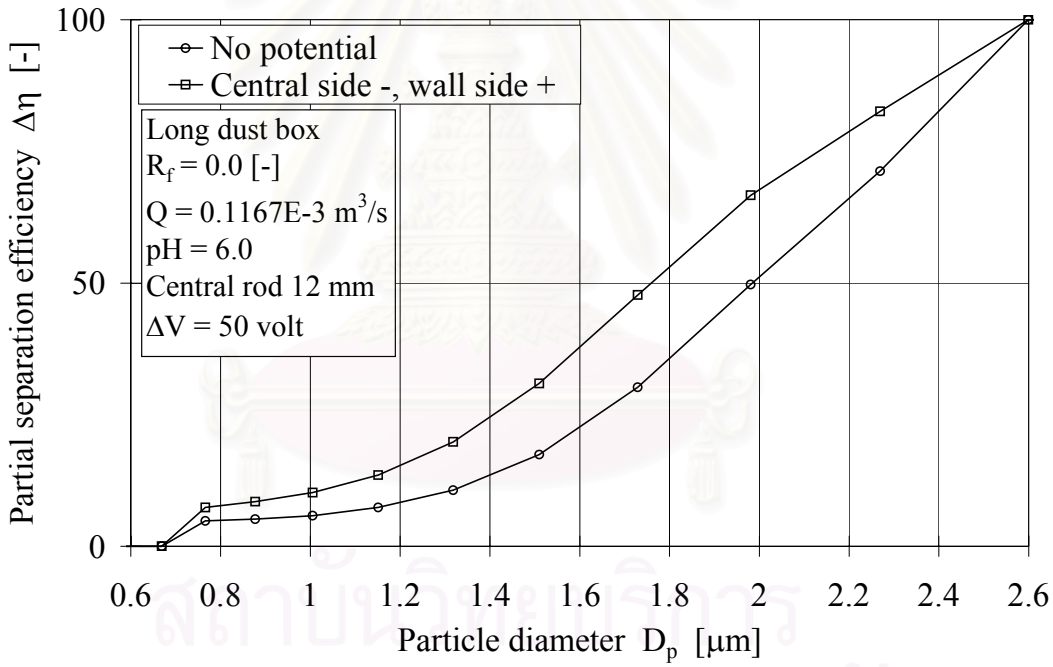

Figure 5.28 Effect of electrical potential on the long dust box of the hydrocyclone in the absence of the underflow at feed flow rate $0.1167*10^{-3}$ m^3/s (7 L/min), pH of suspension 6.0 and central rod diameter 12 mm.

5.6.2.2 pH of suspension 9.0

The effects of central rod diameter on the classification efficiency in the absence of the underflow were investigated by using the 0.2% solid content by weight of silica suspension fed into the present hydrocyclone. **Figure 5.29** shows the partial separation efficiency when electrical potential was applied to the long dust box (106 mm) of the hydrocyclone in the absence of the underflow at feed flow rate $0.1167*10^{-3}$ m^3/s (7 L/min), pH of suspension 9.0 and central rod diameter 12 mm. The 50% particle cut sizes, d_{50}, obtained from experiments of applying electrical potential to the hydrocyclone were

a) No potential; 1.961 μm
c) Central side -, wall side +; 1.653 μm

The appropriated high pH of suspension for investigating effect of central rod diameter was 9.0 because the variation of conductivity of deionized water. At high pH, pH 10.0 for example, suspension had too many sodium and hydroxide ions that interfered the system to achieve the voltage set point. The DC power generator was set to constantly supply voltage at 50 volt and maximum current at 400 mA for security reason. The total ions in the suspension consisted of original ions from deionized water plus sodium and hydroxide ions from addition of NaOH. From experiment, these were found that, if the suspension had too many ions, it was impossible to accomplish both targets of voltage and current at the same time. The voltage was not attaining set point although the current reached the maximum current. In order to ignore the problem from the variation of conductivity of deionized water, the investigated pH of suspension should not too high. Therefore, pH of suspension 9.0 was suitable.

It was found that the electrical potential for positive pole at the side wall decreased the 50% particle cut size when compared with no application of electrical potential.

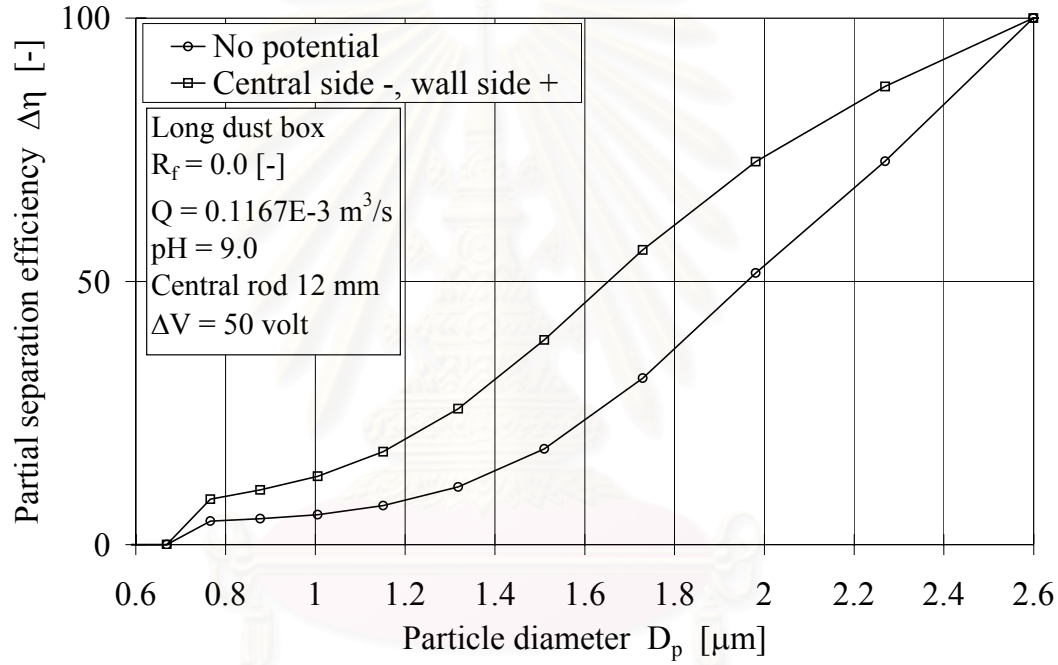

Figure 5.29 Effect of electrical potential on the long dust box of the hydrocyclone in the absence of the underflow at feed flow rate $0.1167*10^{-3}$ m^3/s (7 L/min), pH of suspension 9.0 and central rod diameter 12 mm.

5.6.3 Central rod diameter 16 mm

5.6.3.1 pH of suspension 6.0

The effects of central rod diameter on the classification efficiency in the absence of the underflow were investigated by using the 0.2% solid content by weight of silica suspension fed into the present hydrocyclone. **Figure 5.30** shows the partial separation efficiency when electrical potential was applied to the long dust box (106 mm) of the hydrocyclone in the absence of the underflow at feed flow rate $0.1167*10^{-3}$ m^3/s (7 L/min), pH of suspension 6.0 and central rod diameter 16 mm. The 50% particle cut sizes, d_{50}, obtained from experiments of applying electrical potential to the hydrocyclone were

a) No potential; 2.020 μm
c) Central side -, wall side +; 1.767 μm

It was found that the electrical potential for positive pole at the side wall decreased the 50% particle cut size when compared with no application of electrical potential.

สถาบันวิทยบริการ
จุฬาลงกรณ์มหาวิทยาลัย

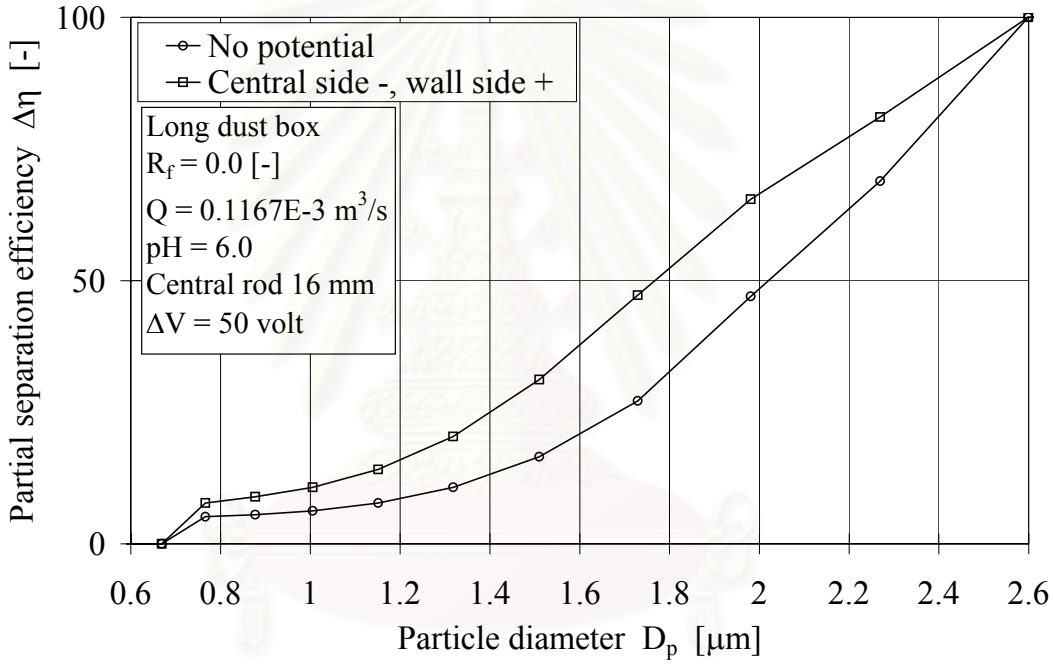

Figure 5.30 Effect of electrical potential on the long dust box of the hydrocyclone in the absence of the underflow at feed flow rate $0.1167*10^{-3}$ m^3/s (7 L/min), pH of suspension 6.0 and central rod diameter 16 mm.

5.6.3.2 pH of suspension 9.0

The effects of central rod diameter on the classification efficiency in the absence of the underflow were investigated by using the 0.2% solid content by weight of silica suspension fed into the present hydrocyclone. **Figure 5.31** shows the partial separation efficiency when electrical potential was applied to the long dust box (106 mm) of the hydrocyclone in the absence of the underflow at feed flow rate $0.1167*10^{-3}$ m^3/s (7 L/min), pH of suspension 9.0 and central rod diameter 16 mm. The 50% particle cut sizes, d_{50}, obtained from experiments of applying electrical potential to the hydrocyclone were

a) No potential; 1.998 μm
c) Central side -, wall side +; 1.631 μm

It was found that the electrical potential for positive pole at the side wall decreased the 50% particle cut size when compared with no application of electrical potential.

สถาบันวิทยบริการ
จุฬาลงกรณ์มหาวิทยาลัย

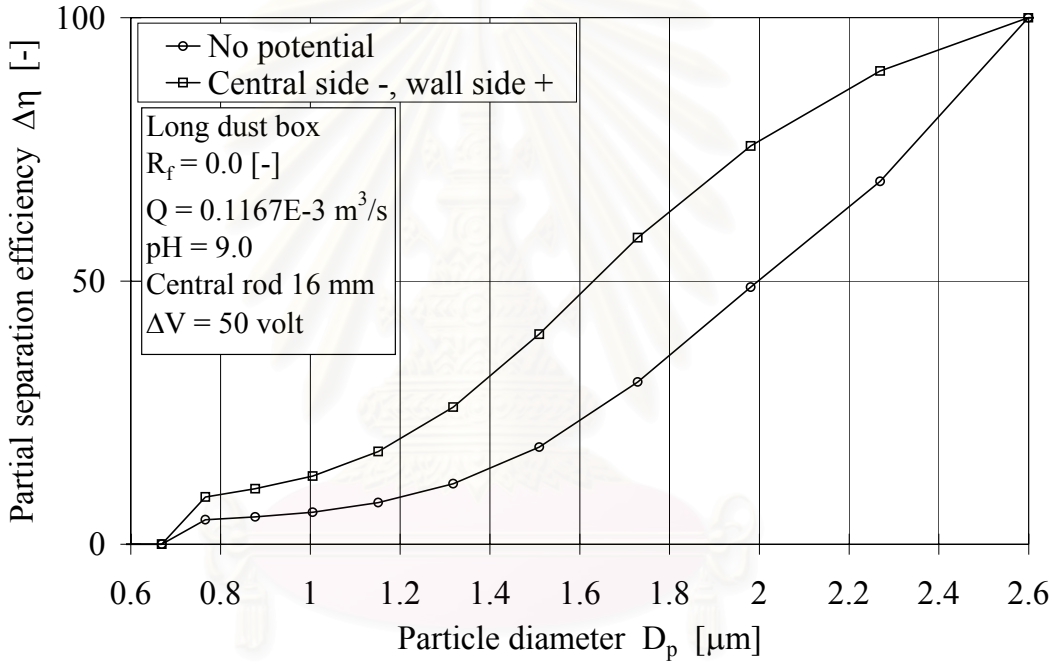

Figure 5.31 Effect of electrical potential on the long dust box of the hydrocyclone in the absence of the underflow at feed flow rate $0.1167*10^{-3}$ m^3/s (7 L/min), pH of suspension 9.0 and central rod diameter 16 mm.

5.6.4 Central rod diameter 20 mm

5.6.4.1 pH of suspension 6.0

The effects of central rod diameter on the classification efficiency in the absence of the underflow were investigated by using the 0.2% solid content by weight of silica suspension fed into the present hydrocyclone. **Figure 5.32** shows the partial separation efficiency when electrical potential was applied to the long dust box (106 mm) of the hydrocyclone in the absence of the underflow at feed flow rate $0.1167*10^{-3}$ m^3/s (7 L/min), pH of suspension 6.0 and central rod diameter 20 mm. The 50% particle cut sizes, d_{50}, obtained from experiments of applying electrical potential to the hydrocyclone were

a) No potential; 2.040 μm
c) Central side -, wall side +; 1.732 μm

It was found that the electrical potential for positive pole at the side wall decreased the 50% particle cut size when compared with no application of electrical potential.

สถาบันวิทยบริการ
จุฬาลงกรณ์มหาวิทยาลัย

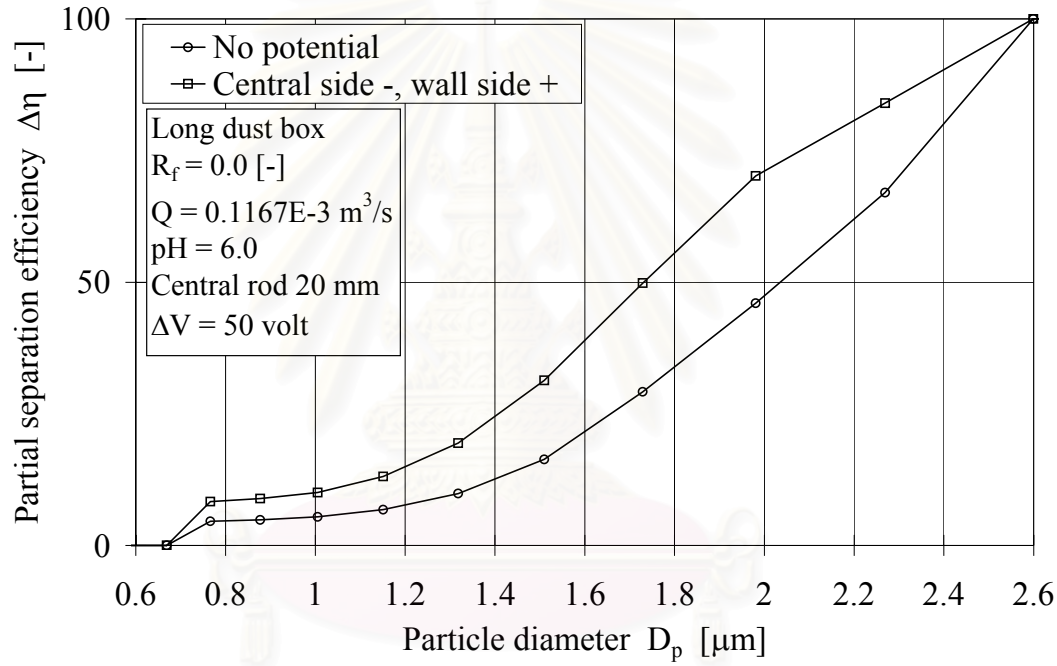

Figure 5.32 Effect of electrical potential on the long dust box of the hydrocyclone in the absence of the underflow at feed flow rate $0.1167*10^{-3}$ m^3/s (7 L/min), pH of suspension 6.0 and central rod diameter 20 mm.

5.6.4.2 pH of suspension 8.0

The effects of central rod diameter on the classification efficiency in the absence of the underflow were investigated by using the 0.2% solid content by weight of silica suspension fed into the present hydrocyclone. **Figure 5.33** shows the partial separation efficiency when electrical potential was applied to the long dust box (106 mm) of the hydrocyclone in the absence of the underflow at feed flow rate $0.1167*10^{-3}$ m^3/s (7 L/min), pH of suspension 8.0 and central rod diameter 20 mm. The 50% particle cut sizes, d_{50}, obtained from experiments of applying electrical potential to the hydrocyclone were

a) No potential; 2.070 μm
c) Central side -, wall side +; 1.705 μm

It was found that the electrical potential for positive pole at the side wall decreased the 50% particle cut size when compared with no application of electrical potential.

สถาบันวิทยบริการ
จุฬาลงกรณ์มหาวิทยาลัย

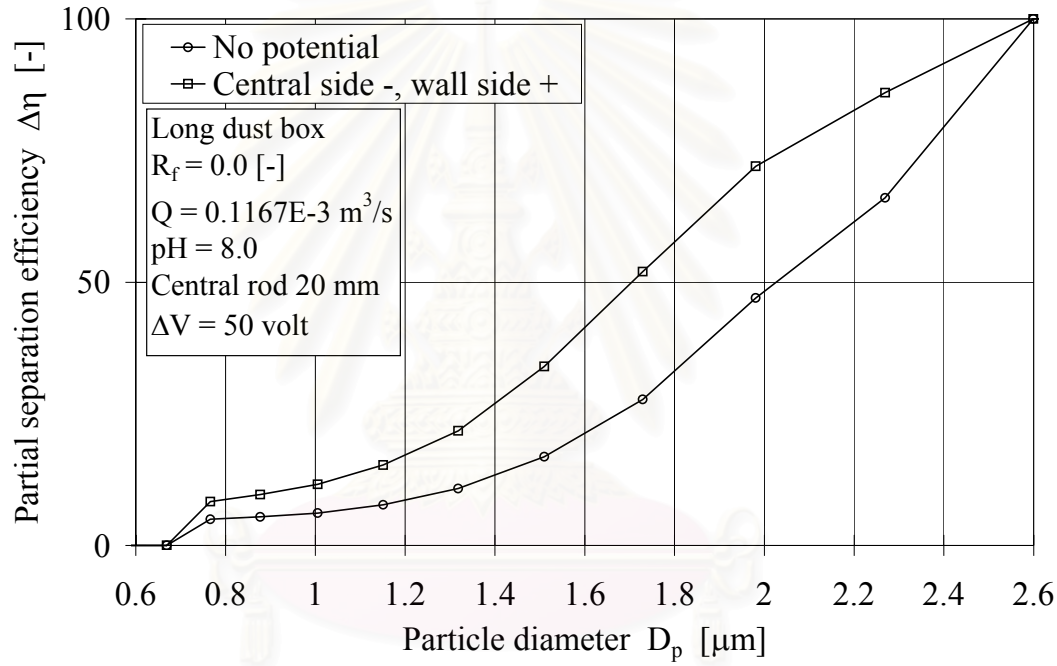

Figure 5.33 Effect of electrical potential on the long dust box of the hydrocyclone in the absence of the underflow at feed flow rate $0.1167*10^{-3}$ m^3/s (7 L/min), pH of suspension 8.0 and central rod diameter 20 mm.

5.6.4.3 pH of suspension 9.0

The effects of central rod diameter on the classification efficiency in the absence of the underflow were investigated by using the 0.2% solid content by weight of silica suspension fed into the present hydrocyclone. **Figure 5.34** shows the partial separation efficiency when electrical potential was applied to the long dust box (106 mm) of the hydrocyclone in the absence of the underflow at feed flow rate $0.1167*10^{-3}$ m^3/s (7 L/min), pH of suspension 9.0 and central rod diameter 20 mm. The 50% particle cut sizes, d_{50}, obtained from experiments of applying electrical potential to the hydrocyclone were

a) No potential; 2.029 μm
c) Central side -, wall side +; 1.588 μm

It was found that the electrical potential for positive pole at the side wall decreased the 50% particle cut size when compared with no application of electrical potential.

สถาบันวิทยบริการ
จุฬาลงกรณ์มหาวิทยาลัย

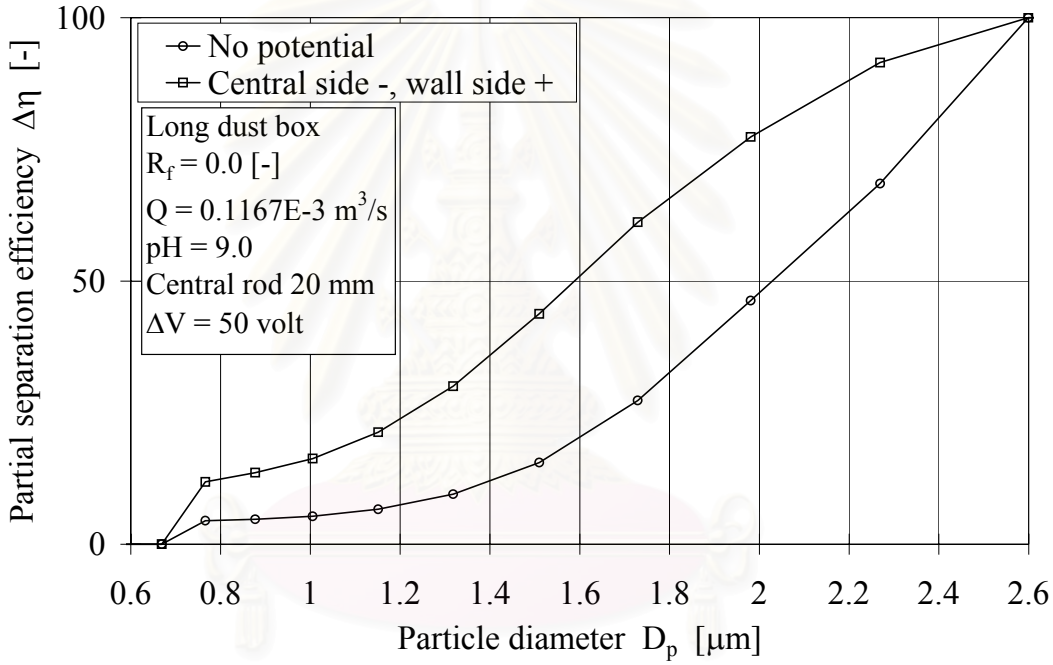

Figure 5.34 Effect of electrical potential on the long dust box of the hydrocyclone in the absence of the underflow at feed flow rate $0.1167*10^{-3}$ m^3/s (7 L/min), pH of suspension 9.0 and central rod diameter 20 mm.

5.6.4.4 pH of suspension 10.0

The effects of central rod diameter on the classification efficiency in the absence of the underflow were investigated by using the 0.2% solid content by weight of silica suspension fed into the present hydrocyclone. **Figure 5.35** shows the partial separation efficiency when electrical potential was applied to the long dust box (106 mm) of the hydrocyclone in the absence of the underflow at feed flow rate $0.1167*10^{-3}$ m^3/s (7 L/min), pH of suspension 10.0 and central rod diameter 20 mm. The 50% particle cut sizes, d_{50}, obtained from experiments of applying electrical potential to the hydrocyclone were

a) No potential; 2.023 μm
c) Central side -, wall side +; 1.563 μm

It was found that the electrical potential for positive pole at the side wall decreased the 50% particle cut size when compared with no application of electrical potential.

สถาบันวิทยบริการ
จุฬาลงกรณ์มหาวิทยาลัย

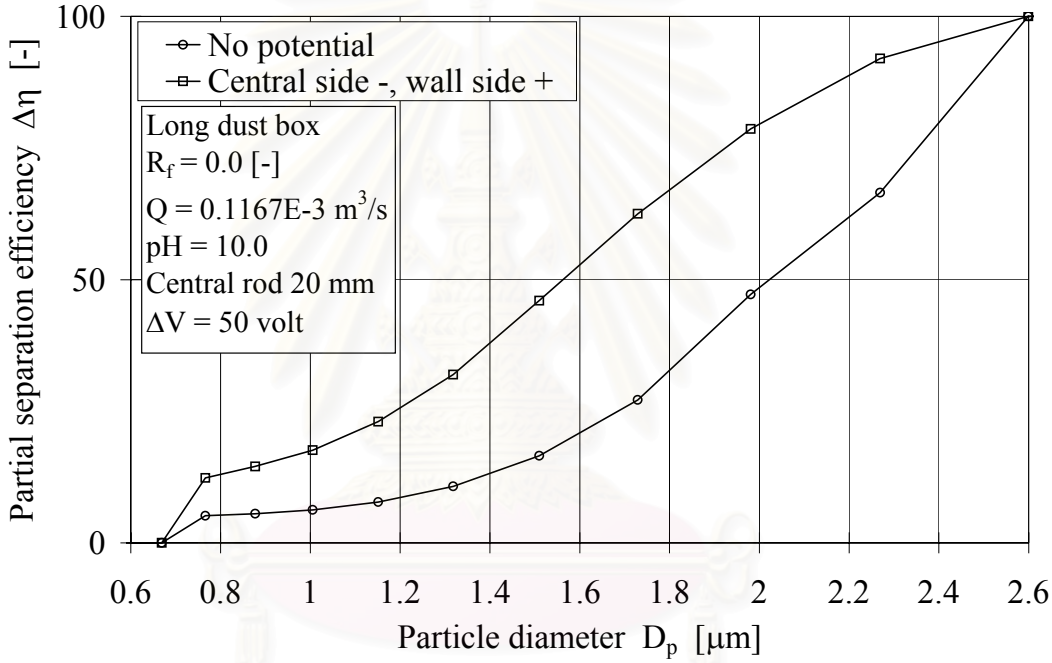

Figure 5.35 Effect of electrical potential on the long dust box of the hydrocyclone in the absence of the underflow at feed flow rate $0.1167*10^{-3}$ m^3/s (7 L/min), pH of suspension 10.0 and central rod diameter 20 mm.

5.6.5 Summary of effect of central rod diameter in the absence of the underflow

Figure 5.36 shows the relationship between 50% particle cut size, d_{50}, and central rod diameter when electrical potential was applied to the long dust box (106 mm) of the hydrocyclone in the absence of the underflow at appropriated feed flow rate $0.1167*10^{-3}$ m^3/s (7 L/min) and either pH of suspension 6.0 or 9.0. The larger the central rod diameter, the smaller the 50% particle cut size became. The results summarized the effect of electrical potential in **Figure 5.17, 5.23, 5.28-5.32** and **5.34**. Subsequently, the electrical potential exhibited a stronger effect when the suspension has higher the pH of suspension.

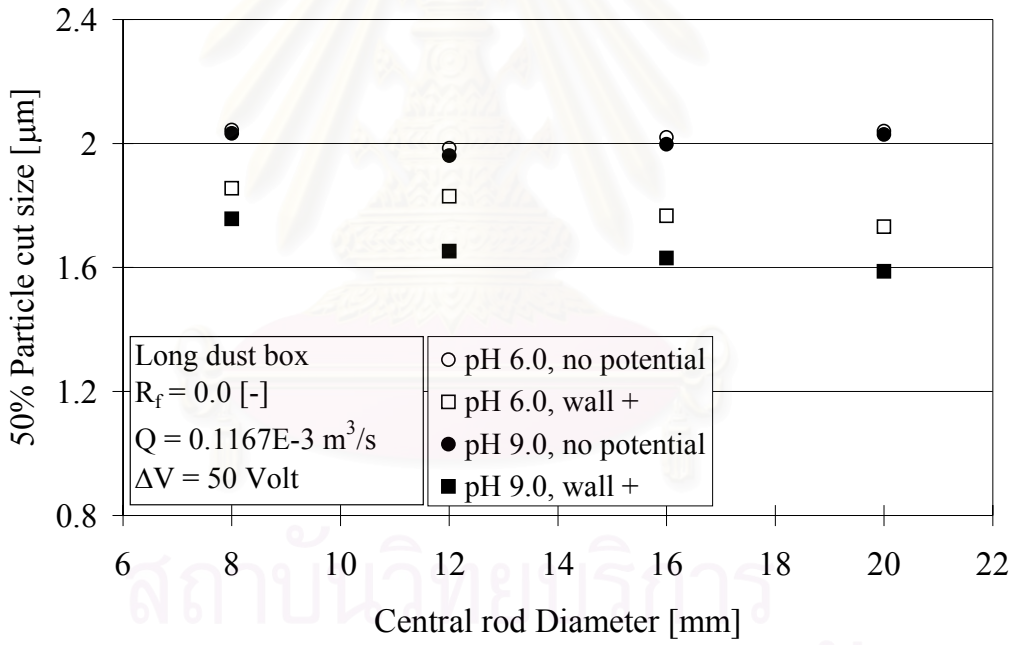

Figure 5.36 Relationship between 50% particle cut size, d_{50}, and central rod diameter when electrical potential was applied to the long dust box (106 mm) of the hydrocyclone in the absence of the underflow at feed flow rate $0.1167*10^{-3}$ m^3/s (7 L/min) and either pH of suspension 6.0 or 9.0.

It was found that the electrical potential exhibited a stronger effect when the central rod had larger diameter because electric field strength in the dust box was increased. The effect of central rod diameter at 20 mm with electrical potential can reduced the 50% particle cut size by up to 9.62% compared to the central rod diameter at 8 mm with electrical potential. Interestingly, the electrical potential with reinforcement of highest pH and largest central rod diameter can reduced the 50% particle cut size by up to 21.73% compared to the absence of electricity. Since the electrostatic force will act on a charged particle under the influence of an electric field. The magnitude of electrostatic force was dependent upon the charge on the particle and the strength of the electric field. As the distance between the central rod and side wall was decreased, the electric field strength increased. The larger the central rod diameter, the shorter the distance between two electrodes that resulted the stronger electric field strength accompanied with the stronger electrostatic force. Therefore, not only the silica particles in the dust box easily hold on the positive electrode but also amount of attached particles was increased as shown in **Figure 5.37**. On the other hand, the classification efficiency was increased. However, the change of central rod diameter was no effect when the system was operated with no application of electrical potential.

In order to obtain the smallest cut size the long dust box should be selected and the system operated with positive electrical potential applied at the side wall and negative electrical potential at the central rod side with the reinforcement of the highest pH of suspension and largest central rod diameter.

จุฬาลงกรณ์มหาวิทยาลัย

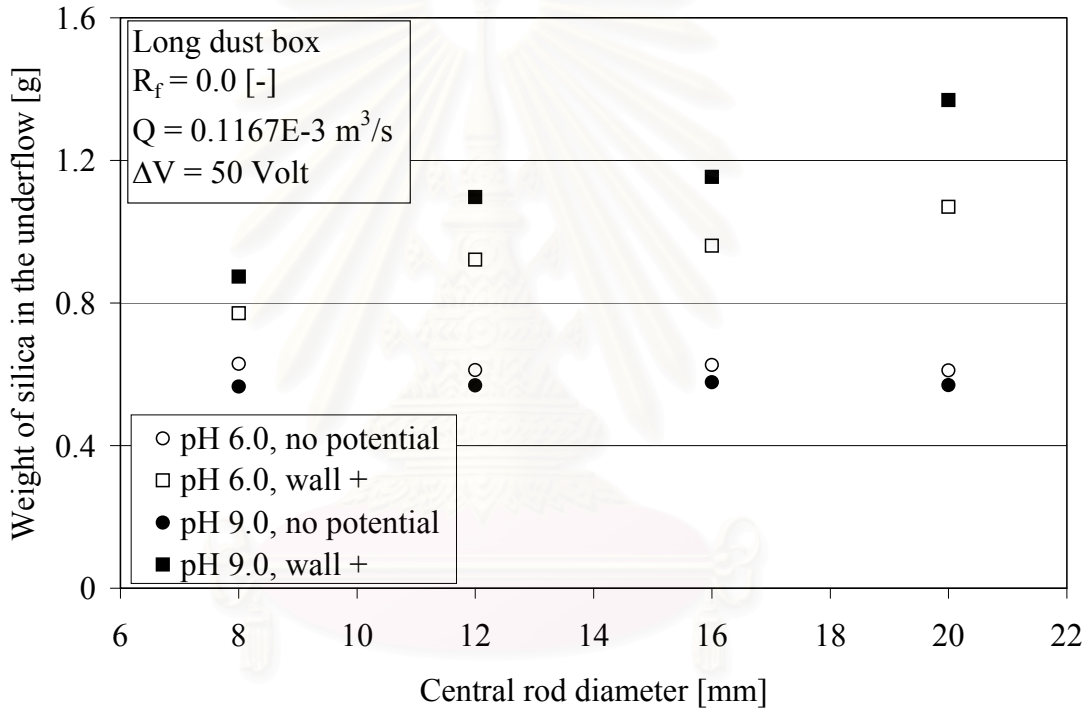

Figure 5.37 Relationship between weight of silica in the underflow and central rod diameter when electrical potential was applied to the long dust box (106 mm) of the hydrocyclone in the absence of the underflow at feed flow rate $0.1167*10^{-3}$ m^3/s (7 L/min) and either pH of suspension 6.0 or 9.0.

5.7 Comparison of effect of pH between central rod diameter 8 and 20 mm in the absence of the underflow

Figure 5.38 compares the partial separation efficiency when applied positive electrical potential at the side wall and negative electrical potential at the central rod with the long dust box (106 mm) of the hydrocyclone in the absence of the underflow at feed flow rate $0.1167*10^{-3}$ m^3/s (7 L/min), pH of suspension 6.0, 8.0, 9.0 and 10.0 and either central rod diameter 8 or 20 mm.

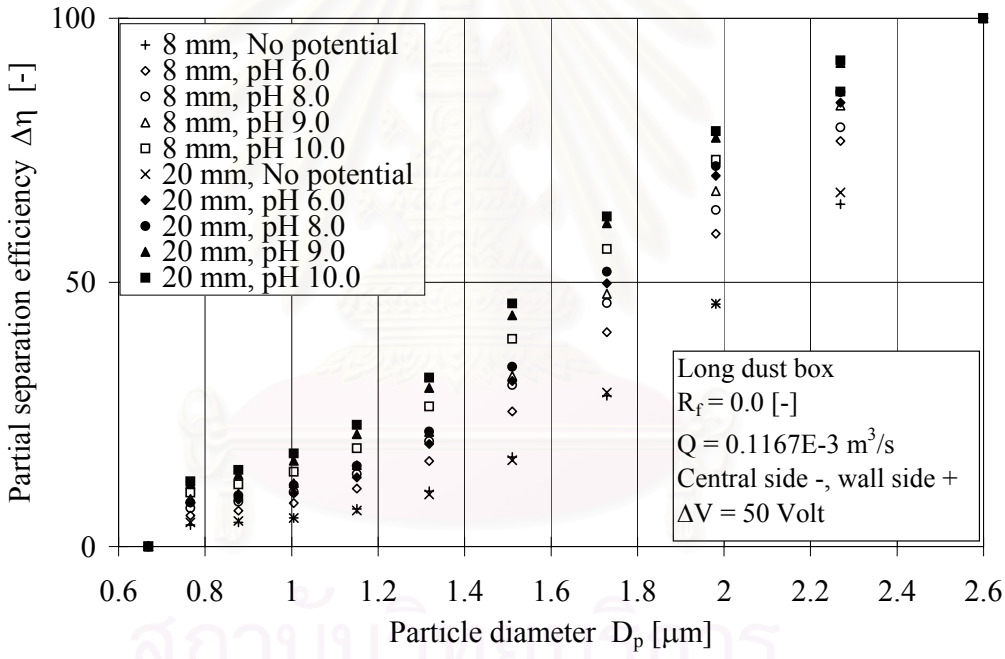

Figure 5.38 Comparison of effect of pH between central rod diameter 8 and 20 mm when applied positive electrical potential at the side wall and negative electrical potential at the central rod on the long dust box (106 mm) of the hydrocyclone in the absence of the underflow at feed flow rate $0.1167*10^{-3}$ m^3/s (7 L/min) and pH of suspension 6.0, 8.0, 9.0 and 10.0.

Figure 5.39 shows the relationship between 50% particle cut size, d_{50}, and central rod diameter when electrical potential was applied to the long dust box (106 mm) of the hydrocyclone in the absence of the underflow at appropriated feed flow rate $0.1167*10^{-3}$ m^3/s (7 L/min), pH of suspension 6.0, 8.0, 9.0 and 10.0 and either central rod diameter 8 or 20 mm. The results summarize the effect of electrical potential in **Figure 5.17, 5.21, 5.23, 5.25** and **5.32-5.35.**

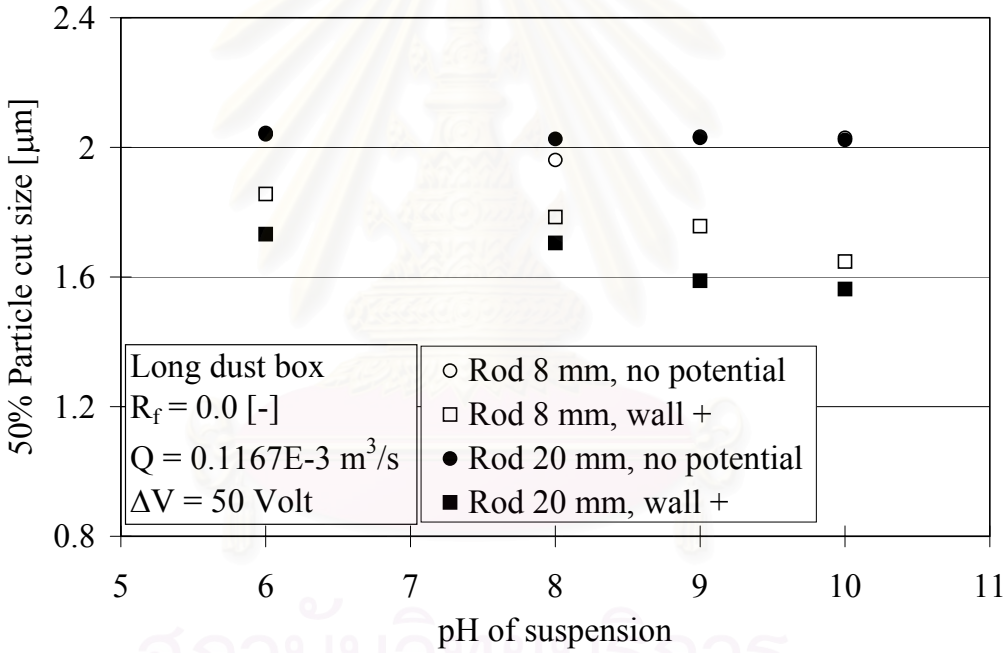

Figure 5.39 Relationship between 50% particle cut size, d_{50}, and central rod diameter when electrical potential was applied to the long dust box (106 mm) of the hydrocyclone in the absence of the underflow at feed flow rate $0.1167*10^{-3}$ m^3/s (7 L/min), pH of suspension 6.0, 8.0, 9.0 and 10.0 and either central rod diameter 8 or 20 mm.

It was found that the higher the pH of suspension, the smaller the 50% particle cut size became. Subsequently, the larger the central rod diameter, the smaller the 50% particle cut size. The electrical potential exhibited a stronger effect when the suspension had higher pH and operated with larger central rod diameter. The effect of pH of suspension at 10.0 and either central rod diameter 8 or 20 mm with electrical potential can reduced the 50% particle cut size by up to either 11.21% or 9.76% compared to the pH of suspension at 6.0. Moreover, the electrical potential with reinforcement of pH and operated with either central rod diameter 8 or 20 mm can reduced the 50% particle cut size by up to either 18.78% or 22.74% compared to the absence of electricity. At the high pH of suspension condition, particles had high zeta potential caused to increase the magnitude of charge that mean not only the silica particles in the dust box easily hold on the positive electrode but also amount of attached particles was increased. Amount of attached particles depended on the magnitude of electrostatic force that proportional to the magnitude of charge and electric field strength. Therefore, amount of attached particles when suspension had higher pH was more than that amount of attached particles when suspension had lower pH. Subsequently, amount of attached particles when operated with larger central rod diameter was more than that amount of attached particles when operated with smaller central rod diameter because the increasing of the electric field strength in the dust box as shown in **Figure 5.40**. The separation efficiency was proportional to amount of collected particles. It was mean that, the classification efficiency in case of operated with large central rod diameter was higher than case of operated with small central rod diameter. However, the pH of suspension was no effect when the system was operated with no application of electrical potential on both large and small central rod diameter.

In order to obtain the smallest cut size the long dust box should be selected and the system was operated with largest central rod diameter with the reinforcement of the highest pH of suspension.

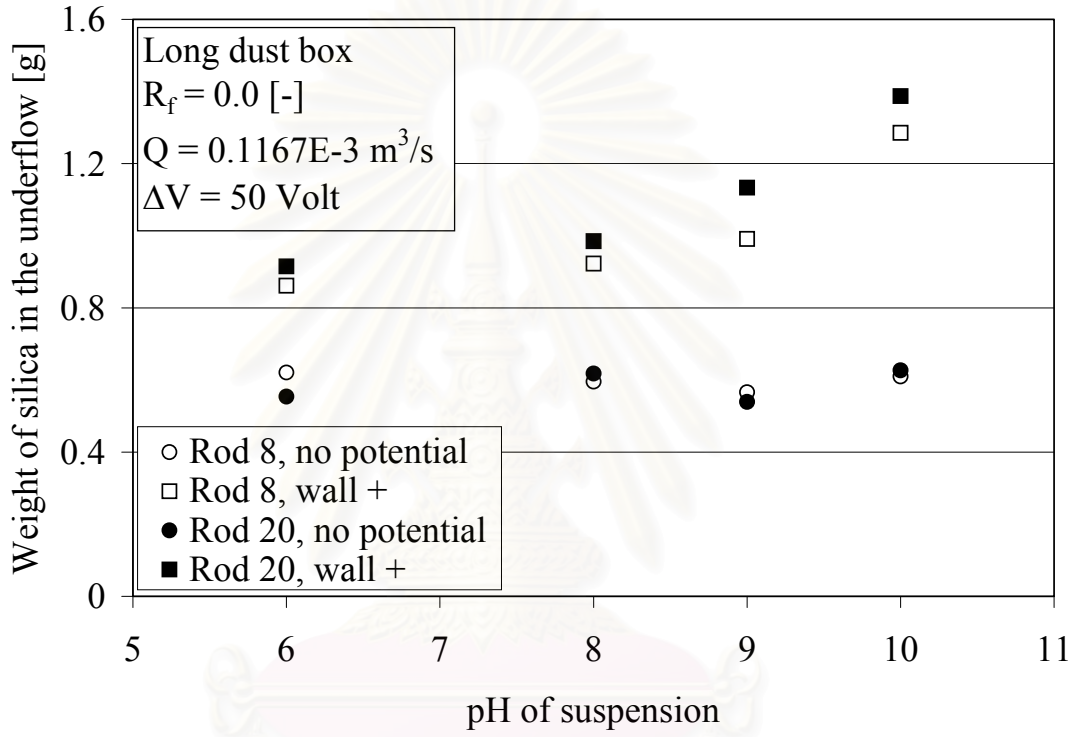

Figure 5.40 Relationship between weight of silica in the underflow and pH of suspension when electrical potential was applied to the long dust box (106 mm) of the hydrocyclone in the absence of the underflow at feed flow rate $0.1167*10^{-3}$ m^3/s (7 L/min) and either central rod diameter 8 or 20 mm.

5.8 Summary of effects of all parameters on the classification efficiency in the presence of the underflow

In this research, all interested parameters that investigated in the presence of the underflow consisted of electrical potential, dust box length, feed flow rate and underflow to throughput ratio. It was found that, the electrical potential for positive pole at both the central rod and side wall decreased the 50% particle cut size when compared with no application of electrical potential. The effect of the electrical potential when the positive pole was connected to the side wall was stronger than when the positive pole was connected to the central rod. The long dust box gave better the classification efficiency than that with a short dust box. The higher feed flow rate the smaller the particle cut size became. The higher the underflow to throughput ratio gave the better the classification efficiency.

In order to clarify the effect of all parameters at above mention, the investigated conditions must be same but only changes the interested parameter. Therefore, the appropriated feed flow rate at $0.1167*10^{-3}$ m^3/s (7 L/min), pH of suspension 6.0 and central rod diameter 8 mm was selected in all conditions. **Table 5.1** shows the comparison of 50% particle cut size, % reduction with short dust box and % reduction with long dust box at feed flow rate $0.1167*10^{-3}$ m^3/s (7 L/min), pH of suspension 6.0 and central rod diameter 8 mm in the presence of the underflow.

สถาบันวิทยบริการ
จุฬาลงกรณ์มหาวิทยาลัย

Table 5.1 Comparison of 50% particle cut size, % reduction with short dust box and % reduction with long dust box at feed flow rate $0.1167*10^{-3}$ m^3/s (7 L/min), pH of suspension 6.0 and central rod diameter 8 mm in the presence of the underflow

Dust box	Potential	Underflow to throughput ratio	d_{50}	%Short	%Long
Short	no	0.1	2.049	-	-10.70
Short	center +	0.1	2.013	1.76	-8.75
Short	wall +	0.1	1.972	3.76	-6.54
Long	no	0.1	1.851	9.66	-
Long	center +	0.1	1.749	14.64	5.51
Long	wall +	0.1	1.696	17.23	8.37
Long	no	0.2	1.575	23.13	14.91
Long	center +	0.2	1.497	26.94	19.12
Long	wall +	0.2	1.452	29.14	21.56
Long	no	0.3	1.325	35.33	28.42
Long	center +	0.3	1.291	36.99	30.25
Long	wall +	0.3	1.255	38.75	32.20

สถาบันวิทยบริการ
จุฬาลงกรณ์มหาวิทยาลัย

5.9 Summary of effects of all parameters on the classification efficiency in the absence of the underflow

In this research, all interested parameters that investigate in the absence of the underflow consisted of electrical potential, dust box length, feed flow rate, pH and central rod diameter. It was found that, the electrical potential for positive pole at both the central rod and side wall decreased the 50% particle cut size when compared with no application of electrical potential. The effect of the electrical potential when the positive pole was connected to the side wall was stronger than when the positive pole was connected to the central rod. The long dust box gave better the classification efficiency than that with a short dust box. The higher feed flow rate the smaller the particle cut size became. The higher pH of suspension resulted the smaller the particle cut size and finally, the larger central rod diameter the better the classification efficiency.

In order to clarify the effect of all parameters at above mention, the investigated conditions must be same but only changes the interested parameter. Therefore, the appropriated feed flow rate at $0.1167*10^{-3}$ m^3/s (7 L/min) was selected in all conditions. **Table 5.2** shows the comparison of 50% particle cut size, % reduction with short dust box and % reduction with long dust box at feed flow rate $0.1167*10^{-3}$ m^3/s (7 L/min) in the absence of the underflow.

สถาบันวิทยบริการ
จุฬาลงกรณ์มหาวิทยาลัย

Table 5.2 Comparison of 50% particle cut size, % reduction with short dust box and % reduction with long dust box at feed flow rate $0.1167*10^{-3}$ m^3/s (7 L/min) in the absence of the underflow

Dust box	Potential	pH	Rod diameter	d_{50}	%Short	%Long
Short	no	6.0	8	2.260	-	-9.56
Short	center +	6.0	8	2.132	5.66	-4.31
Short	wall +	6.0	8	2.107	6.77	-3.08
Long	no	6.0	8	2.044	9.56	-
Long	center +	6.0	8	1.964	13.10	3.91
Long	center +	8.0	8	1.875	17.04	8.27
Long	center +	9.0	8	1.859	17.74	9.05
Long	center +	10.0	8	1.842	18.50	9.88
Long	wall +	6.0	8	1.856	17.88	9.20
Long	wall +	8.0	8	1.785	21.02	12.67
Long	wall +	9.0	8	1.757	22.26	14.04
Long	wall +	10.0	8	1.648	27.08	19.37
Long	wall +	6.0	12	1.830	19.03	10.47
Long	wall +	6.0	16	1.767	21.81	13.55
Long	wall +	6.0	20	1.732	23.36	15.26
Long	wall +	8.0	20	1.705	24.56	16.59
Long	wall +	9.0	12	1.653	26.86	19.13
Long	wall +	9.0	16	1.631	27.83	20.21
Long	wall +	9.0	20	1.588	29.73	22.31
Long	wall +	6.0	20	1.563	30.84	23.53

5.10 Pressure drop

Figure 5.41 shows the relationship between pressure drop, ΔP, and feed flow rate, Q, when electrical potential was applied either to the short or the long dust boxes (53 or 106 mm) of the hydrocyclone in the presence and absence of the underflow at pH of suspension 6.0 and central rod diameter 8 mm.

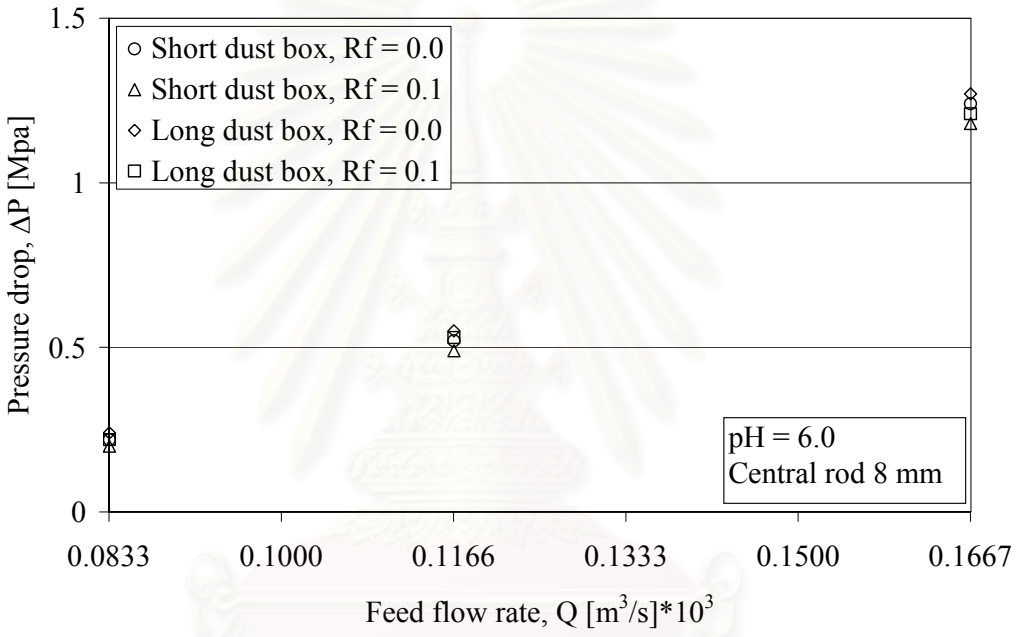

Figure 5.41 Relationship between pressure drop, ΔP, and feed flow rate, Q, when electrical potential was applied either to the short or the long dust boxes (53 or 106 mm) of the hydrocyclone in the presence and absence of the underflow at pH of suspension 6.0 and central rod diameter 8 mm.

It was found that, the pressure drop proportionally increased to the feed flow rate. The long dust box exhibited a little higher the pressure drop when compared with the short dust box. The absence of the underflow exhibited a little higher the pressure drop when compared with the presence of the underflow. The electrical potential had not affect to the pressure drop.

Figure 5.42 shows the relationship between pressure drop, ΔP, and the underflow to throughput ratio, R_f, when electrical potential was applied to the long dust box (106 mm) of the hydrocyclone in the presence of the underflow at feed flow rate $0.1167*10^{-3}$ m^3/s (7 L/min), pH of suspension 6.0 and central rod diameter 8 mm.

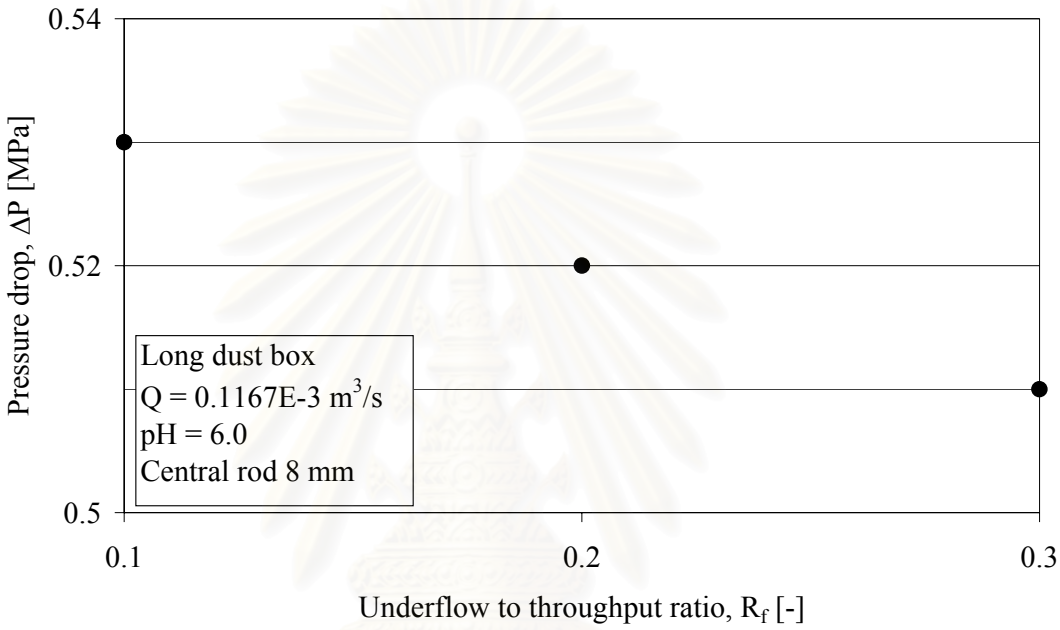

Figure 5.42 Relationship between pressure drop, ΔP, and the underflow to throughput ratio, R_f, when electrical potential was applied to the long dust box (106 mm) of the hydrocyclone in the presence of the underflow at feed flow rate $0.1167*10^{-3}$ m^3/s (7 L/min), pH of suspension 6.0 and central rod diameter 8 mm.

It was found that, the pressure drop proportionally decreased to the underflow to throughput ratio. The electrical potential had not affect to the pressure drop.

Figure 5.43 shows the relationship between pressure drop, ΔP, and the central rod diameter when electrical potential was applied to the long dust box (106 mm) of the hydrocyclone in the absence of the underflow at feed flow rate $0.1167*10^{-3}$ m^3/s (7 L/min) and pH of suspension 6.0.

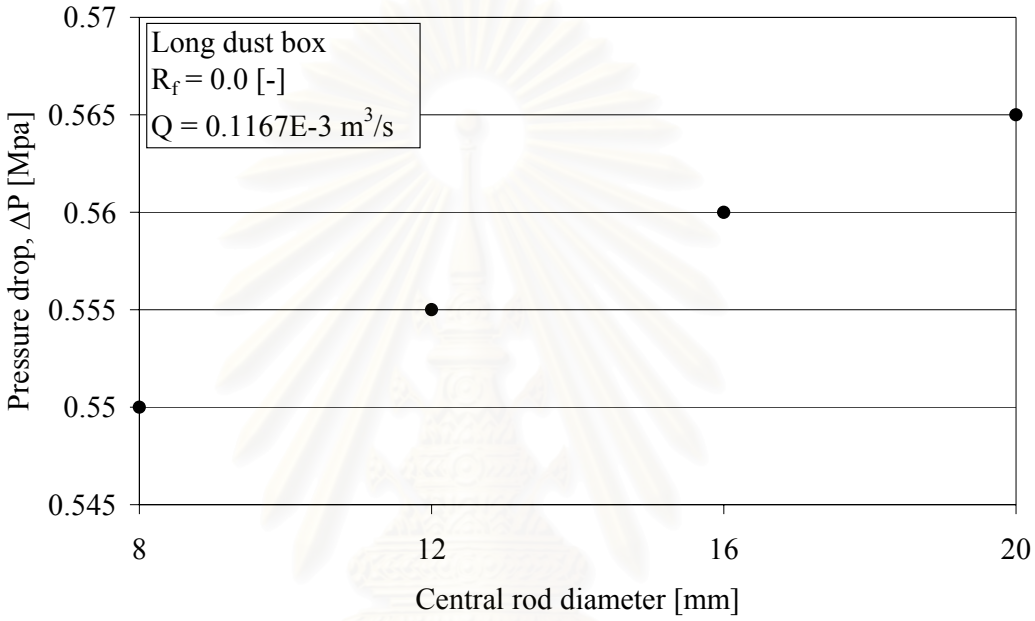

Figure 5.43 Relationship between pressure drop, ΔP, and the central rod diameter when electrical potential was applied to the long dust box (106 mm) of the hydrocyclone in the absence of the underflow at feed flow rate $0.1167*10^{-3}$ m^3/s (7 L/min) and pH of suspension 6.0.

It was found that, the pressure drop proportionally increased to the central rod diameter. The electrical potential had not affect to the pressure drop.

5.11 Models

The correlation was derived from equation of motion:

$$m \frac{du_r}{dt} = -3\pi\mu d_p \left| u_r - v_r \right| + \frac{mv_\theta^2}{r} \tag{5.1}$$

where u and v were particle and fluid velocity that respect to coordinate, respectively. At steady state the left hand term was zero, so that:

$$d_p = \sqrt{\frac{18 \mu r \left| u_r - v_r \right|}{(\rho_p - \rho) v_\theta^2}} \tag{5.2}$$

At critical particle velocity, $u_r = 0$:

$$d_{50} = \left(\frac{18 \mu r v_r}{(\rho_p - \rho) v_\theta^2} \right)^{0.5} \tag{5.3}$$

Normally, $v_\theta = v_i$, $v_r = \alpha v_i$, $v_i = Q/ab$ and $r = \beta D_c$ where a and b were width and length of inlet.

$$d_{50} = (18 \alpha\beta)^{0.5} \left(\frac{\mu D_c ab}{(\rho_p - \rho) Q} \right)^{0.5} = K \left(\frac{\mu D_c ab}{(\rho_p - \rho) Q} \right)^{0.5} \tag{5.4}$$

Substituted with the cyclone dimensions and properties:

$$d_{50} = K \left(\frac{0.8328 * 10^{-3} * 0.020 * (0.002 * 0.006)}{(2210 - 995.647) Q} \right)^{0.5}$$

$$d_{50} = K \left(\frac{1.646 * 10^{-13}}{Q} \right)^{0.5} \tag{5.5}$$

where α, β, K were semi-empirical constants.

$$K = (18\,\alpha\beta)^{0.5} = \left(18\,\frac{v_r}{v_i}\frac{r}{D_c}\right)^{0.5} = \left(18\,\frac{\sigma u_r}{Q/ab}\frac{A/2\pi h}{D_c}\right)^{0.5}$$

$$= \left(18\,\frac{\sigma ab}{2\pi h D_c}\left(\frac{u_r A}{Q}\right)\right)^{0.5} = \left(\frac{18\,\sigma ab}{2\pi h D_c}\right)^{0.5}\left(\frac{u_r A}{Q}\right)^{0.5}$$

$$= \delta\left(\frac{u_r A}{Q}\right)^{0.5} \qquad (5.6)$$

The effect of electrical potential was depended not only the feed flow rate, Q and the migration velocities, u_r of the particles but also on the collecting area, A of the electrode in the dust box. The electrical potential effect can be determined from: u_rA/Q.

From equation (2.16) the migration velocity of the particle was:

$$u_r = \frac{2\varepsilon\zeta}{3\mu}\frac{1}{r}\frac{V}{\ln(R_o/R_i)} \qquad (5.7)$$

The particle located somewhere between the central rod and the side wall.

$$r = \gamma(R_o + R_i) \qquad (5.8)$$

where γ was a constant. Substitution gave:

$$u_r = \frac{2\varepsilon\zeta}{3\mu\gamma}\frac{1}{(R_o + R_i)}\frac{V}{\ln(R_o/R_i)} \qquad (5.9)$$

The collecting area of the electrode in the dust box was obtained from

$$A = 2\pi Rh \qquad (5.10)$$

where R = R_i when positive pole was connected to the central rod side

R = R_o when positive pole was connected to the side wall

h was the length of dust box that was approximately same as the height of the central rod.

$$\frac{u_r A}{Q} = \left(\frac{4\pi\varepsilon}{3\mu\gamma}\right)\frac{Rh\zeta V}{Q(R_o + R_i)\ln(R_o/R_i)} \tag{5.11}$$

Substitution equation (5.11) to (5.6) yield:

$$K = \delta\left(\frac{u_r A}{Q}\right)^{0.5} = \delta\left(\frac{4\pi\varepsilon}{3\mu\gamma}\right)^{0.5}\left(\frac{Rh\zeta V}{Q(R_o + R_i)\ln(R_o/R_i)}\right)^{0.5}$$

$$= \psi\left(\frac{Rh\zeta V}{Q(R_o + R_i)\ln(R_o/R_i)}\right)^{0.5} \tag{5.12}$$

The semi-empirical constants *K* for the presence of the underflow were:

Case a) no potential

$$K = \frac{20,063}{Q^{0.023} R_f^{0.297}}\left(\frac{0.106}{h}\right)^{0.137} \tag{5.13}$$

Case b) positive potential was applied at the central rod side and negative potential at the side wall

$$K = \frac{20{,}063}{Q^{0.023} R_f^{0.297}}\left(\frac{0.106}{h}\right)^{0.137} - 53.81\left[\frac{R_i h\zeta V}{QR_f(R_o + R_i)\ln(R_o/R_i)}\right]^{0.5} \tag{5.14}$$

Case c) positive potential was applied at the side wall and negative potential at the central rod side

$$K = \frac{20{,}063}{Q^{0.023} R_f^{0.297}}\left(\frac{0.106}{h}\right)^{0.137} - 38.18\left[\frac{R_o h\zeta V}{QR_f(R_o + R_i)\ln(R_o/R_i)}\right]^{0.5} \tag{5.15}$$

Figure 5.41 shows the correlation results for the d_{50} in the presence of underflow using parameter *K* compared with experimental results. The estimated parameters agreed well with experimental results.

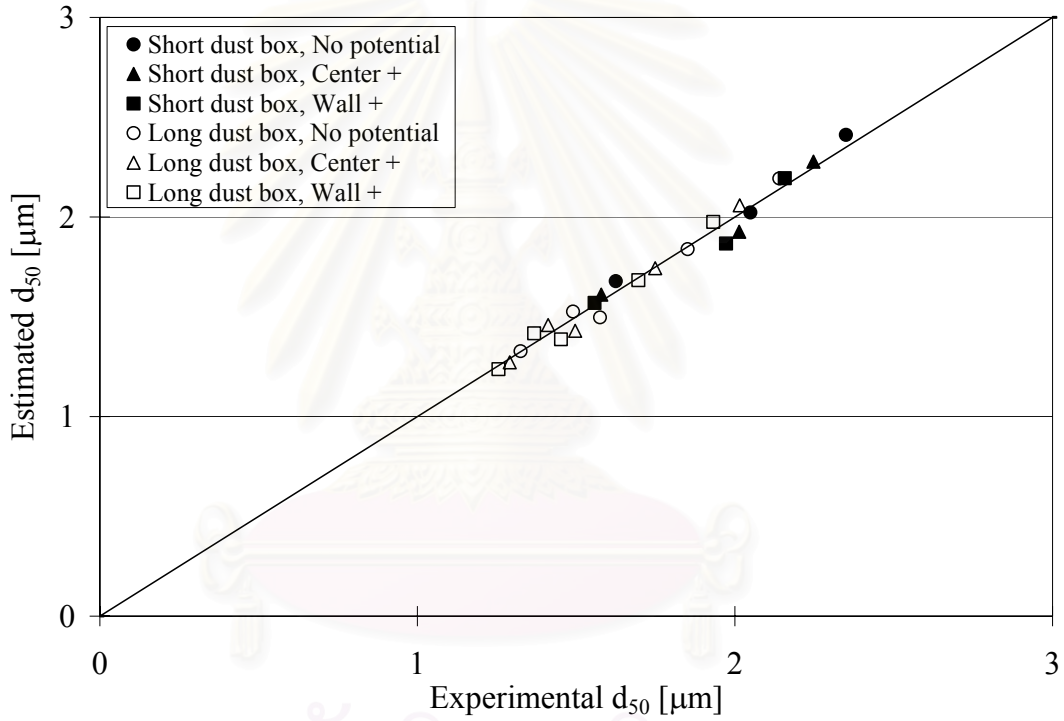

Figure 5.41 Correlation results for the d_{50} in the presence of underflow using parameter *K* compared with experimental results

The semi-empirical constants *K* for the absence of the underflow were:

Case a) no potential

$$K = 90{,}877 Q^{0.06} \left(\frac{0.106}{h} \right)^{0.164} \tag{5.16}$$

Case b) positive potential was applied at the central rod side and negative potential at the side wall

$$K = 90{,}877 Q^{0.06} \left(\frac{0.106}{h} \right)^{0.164} - 191 \left[\frac{R_i h \zeta V}{Q(R_o + R_i)\ln(R_o / R_i)} \right]^{0.5} \tag{5.17}$$

Case c) positive potential was applied at the side wall and negative potential at the central rod side

$$K = 90{,}877 Q^{0.06} \left(\frac{0.106}{h} \right)^{0.164} - 169 \left[\frac{R_o h \zeta V}{Q(R_o + R_i)\ln(R_o / R_i)} \right]^{0.5} \tag{5.18}$$

Figure 5.42 shows the correlation results for the d_{50} in the absence of underflow using parameter *K* compared with experimental results. The estimated parameters agreed well with experimental results.

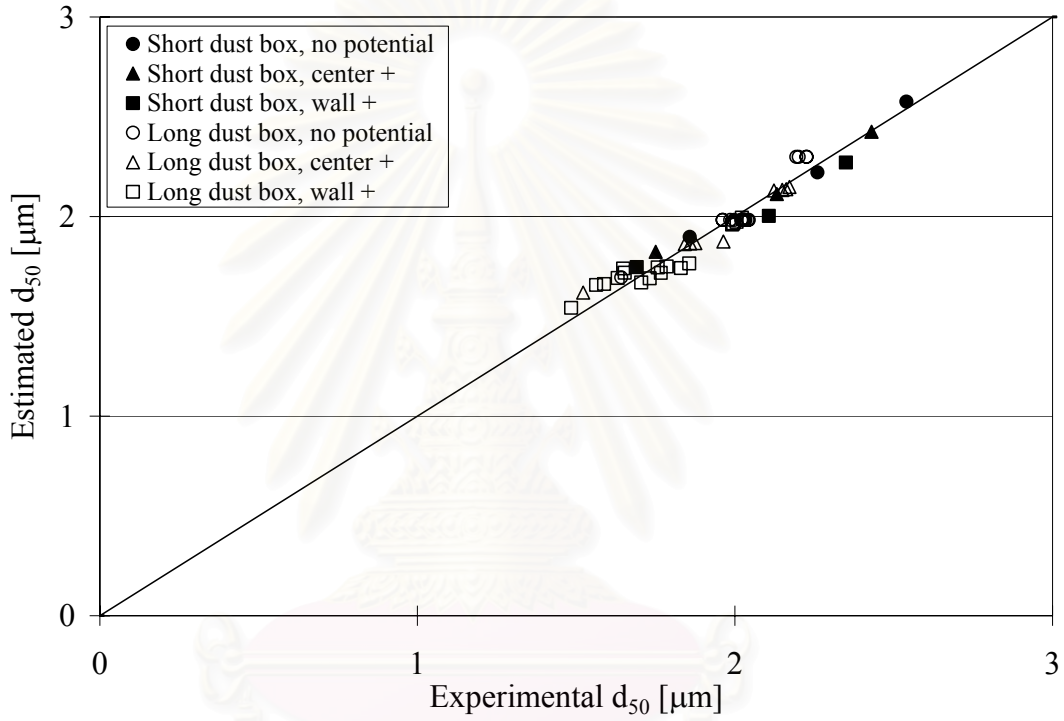

Figure 5.42 Correlation results for the d_{50} in the absence of underflow using parameter *K* compared with experimental results

สถาบันวิทยบริการ
จุฬาลงกรณ์มหาวิทยาลัย

CHAPTER VI

CONCLUSIONS AND RECOMMENDATIONS

6.1 Conclusions

The main purposes of the present research were to increase the particle classification efficiency using a novel electrical hydrocyclone. The additional parameters investigated were electrical potential, dust box length, feed flow rate, underflow to throughput ratio, the effect of the underflow, pH and central rod diameter. Finally, to determine the best conditions to obtain the smallest 50% particle cut size.

6.1.1 Effect of dust box length on the classification efficiency

In both the presence and absence of the underflow and both for the presence and absence of electrical potential, the hydrocyclone with a long dust box was found to give better classification efficiency than that with a short dust box.

6.1.2 Effect of feed flow rate on the classification efficiency

In both the presence and absence of the underflow and both for the presence and absence of electrical potential, the higher the feed flow rate, the better classification efficiency became. In the presence of the underflow, the electrical potential exhibited a stronger effect at the slower the feed flow rate. However, the feed flow rates had not affected corresponding to the electrical potential in the absence of the underflow.

6.1.3 Effect of underflow to throughput ratio on the classification efficiency

In both the presence and absence of electrical potential, the higher the underflow to throughput ratio, the smaller the particle cut size became. It was mean that the better classification efficiency. The lower the underflow to throughput ratio, the electrical potential exhibited a stronger effect.

6.1.4 Effect of electrical potential on the classification efficiency

In both the presence and absence of the underflow, the effect of the electrical potential when the positive pole was connected to the side wall was stronger than when the positive pole was connected to the central rod.

6.1.5 Effect of the underflow on the classification efficiency

Both the presence and absence of the underflow decreased the 50% particle cut size when electrical potential was applied for positive pole at both the central rod and side wall compared with no application of electrical potential. Moreover, the presence of the underflow gave better classification efficiency than the absence of the underflow.

6.1.6 Effect of pH of suspension on the classification efficiency

The higher pH of suspension, the electrical potential exhibited a stronger effect because of the higher zeta potential. The higher pH increased the classification efficiency. However, the pH of suspension was no effect when the system was operated with no application of electrical potential.

6.1.7 Effect of central rod diameter on the classification efficiency

The larger the central rod diameter, the electrical potential exhibits a stronger effect because of the stronger the electric field strength. The larger central rod diameter increased the classification efficiency. However, the central rod diameter was no effect when the system was operated with no application of electrical potential.

6.1.8 The best conditions to obtain the smallest the 50% particle cut size

The best conditions to obtain the smallest 50% particle cut size were that the long dust box be used, the system was operated with a highest pH of suspension, the largest central rod diameter and positive electrical potential applied at the side wall and negative electrical potential at the central rod be employed in the presence of the underflow.

6.2 Recommendation for the future work

From the experimental results, dust box length and electrical potential had affected on the classification efficiency. More investigation of the various lengths of dust box and magnitude of electrical potential should be carried out for appropriating the dust box length and magnitude of electrical potential. The increasing of zeta potential for particles was interested point. Additionally, the tested hydrocyclone should be made from transparency material in order to investigate the phenomenon that happens in the dust box.

REFERENCES

Anderson, B. and Jackson, R. A. & EC Fundamentals. 6 (1967): 527.

Apling, A. C., Montaldo, D. and Young P. A. Hydrocyclone models in an ore-grinding context. Int. Conf. Hydrocyclones (Cambridge, 1980): Paper 9, 113-125. Cranfield: BHRA Fluid Engineering, 1980.

Asomah, A. K. and Napier-Munn, T. J. An empirical model of hydrocyclones, incorporating angle of cyclone inclination. Minerals Engineering 10, 3 (1997): 330-347.

Bloor, M. I. G. On axially symmetric flow models for hydrocyclones. BHRA 3rd Int. Conf. on Hydrocyclones (Oxford, 1987): Paper D2. Barking: Elsevier Applied Science Publishers, 1987.

Bloor, M. I. G. and Ingham, D. B. On the efficiency of the industrial cyclone. Trans. Instn Chem. Engrs. 51 (1973b): 173-176.

Bloor, M. I. G. and Ingham, D. B. Theoretical analysis of the conical cyclone. First European Conf. On Mixing and Centrifugal Separation (Cambridge, 1974): Paper E6. Cranfeild: BHRA Fluid Engineering, 1974.

Bloor, M. I. G. and Ingham, D. B. Theoretical investigation of the flow in a conical hydrocyclone. Trans. Instn Chem. Engrs. 51 (1973a): 36-41.

Bloor, M. I. G. and Ingham, D. B. Trans. Ind. Chem. Eng. 53 (1975): 1.

Bloor, M. I. G., Ingham, D. B. and Ferguson, J. W. J. A viscous model for flow in the hydrocyclone. 397th Event of the European Federation of Chemical Engineering (Bradford, 1989): Session I, Solid-Liquid Separation Practice III.

Bloor, M. I. G., Ingham, D. B. and Laverack, S. D. An analysis of boundary layer effects in a hydrocyclone. Proc. Int. Conf. on hydrocyclones (Cambridge, 1974): Paper 5, 49-62. Cranfield: BHRA Fluid Engineering, 1980.

Bohnet, M. Neuere Untersuchungen uber die Trennwirkung und den Druckverlust von Hydrozyklonen. Chemische Technik. 20, 9 (1969): 376-381.

Boyson, F., Ayers, W. H. and Swithenbank, J. A fundamental mathematical modeling approach to cyclone design. Trans. Ind. Chem. Eng. 60 (1982): 222-236.

Bradley, D. Ind. Chemist 34 (September 1958): 473.

Bradley, D. The Hydrocyclone. London: Pergamon Press, 1965.

Bradley, D. and Pulling, D. J. Flow patterns in the hydraulic cyclone and their interpretation in terms of performance. Trans. Instn Chem. Engrs. 37 (1959): 34-45.

Braun, T. Theoretische und experimentelle Untersuchungen des Einflubes der Feststoffkonzentration und der Partikelgrobenverteilung auf das Trennverhalten von Hydrozyklonen. Doctoral Dissertation, Technical University of Braunschweig, Braunschweig, Germany. 1989.

Castilho, L. R. and Medronho, R. A. A simple procedure for design and performance prediction of Bradley and Rietema hydrocyclones. Minerals Engineering 13, 2 (2000): 183-191.

Chen, W., Zydex, N. and Parma F. Evaluation of hydrocyclone models for practical applications. Chemical Engineering J. 80 (2000): 295-303.

Chine, B. and Concha, F. Flow patterns in conical and cylindrical hydrocyclones. Chemical Engineering J. 80 (2000): 267-273.

Chu, L. Y., Chen, W. M. and Lee, X. Z. Effect of structural modification on hydrocyclone performance. Separation and Purification Technology 20 (2000): 71-86.

Cilliers, J. J. and Harrison, S. T. L. The application of mini-hydrocyclones in the concentration of yeast suspensions. Chemical Engineering J. 65 (1997): 21-26.

Coelho, M. A. Z. and Medronho, R. A. A model for performance prediction of hydrocyclones. Chemical Engineering J. 84 (2001): 7-14.

Criner, H. E. The vortex Thickener. Int. Conf. on Coal Preparation Paris: 1950.

Crowley, J. M. Fundamentals of applied electrostatics. United States: John Wiley & Sons, 1986.

Dahlstrom, D. A. Series No. 15. Chem. Engng. Progr. Symp. Mineral Engineering Techniques 50 (1954): 41.

de Gelder, A. L. Paper S47. Symp. on Scaling-up of chemical plant and processes. Inst. Chem. Engrs. London, (May 1957).

Driessen, M. G. Rev. Ind. Mining Special Issue 4 (1951): 449-461.

Driessen, M. G. Trans. Am. Inst. Min. (Metall.) Eng. 177 (1948): 240.

Duggins, R. K. and Frith, P. C. W. Turbulence effects in hydrocyclones. 3rd International Conference on Hydrocyclones (Oxford, 1987): Paper D1. Barking: Elsevier Applied Science Publisher, 1987.

Dwari, R. K., Biswas, M. N. and Meikap, B. C. Performance characteristics for particles of sand FCC and fly ash in a novel hydrocyclone. Chemical Engineering Science 59 (2004): 671-684.

Dyakowski, T. and Williams, R. A. Modelling turbulent flow within a small diameter hydrocyclone. Chemical Engineering Science 48, 6 (1993): 1143-1152.

Fahlstrom, P. H. Discussion Proc. Int. Min. Proicessing Congress 1960. Inst. Mining and Metallurgy (1960): 632-643.

Flintoff, B. C., Plitt, L. R. and Turak, A. A. Cyclone modelling: a review of present technology. CIM Bull. 80, 905 (1987): 39-50.

Gerrard, A. M. and Liddle, C. J. Numerical optimization of multiple hydrocyclone systems. Chem. Eng. (February, 1978): 107-109.

Gibson, K. Large scale tests on sedimenting centrifuges and hydrocyclones for mathematical modelling of efficiency. Proc. Symp. Solid-Liquid Separaion Practice (Leeds, 1979): 1-10. Leeds: Yorkshire Branch of the Institute of Chemical Engineers, 1979.

Gotoh, K. Powder Technology Handbook. 2nd ed. Revised and Expanded. New York: Marcel Dekker, 1997.

Haas, P. A., et al. Chem. Engng. Progr. 53 (April 1957): 203.

Holland-Batt, A. B. A bulk model for separation in hydrocyclones. Trans. Inst Min. Metall. (Sect. C: Min. Process Extr. Metall.) 91 (1982).

Hsieh, K. T. and Rajamani, R. K. Mathematical model of the hydrocyclone based on physics of fluid flow. AIChE J. 37, 5 (1991): 735-746.

Kawatra, S. K., Bakshi, A. K. and Rusesky, M. T. Effect of viscosity on the cut (d_{50}) size of hydrocyclone classifiers. Minerals Engineering 9, 8 (1996a): 881-891.

Kawatra, S. K., Bakshi, A. K. and Rusesky, M. T. The effect of slurry viscosity on hydrocyclone classification. Int. J. Mineral Processing 48 (1996b): 39-50.

Kelsall, D. F. A further study of the hydraulic cyclone. Chemical Engineering Science 2 (1953): 254-272.

Kelsall, D. F. A study of motion of solid particles in a hydraulic cyclone. Tran. Inst. Chem. Eng. 30 (1952): 87-104.

Kutepov, A. M. Study and calculation of the separation efficiency of hydrocyclones. Zh. Prikl. Khim. 51 (1978): 614-619.

Kutepov, A. M., et al. Calculation of separation efficiencies in hydrocyclones. Izv. Vuzov, Chim. Chim. Technol 20 (1977): 144-145.

Laverack, S. D. Trans. Ind. Chem. Eng. 58 (1980): 33.

Lynch, A. J. and Roa, T. C. Ind. J. Technol. 6 (1968): 106-114.

Lynch, A. J. and Roa, T. C. Modeling and scale-up of hydrocyclone classifiers. 11th Int. Mineral Processing Congress (Cagliari, 1975): Paper 9, 9-25. Instituto di Arte Mineraria, 1975.

Lynch, A. J., Roa, T. C. and Prisbrey, K. A. Int. J. Min. Proc. 1 (1974): 173-181.

Malcolm, R. D. Similarity solutions for flow in hydrocyclones. Chemical Engineering Science 43, 7 (1988): 1499-1505.

Matschke, D. E. and Dahlstrom, D. A. Chem. Engng. Progr. 55 (January 1959): 79.

Medronho, R. A. Scale-up of hydrocyclones at low concentrations. Doctoral Dissertation, University of Bradford, 1984.

Medronho, R. A. and Svarovsky, L. Tests to verify hydrocyclone scale-up procedure. 2nd Int. Conf. on Hydrocyclones (Bath, 1984): Paper A1, 1-14. Cranfield: BHRA Fluid Engineering, 1984.

Mitzmager, A. and Mizrahi, J. Correlation of the pressure drop through small cyclones operating with dilute pulps of various liquids. Trans. Instn Chem. Engrs 42 (1964): T152-T157.

Mueller, M. and Bohnet M. Pressure drop and grade efficiency of a newly developed hydrocyclone for the separation of two different solids from a liquid flow. 3rd Int. Conf. on Multiphase Flow Lyon, France, 1998.

Nageswararao, K. A critical analysis of the fish hook effect in hydrocyclone classifiers. Chemical Engineering J. 80 (2000): 251-256.

Nageswararoa, K. Further developments in the modelling and scale-up of industrial hydrocyclones. Doctoral Dissertation, University of Queenland (JKMRC), Brisbane, Australia, 1978.

Nageswararoa, K. Reduced efficiency curves of industrial hydrocyclones-an analysis for plant practice. Minerals Engineering 12, 5 (1999): 517-544.

Nageswararoa, K., Wiseman, D. M. and Napier-Munn, T. J. Two empirical hydrocyclone models revisited. Minerals Engineering 17 (2004): 671-687.

Narasimha, M., Sripriya, R. and Banerjee P. K. CFD modelling of hydrocyclone-prediction of cut size. Int. J. of Mineral Processing 75 (2005): 53-68.

Neesse, T. and Schubert, H. Die Trennkorngrosse des Hydrozyklonen bei Dunnstrom und Dicht-stromtrennungen. First European Symposium on Particle Classification in Gases and Liquids (Nuremberg, 1984).

Neesse, T. and Schubert, H. Praktische und theoretische aspekte der dichtstromklassierung. Aufbereitungstechnik 32, 9 (1991): 459-472.

Neesse, T., Dueck, J. and Minkov, L. Separation of finest particles in hydrocyclones. Minerals Engineering 17 (2004): 689-696.

Ogawa, A. and Suzuki, T. Theory of the cut-size, the fractional collection efficiency, and the vortex breakdown in the axial flow hydrocyclone. Particulate Science and Technology 19 (2001): 257-299.

Plitt, L. R. A mathematical model of the hydrocyclone classifier. CIM Bull. (December 1976): 114-122.

Rhodes, N., Pericleous, K. A. and Drake, S. N. The prediction of hydrocyclone performance with a mathematical model. BHRA 3rd Int. Conf. on Hydrocyclones (Oxford, 1987): Paper B3. Barking: Elsevier Applied Science Publishers, 1987.

Rietema, K. Performance and design of hydrocyclones Part I to IV. Chem. Eng. Sci. 15 (1961a): 298-325.

Rietema, K. The mechanism of the separation of finely dispersed solids in cyclones. in Rietema, K. and Verver, C. G. (Eds), Cyclones in Industry, Chap. 4. Amsterdam: Elsevier, 1961b.

Roa, T. C., Nageswararao, K. and Lynch, A. J. Int. J. Min. Proc. 3 (1976) 357-363.

Schubert, H. and Neesse, T. A hydrocyclone separation model in consideration of the turbulent multi-phase flow. Proc. Int. Conf. on hydrocyclones (Cambridge, 1980): Paper 3, 23-36. Cranfield: BHRA Fluid Engineering, 1980.

Schubert, H., et al. Classification in turbulent two-phase flows. Aufbereitungs-Technik 6 (1986): 295-306.

Souza, F. J., et al. Analysis of the influence of the filtering medium on the behavior of the filtering hydrocyclone. Powder Technology 107 (2000): 259-267.

Svarovsky, L. Hydrocyclones. London: Holt, Rinehart and Winston, 1984.

Svarovsky, L. Hydrocyclones. Lancaster: Technomics, 1994.

Svarovsky, L. Selection of hydrocyclone design and operation using dimensionless groups. BHRA 3rd Int. Conf. on Hydrocyclones (Oxford, 1987): Paper A1. Barking: Elsevier Applied Science Publishers, 1987.

Svarovsky, L. Solid-Liquid Separation. 3rded. London: Butterworth & Co. (Publishers), 1990.

Tavares, L. M., et al. Modeling classification in small-diameter hydrocyclones under variable rheological conditions. Minerals Engineering 15 (2002): 613-622.

Trawinski, H. F. Filtration and Separation 6 (1969).

Vallebuona, et al. Technical note modelling for small diamete hydrocyclones. Minerals Engineering 8, 3 (1995): 321-327.

Yopps, S. W., et al. A study of the effect of slurry rheology on hydrocyclone performance. 3rd International Conference on Hydrocyclones (Oxford, 1987): Paper C1. Barking: Elsevier Applied Science Publisher, 1987.

Yoshioka, H. and Hotta, Y. Chem. Engng., Japan. 19 (1955): 632.

APPENDICES

สถาบันวิทยบริการ
จุฬาลงกรณ์มหาวิทยาลัย

APPENDIX A

PUBLICATION IN THIS RESEARCH WORK

International research paper

1. **P. Wongsarivej**, W. Tanthapanichakoon, and H. Yoshida, "Classification of silica fine particles using a novel electric hydrocyclone*" accepted for Science and Technology for Advanced Materials*, **2005**.

International Proceedings

1. **P. Wongsarivej**, and H. Yoshida, "Fine particle classification by using new type of electric hydrocyclone," *Proceedings of the 69th Annual Convention of Society of Chemical Engineers Japan,* B119, April 2-4, **2004**, Osaka, Japan.

2. **P. Wongsarivej**, W. Tanthapanichakoon, and H. Yoshida, "Classification of silica fine particles using a novel electric hydrocyclone," *Proceedings of International Symposium on Nanotechnology in Environmental Protection and Pollution (ISNEPP 2005),* January 12-14, **2005**, Bangkok, Thailand.

สถาบันวิทยบริการ
จุฬาลงกรณ์มหาวิทยาลัย

APPENDIX B

CURRENT, POWER, VOLTAGE AND RESISTANCE

The effects of electrical potential on the classification efficiency were carried out by the present hydrocyclone that the conical part was connected to a cylindrical dust box. This dust box had a central metal rod cone and a cylindrical metal wall between which the desired 50-volt DC electrical potential or no potential was applied by a DC power generator (BIO RAD POWER PAC3000). **Figure B1** shows the relationship between current that supplies from the DC power generator and time at various pH of suspensions when electrical potential was applied to the long dust box (106 mm) of the hydrocyclone in the absence of the underflow at feed flow rate $0.1167*10^{-3}$ m^3/s (7 L/min) and central rod diameter 20 mm. It was shown that, the steady state of the system at all pH of suspension occurs when the hydrocyclone operates 600 seconds (10 min). Therefore, the operating time 20 minutes can be assured that the system was in steady state.

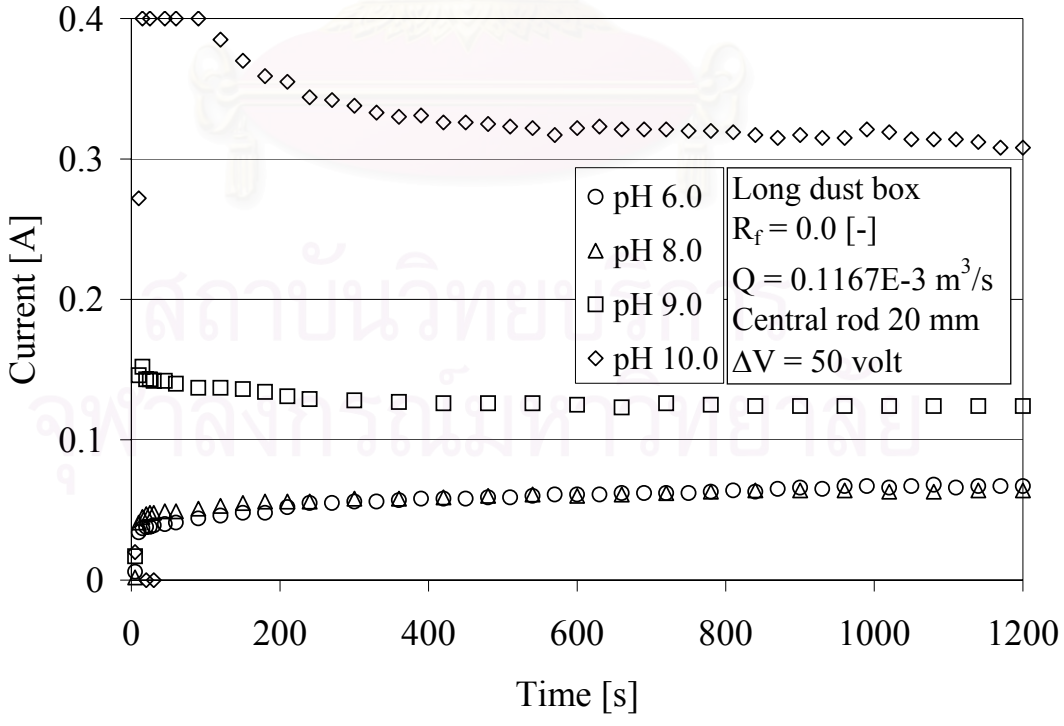

Figure B1 Relationship between current and time

Figure B2 shows the relationship between power that supplies from the DC power generator and time at various pH of suspensions when electrical potential was applied to the long dust box (106 mm) of the hydrocyclone in the absence of the underflow at feed flow rate $0.1167*10^{-3}$ m^3/s (7 L/min) and central rod diameter 20 mm. It was shown that, the steady state of the system at all pH of suspension occurred when the hydrocyclone operates 600 seconds (10 min). The results again confirmed the previous results. Therefore, the operating time 20 minutes can be assured that the system was in steady state.

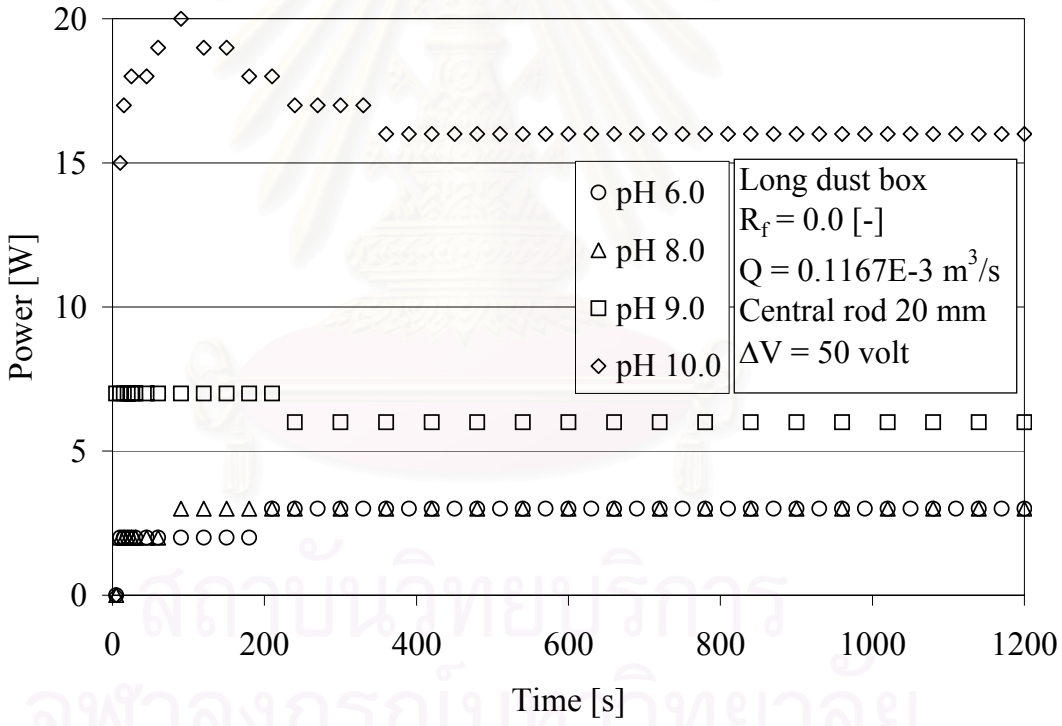

Figure B2 Relationship between power and time

Figure B3 shows the relationship between voltage that supplies from the DC power generator and time at various pH of suspensions when electrical potential was applied to the long dust box (106 mm) of the hydrocyclone in the absence of the underflow at feed flow rate $0.1167*10^{-3}$ m^3/s (7 L/min) and central rod diameter 20 mm. It was shown that, the electrical potential could not constantly supply at 50 volt in the beginning 90 seconds when the pH of suspension was 10.0. It can be explained as following. In the first period, the DC power generator attempted to increase the magnitude of current for achieving the voltage set point. Since at pH of suspension 10.0, the suspension had a lot of sodium and hydroxide ions that mean it was a good conductivity (low resistance). Although the current reached the maximum set current (400 mA), the voltage was not attaining the set point at 50 volt regarding to V=Ri. After 90 seconds, some of sodium and hydroxide ions were deposited on the electrodes as well as amount of silica particles that suspend in the suspension of the dust box increased. Decreasing of sodium and hydroxide ions exhibited a stronger effect than the increasing of silica particles. Therefore, the conductivity of suspension decreased (increasing resistance) and the voltage attained the set point. When the time was gone, the deposit of sodium and hydroxide ions on the electrodes increased, as well as amount of silica particles that suspend in the suspension of the dust box also increased. The suspension had lower conductivity (higher resistance) caused to decrease the supplied current for achieving voltage set point. When the hydrocyclone was operated 600 seconds (10 min), the system was in steady state.

สถาบันวิทยบริการ
จุฬาลงกรณ์มหาวิทยาลัย

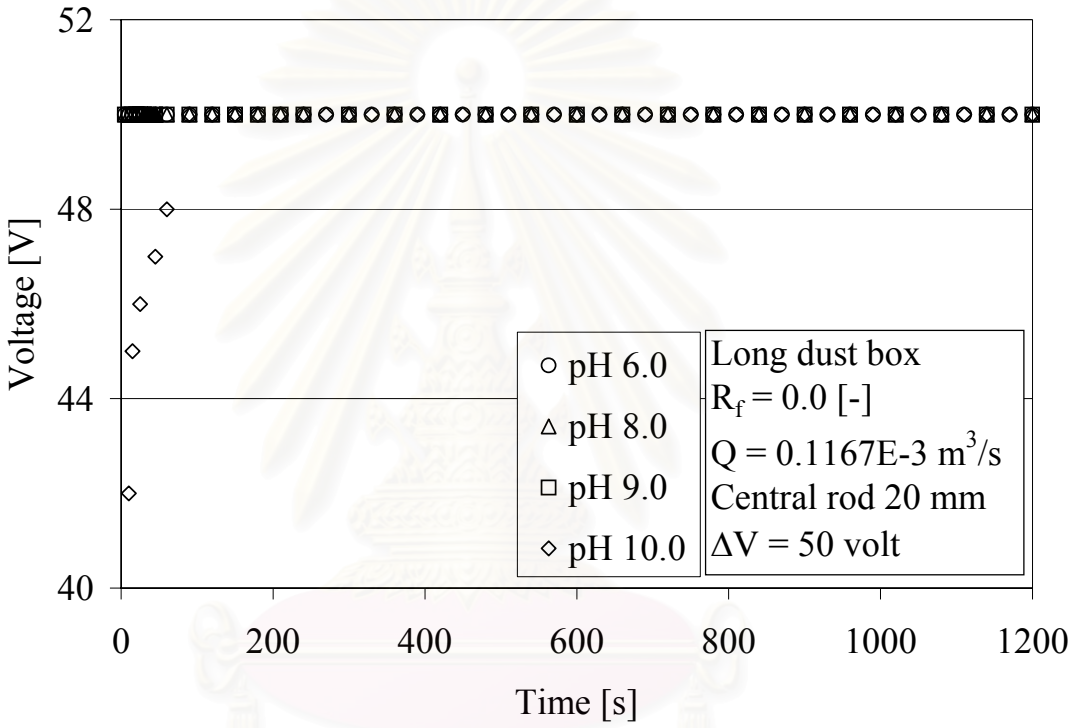

Figure B3 Relationship between voltage and time

สถาบันวิทยบริการ
จุฬาลงกรณ์มหาวิทยาลัย

Figure B4 shows the relationship between resistance of suspension and time at various pH of suspensions when electrical potential was applied to the long dust box (106 mm) of the hydrocyclone in the absence of the underflow at feed flow rate $0.1167*10^{-3}$ m^3/s (7 L/min) and central rod diameter 20 mm.

The pH of suspension 6.0 reveals the highest resistance of suspension when compared to other pH. When the time was gone, amount of silica particles that suspended in the suspension of the dust box increased, caused to increase the conductivity of suspension (decreasing resistance). Therefore, the current increased for maintaining the constant voltage set point.

The pH of suspension 8.0 results the lower resistance when compared to pH of suspension 6.0 because the suspension had a few of sodium and hydroxide ions from addition of NaOH. All of a few of sodium and hydroxide ions were deposited on the electrodes. The behavior of the pH of suspension 8.0 was the same as pH of suspension 6.0.

The pH of suspension 9.0 shows the lower resistance when compared to pH of suspension 6.0 and 8.0 because the suspension had many sodium and hydroxide ions from addition of NaOH. First, the DC power generator increased the magnitude of current for achieving the voltage set point because the suspension had good conductivity (low resistance). Then, some of sodium and hydroxide ions were deposited on the electrodes as well as amount of silica particles that suspend in the suspension of the dust box increased. Decreasing of sodium and hydroxide ions exhibited a stronger effect than the increasing of silica particles. Therefore, the conductivity of suspension decreased (increasing resistance) caused to decrease the supplied current for achieving voltage set point.

The pH of suspension 10.0 expresses the lowest resistance when compared to pH of suspension 6.0, 8.0 and 9.0 because the suspension had huge of sodium and hydroxide ions from addition of NaOH. The behavior of the pH of suspension 10.0 was the same as pH of suspension 9.0 excepted the electrical potential could not constantly supplied at 50 volt in the beginning 90 seconds as explained previously on **Figure B3**.

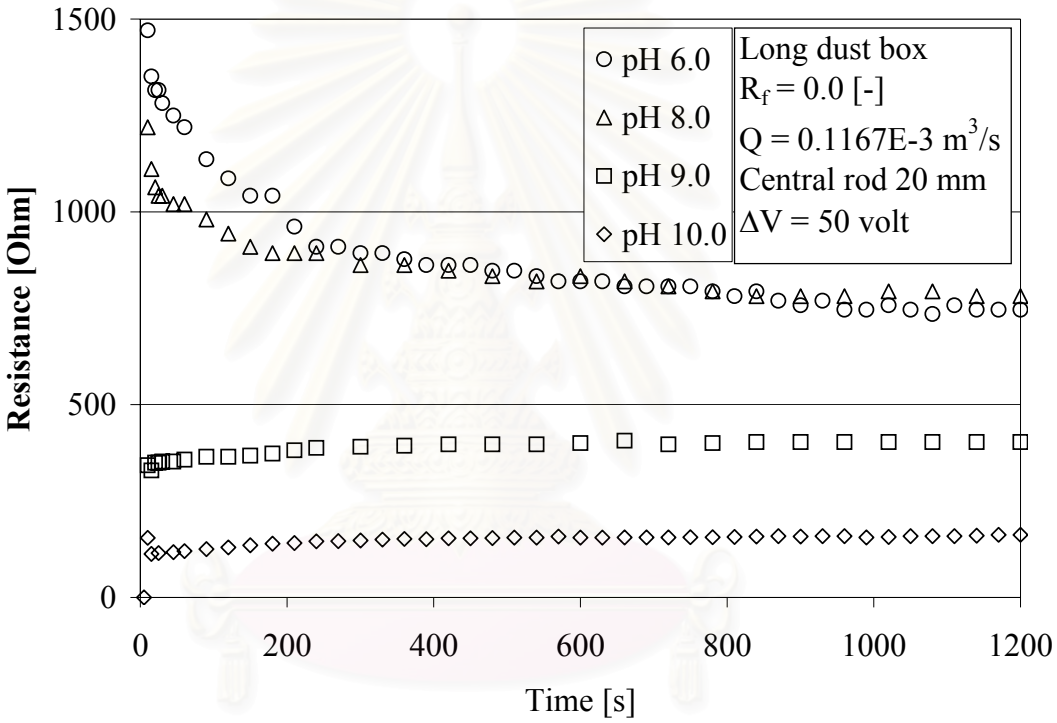

Figure B4 Relationship between resistance of suspension and time

ศูนย์วิทยทรัพยากร
จุฬาลงกรณ์มหาวิทยาลัย

APPENDIX C

ZETA POTENTIAL MEASUREMENT

A graph of zeta potential versus pH is shown in **Figure C1**. This data was obtained on the 0.2 wt% silica suspension using zeta potential instrument (Zetasizer 2000, MALNERN INSTUMENTS). Sodium hydroxide was used to adjust the pH of suspension. The addition of NaOH increased the zeta potential of surface and changed the surface to higher the negative charge. The zeta potential was less negative for low pH values and more negative for high pH values. The pH at which the zeta is zero is the isoelectric point (IEP) of the colloid. The IEP is a property of the particle surface. For silica, the IEP is usually around 3. Thus, silica suspensions are usually stable above about pH 4.

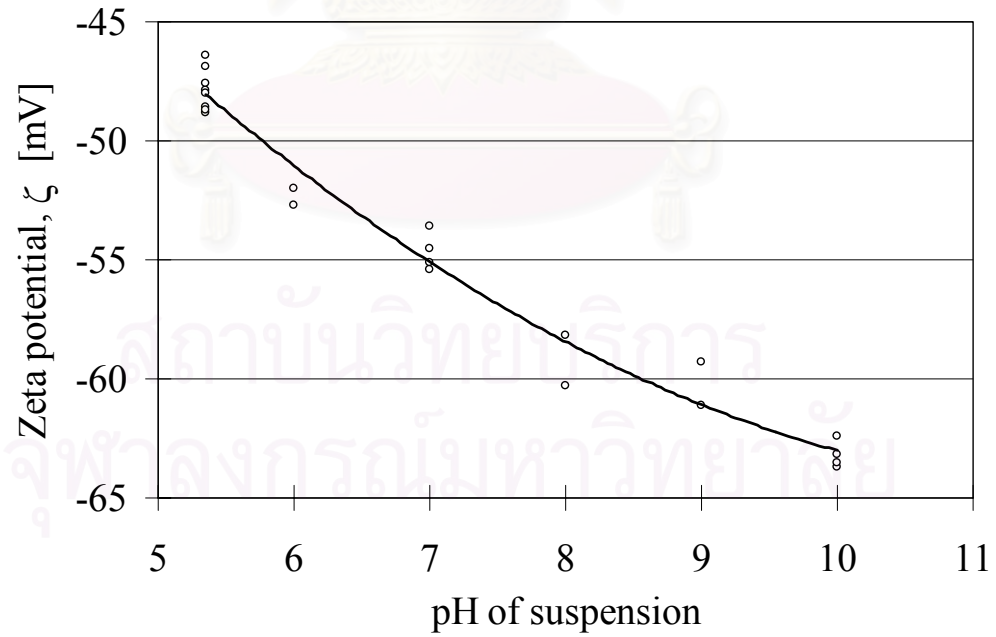

Figure C1 Effect of pH on zeta potential

VITA

Mr. Pratarn Wongsarivej, the first son of Mr. Kamrop and Mrs. Saichol Wongsarivej, was born on March 29, 1969 in Hadyai, Songkhla, Thailand. He spent 6 years studying in primary and secondary educations at Hadyaiwittayalai School, Songkhla. He graduated from Prince of Songkhla University, with a Bachelor of Engineering in Chemical Engineering with 1st class honor in 1991 and from Chulalongkorn University, with a Master of Engineering in Chemical Engineering in 1998. Prior to study in Doctor's program he received the 2001 Royal Golden Jubilee Ph.D. scholarship from the Thailand Research Fund, TRF-RGJ. He was a grantee of Association of International Education, Japan (AIEJ) Short-term Student Exchange Promotion Program (Inbound) Scholarship under the Memorandum of Understanding (MOU) between TRF and AIEJ. He had been admitted to Graduate School of Engineering, Hiroshima University as a Special Research Student from October 1, 2003 to September 31, 2004 to carry out a part of his dissertation. He was awarded a Ph.D. degree in Chemical Engineering from Chulalongkorn University in April 2005.

สถาบันวิทยบริการ
จุฬาลงกรณ์มหาวิทยาลัย